BINDING, KINETICS, AND CELLULAR PROCESSING OF OVINE INTERFERON TAU AND THE TYPE I INTERFERON RECEPTOR

BY

KENDRA INDHIRA SILER

A DISSERTATION PRESENTED TO THE GRADUATE SCHOOL
OF THE UNIVERSITY OF FLORIDA IN PARTIAL FULFILLMENT
OF THE REQUIREMENTS FOR THE DEGREE OF
DOCTOR OF PHILOSOPHY

UNIVERSITY OF FLORIDA

2001

To the loving memory of my abuelita, Gwendolyn Matthews, who taught me patience, perseverance, compassion, and how to read.

ACKNOWLEDGMENTS

I would like to recognize the chairman of my committee, Dr. Phillip M. Achey; and the members of my committee, Dr. Daniel C. Sharp, Dr. Edward M. Hoffmann, and Dr. James F. Preston for their positive contributions to my research and education. I am grateful to Dr. Rachel Shireman, Dr. Gerard Shaw, Dr. William W. Thatcher, Dr. Ben Dunn, Dr. Paul Chun, Dr. Martez M. Green, and Dr. Michael B. Porter for assisting with experimental design, data analysis and research presentation. I also greatly appreciate the technical advice and services provided by Alfred Chung, Tim Vaught, Frank Michel, George Rawls, Jose Clemente and Sam Frank. I was so fortunate to have the opportunity to interact with Dr. Daniel C. Sharp, Dr. Rachel Shireman, and Dr. B.D. Sivazlian. They are all excellent role models and mentors because they do not limit what they teach to science; they truly care about the well being of others. Dr. Samuel R. Farrah deserves my deepest gratitude for his kindness; he treated me as if I were one of his own students. I appreciate the time and laughter shared with my fellow graduate students, especially those in Dr. Daniel C. Sharp's laboratory, Dr. Samuel R. Farrah's laboratory, Dr. Linda Bloom's laboratory, and Dr. Ben Dunn's laboratory. I am grateful for

the positive attitude, support, work ethic, and expertise of the integral employees of the Microbiology and Cell Science Department, especially Cathy Cassidy, Linda Parsons, and Barbara Perry. I will always cherish the kindness and love that can only be provided by true friends. My family, especially James H. Siler, Kumari Siler, and James K. Siler, will always be adored for their love, moral support, and for teaching me what is important in life.

TABLE OF CONTENTS

page

ACKNOWLEDGMENTS iv

LIST OF TABLES ix

LIST OF FIGURES x

1 BACKGROUND AND SIGNIFICANCE 1
Structural and Biochemical Characteristics of Ovine IFNτ 1
Biological Properties of Ovine IFNτ 2
Functional Regions on the Ovine IFNτ Molecule 6
Structural Characteristics of the Type I IFN Receptor 8
Binding and Biochemical Features of the Type I IFNs to the Type I IFN Receptor 9
Interactions between the Type I IFN Receptor and Intracellular Signalling Molecules 10
Signal Transduction and Biological Response to Ovine IFNτ 11
Cellular Internalization and Processing 12
Equilibrium Binding of the Type I IFNs to the Type IFN Receptor 14
Steady-state Models and Kinetics of the Type I IFNs and the Type I IFN Receptor in Whole Cells 17

2 MATERIALS AND METHODS 24
Cell Lines 24
Recombinant Ovine IFNτ 24
Peptide Synthesis and Purification 24
Biotin Labeling of IFNτ Peptides and Ovine IFNτ for Synthetic Peptide Studies 25
Radioiodination of Ovine IFNτ for Synthetic Peptide Studies 26
Direct Binding Assays 27
Competitive Binding Assays on Viable Cells 28
Solid-phase Competition Assays 28
Vesicular Stomatis Virus (VSV) Propagation 29
Antiviral Cytopathic Effect Inhibition Assay 30
Localization of IFNAR2 in MDBK Cells Using Immunofluorescence 30

Localization of Ovine IFNτ with respect to the Lysosomes in MDBK Cells Using Immunofluorescence....31
Iodogen Radioiodination of Ovine IFNτ and Human IFNαA for Equilibrium Binding and Kinetic Assays....33
Cellular Binding and Internalization Kinetic Assays....34
Equilibrium Binding Assay....36
Steady State Binding Assays....37
Unoccupied Receptor Turnover Binding Assays....39

3 DETERMINATION OF STRUCTURAL AND FUNCTIONAL REGIONS OF OVINE IFNτ AND THE TYPE I IFN RECEPTOR....41
Direct Binding of Biotinylated Ovine IFNτ to IFNAR2 Extracellular Domain Peptides....41
Extracellular Domain Receptor Peptides Block Ovine ^{125}I-IFNτ Binding to Viable MDBK Cells....44
Differential Binding Affinities of IFNAR2(1-38) and IFNAR2(34-67) for Ovine ^{125}I-IFNτ....47
Structurally Important Extracellular IFNAR2 Peptides Block Antiviral Activity of Ovine IFNτ....49
Human IFNαD Antagonizes Biotinylated Ovine IFNτ Binding to IFNAR2(34-67)....50
Direct Binding of Biotinylated Ovine IFNτ to IFNAR2 Intracellular Domain Peptides....50
An Intracellular Peptide Inhibits Ovine ^{125}I-IFNτ Binding to IFNAR2 on Viable and Intact MDBK Cells....54
An Intracellular Peptide Inhibits Ovine IFNτ Antiviral Activity....59
Direct Binding of Biotin-conjugated Ovine IFNτ Peptides to Extracellular IFNAR2 Peptides....59
Direct Binding of Biotin-conjugated Ovine IFNτ Peptides to Intracellular IFNAR2 Peptides....60
Ovine IFNτ Peptides Compete with Ovine ^{125}I-IFNτ for IFNAR2(1-38)....63
Ovine IFNτ Peptides Compete with Ovine ^{125}I-IFNτ for IFNAR2(34-67)....73
Ovine IFNτ and Ovine IFNτ Peptides Specifically Recognize IFNAR2(287-315)....80
Saturation Binding Studies with ^{125}I-Ovine IFNτ Further Reveal Specific Recognition of IFNAR2(287-315)....91
Determination of Binding Regions on Ovine IFNτ for the Type I IFN Receptor....92
Discussion....92

4 TOPOGRAPHICAL FATE OF OVINE IFNτ AND THE TYPE I IFN RECEPTOR AS DETERMINED BY INDIRECT FLUORESCENT MICROSCOPY 98
Ovine IFNτ Colocalizes with the Lysosomal Associated Matrix Protein 1 98
Ovine IFNτ is Degraded in the Lysosomes 112
IFNAR2 is Internalized in MDBK Cells Following Ovine IFNτ Stimulation 112
Discussion 113

5 BINDING, INTERNALIZATION, AND PROCESSING OF OVINE IFNτ, HUMAN IFNαA, AND THE TYPE I IFN RECEPTOR BY MDBK CELLS: A COMPARATIVE BIOCHEMICAL ANALYSIS 116
Equilibrium Binding of Ovine IFNτ and Human IFNαA to the Type I IFN Receptor on MDBK Cells 116
Dissociation Rate Constant (k_d) of Ovine IFNτ and Human IFNαA from the Type I IFN Receptor on MDBK Cells 123
Association Rate Constants (k_a) of Ovine IFNτ and Human IFNαA from the Type I IFN Receptor on MDBK Cells 124
Endocytotic Rate Constant (k_e) of Human IFNαA is Significantly Faster than that of Ovine IFNτ into MDBK Cells 127
Surface Binding and Internalization Patterns of Human IFNαA and Ovine IFNτ in MDBK Cells 128
Rate Constants of Hydrolysis (k_h) of Ovine IFNτ and Human IFNαA in MDBK Cells 133
Steady State Binding Constants (K_{ss}) of Ovine IFNτ and Human IFNαA for the Type I IFN Receptor 134
Reinsertion of Type I IFN Receptors into the Plasma Membrane Occurs at a Faster Rate in MDBK Cells Stimulated with Human IFNαA than Ovine IFNτ 135
Human IFNαA and Ovine IFNτ Accelerate the Internalization of Ligand-Occupied Type I IFN Receptors into MDBK Cells 140
Discussion 147

6 DISCUSSION 153

LIST OF REFERENCES 158

BIOGRAPHICAL SKETCH 173

LIST OF TABLES

Table Page

3-1. Sequences and secondary structure predictions of the synthetic extracellular domain peptides of IFNAR2.....42

3-2. Sequences and secondary structure predictions of the synthetic intracellular domain peptides of IFNAR2. 53

3-3. Sequences and secondary structure of the synthetic ovine IFNτ peptides of IFNAR2.....64

LIST OF FIGURES

Figure Page

3-1. Direct binding of biotinylated ovine IFNτ to overlapping synthetic peptides of the extracellular domain of IFNAR2 43

3-2. Dose-response of unlabeled ovine IFNτ and extracellular IFNAR2 peptide competitors on ovine IFNτ binding to the type I IFN receptor on viable MDBK cells.....45

3-3. Dose-response of extracellular IFNAR2 peptide competitors, IFNAR2(1-38) and IFNAR2(34-67) on ovine ^{125}I-IFNτ binding to the type I IFN receptor on MDBK cells 46

3-4. Extracellular IFNAR2 peptide, IFNAR2(186-217), does not effect ovine ^{125}I-IFNτ binding to the type I IFN receptor on MDBK cells 48

3-5. Extracellular IFNAR2 peptides inhibition of ovine IFNτ antiviral activity.. 51

3-6. Dose-dependent inhibition of biotinylated ovine IFNτ binding to IFNAR2(34-67) by unlabeled ovine IFNτ and human IFNαD 52

3-7. Direct binding of biotinylated ovine IFNτ to overlapping synthetic peptides of the intracellular domain of IFNAR2.....55

3-8. Dose-response of unlabeled ovine IFNτ and extracellular IFNAR2 peptide competitors on ovine IFNτ binding to the type I IFN receptor on MDBK cells 56

3-9. Dose-response of intracellular IFNAR2 peptide competitor, IFNAR2(287-315) on ovine ^{125}I-IFNτ binding to the type I IFN receptor on MDBK cells 57

3-10. Intracellular IFNAR2 peptide inhibition of ovine IFNτ antiviral activity 58

3-11. Binding of biotinylated ovine IFNτ, and ovine IFNτ peptides, IFNτ(1-38), IFNτ(118-138), and IFNτ(153-168) to overlapping synthetic peptides corresponding to the extracellular domain of IFNAR2. 61

3-12. Binding of biotinylated ovine IFNτ, and ovine IFNτ peptides, IFNτ(1-38), IFNτ(118-138), and IFNτ(153-168) to overlapping synthetic peptides corresponding to the intracellular domain of IFNAR2. 62

3-13. Dose-dependent binding of ovine ^{125}I-IFNτ to IFNAR2(1-38) in the presence of unlabeled ovine IFNτ peptides. 65

3-14. Dose-dependent binding of ovine ^{125}I-IFNτ to IFNAR2(1-38) in the presence of unlabeled ovine IFNτ. 71

3-15. Dose-response of extracellular IFNAR2 peptide competitors, IFNAR2(1-38) and IFNAR2(186-217), on ovine ^{125}I-IFNτ binding to the type I IFN receptor on MDBK cells.....72

3-16. Dose-dependent binding of ovine ^{125}I-IFNτ to IFNAR2(34-67) in the presence of unlabeled ovine IFNτ peptides 74

3-17. Dose-dependent binding of ovine ^{125}I-IFNτ to IFNAR2(34-67) in the presence of unlabeled ovine IFNτ. 81

3-18. Dose-response of extracellular IFNAR2 peptide competitors, IFNAR2(34-67) and IFNAR2(186-217), on ovine ^{125}I-IFNτ binding to IFNAR2(34-67).. 82

3-19. Dose-dependent binding of biotinylated ovine IFNτ peptides, IFNτ(1-38), IFNτ(118-138), and IFNτ(153-168) to IFNAR2(287-315) in the presence of unlabeled ovine IFNτ peptides.. 83

3-20. Binding of biotinylated ovine IFNτ to IFNAR2(287-315) in the presence of unlabeled ovine IFNτ.. 86

3-21. Dose-dependent binding of biotinylated ovine IFNτ to IFNAR2(287-315) in the presence of IFNAR2(287-315).....87

3-22. Dose-dependent binding of ovine ^{125}I-IFNτ to IFNAR2(287-315) in the presence of unlabeled ovine IFNτ. 88

3-23. Dose-response of intracellular IFNAR2 peptide competitor, IFNAR2(287-315), on ovine ^{125}I-IFNτ binding to IFNAR2(287-315).. 89

3-24. Dose-response of unlabeled ovine IFNτ and extracellular IFNAR2 peptide competitors on ovine IFNτ binding to the type I IFN receptor on MDBK cells. 90

4-1. Translocation of ovine IFNτ in respect to LAMP-1, a lysosomal protein, at 32 minutes.. 99

4-2. Time-dependent translocation of ovine IFNτ in respect to LAMP-1, a lysosomal protein, following ovine IFNτ treatment as shown by indirect immunofluorescence.. 103

4-3. The indirect immunofluorescence of LAMP-1.. 104

4-4. MDBK cells treated only with secondary antibodies against primary antibodies specific for (A) ovine IFNτ and (B) LAMP-1.. 105

4-5. Concentration of degraded ovine ^{125}I-IFNτ from 100 μM final concentration of chloroquine-treated MDBK cells.. 106

4-6. Time-dependent translocation of IFNAR2 following ovine IFNτ treatment as shown by indirect immunofluorescence. 110

4-7. MDBK cells treated only with secondary antibodies that were against primary antibodies specific for IFNAR2. 111

5-1. The equilibrium surface binding of human IFNαA to MDBK cells as determined by (A) Scatchard analysis and (B) nonlinear regression analysis.. 117

5-2. The equilibrium surface binding of ovine IFNτ to MDBK cells as determined by (A) Scatchard analysis and (B) nonlinear regression analysis.. 119

5-3. The dissociation rate constants of human IFNαA and the type I IFN receptor on MDBK cells.. 125

5-4. The dissociation rate constants of ovine IFNτ and the type I IFN receptor on MDBK cells.. 126

5-5. The rate constants of endocytosis and hydrolysis of human IFNαA and the type I IFN receptor on MDBK cells.....129

5-6. The rate constants of endocytosis and hydrolysis of ovine IFNτ and the type I IFN receptor on MDBK cells.....130

5-7. The surface binding and internalization pattern of human IFNαA and the type I IFN receptor in relation to MDBK cells.. 131

5-8. The surface binding and internalization pattern of ovine IFNτ and the type I IFN receptor in relation to MDBK cells.. 132

5-9. The steady state binding of human IFNαA to MDBK cells and the rate of insertion of type I IFN receptors into MDBK cell membranes following human IFNαA stimulation as determined by (A) Scatchard analysis and (B) nonlinear regression analysis.. 136

5-10. The steady state binding of ^{125}I-ovine IFNτ and the rate of insertion of type I IFN receptors into MDBK cell membranes following ovine IFNτ stimulation as determined by (A) Scatchard analysis and (B) nonlinear regression analysis...138

5-11. Total receptor concentration following human IFNαA stimulation at a final concentration of 22 pM as determined by (A) Scatchard analysis and (B) nonlinear regression analysis...142

5-12. Total receptor concentration following ovine IFNτ stimulation at a final concentration of 56 pM as determined by (A) Scatchard analysis and (B) nonlinear regression analysis.. 144

Abstract of Dissertation Presented to the Graduate School
of the University of Florida in Partial Fulfillment of the
Requirements for the Degree of Doctor of Philosophy

Binding, Kinetics, and Cellular Processing of Ovine Interferon Tau and the Type I Interferon Receptor

By

Kendra Indhira Siler

August, 2001

Chairman: Phillip M. Achey
Major Department: Microbiology and Cell Science

Although ovine interferon tau (IFNτ) was originally identified as a pregnancy recognition hormone and IFNτ genes have not been identified in humans, this type I IFN exerts plieotropic biological activities without species-specificity. Ovine IFNτ elicits function by binding the type I IFN receptor, which is shared by all type I IFNs. However, IFNτ is less toxic than FDA approved type I IFNs, yet comparable functionally. This study serves as a comprehensive analysis of the structurally and functionally significant interactions and cellular processing of IFNτ and its receptor. This research may contribute significantly to the design of hybrid type I IFN therapeutic agents.

Biochemical aspects of ovine IFNτ, especially the efficient removal of ovine IFNτ from cells and the reduced rate of insertion of receptor into the cell membrane, may be factors in the reduction of the toxic effects that are characteristic of type I IFNs. For every four human IFNαA internalized one is degraded; the ratio of IFNτ internalization to degradation is 1:1. In addition, receptor is inserted into the cell membrane 70% more slowly in response to IFNτ than human IFNαA. Therefore, accumulation of human IFNαA in cells may contribute to toxicity. The display of these biochemical characteristics of ovine IFNτ by hybrid type I IFN molecules may be indicative of therapeutic potential.

Specific binding regions of ovine IFNτ and IFNAR2 were elucidated to provide primary structure information for hybrid IFN design. Ovine IFNτ residues 1-38 and 77-138 interact with the N-terminus of IFNAR2 at residues 1-67.

CHAPTER 1
BACKGROUND AND SIGNIFICANCE

Type I interferons (IFNs) are structurally and functionally related cytokines that exert strong antiviral, antiproliferative, antitumor, and immunomodulatory activities. At least fourteen IFNα subtypes, IFNβ, IFNω, and the newest member IFNτ, originally identified as a pregnancy recognition hormone for sheep, make up the type I IFN family [1, 2]. Because of successful basic research and clinical trials, IFNα has been approved by the FDA for treating hairy cell leukemia, Kaposi's sarcoma, and chronic hepatitis B and C [1, 2, 3]. Interferonβ has received FDA approval for the treatment of relapsing-remitting multiple sclerosis [1]. However, undesirable side effects at high doses, such as severe flu-like symptoms and bone marrow suppression limit more extensive and effective use of the type I IFNs [1, 4, 5].

Structural and Biochemical Characteristics of Ovine IFNτ

Ovine IFNτ shares 30 to 70% amino acid sequence identity with type I IFNs of various species and subtypes [6]. The primary sequence of ovine IFNτ is 30% identical to that of ovine IFNβ and 45 to 55% identical when compared to the amino acid sequences of human, mouse, and pig IFNα subtypes. Primary structure identity increases to

70% when ovine IFNτ is aligned with bovine IFNω. Also, like bovine IFNω, the mature form of ovine IFNτ is 172 amino acids in length [7]. The protein's precursor is 195 amino acids long; therefore, 23 amino acids make up the cleaved signal sequence [2]. The molecular weight is approximately 19 kD, equivalent to that of all type I IFNs. The isoelectric point (pI) of various natural and recombinant ovine IFNτ molecules ranges between 5.3 and 5.8 [1, 2]. The pI values of IFNα subtypes average 5.5. All of the type I IFNs are acid stable to pH 2-3 [8].

Ovine IFNτ has the characteristic tertiary structure of the type I IFN family, a four-helix bundle with a tightly associated fifth helix [9, 10]. Cellular response to all type I IFNs depends on ligand recognition and interaction with the type I IFN receptor [7, 11-13]. Ovine IFNτ interacts with this receptor to exert function [8]. No other receptors have been shown to specifically interact with ovine IFNτ. Cytokines that share receptor subunits, like the type I IFNs, elicit both redundant and unique biological responses [14].

Biological Properties of Ovine IFNτ

Like all type I IFNs, ovine IFNτ has been shown to inhibit viral replication. Specifically, ovine IFNτ inhibits vesicular stomatis virus (VSV), human papilloma virus (HPV), human and feline immunodeficiency lentiviruses and ovine progressive pneumonia virus

(OPPV), a concern to sheep ranchers [8]. Therefore, the antiviral activity is not species-specific. In addition, antiviral protection is provided to many cell types including various epithelial cells and fibroblasts [2, 8, 12]. Unlike other type I IFNs, however, neither viral infections nor double-stranded RNA stimulates the production of ovine IFNτ by trophoblasts [15].

Type I IFNs invoke antiviral activity by multiple mechanisms. The upregulation of 2'-5' oligoadenylate synthetase, ds-RNA-dependent protein kinase (PKR) activation, and Mx protein synthesis provides several different cell types with a comprehensive defense against a host of viruses [16-21]. The 2'-5' oligoadenylate synthetase production of 2', 5' oligoadenylates is stimulated by viral dsRNA [22]. The oligoadenylates bind and activate monomers of 2-5A-dependent RNαse L, which then dimerize and cleave ssRNA to block viral replication. The activation of PKR ultimately causes the inhibition of translation [20]. Double-stranded RNA binds to PKR, a serine-threonine kinase, to initiate a kinase cascade that results in the inactivation of guanine diphosphate bound eIF2 and eIF2B. Without these active complexes, all translation, and therefore, viral translation, stops. Both PKR and 2-5A-dependent RNαse L have been implicated in apoptosis, which also provides viral protection [23, 24]. Mx proteins inhibit viral replication at levels of transcription and translation, at

various points in the viral life cycle. These proteins are GTPases of the dynamin family [25]. Type I IFNs, including ovine IFNτ, exert antiretroviral activity by blocking reverse transcriptase [26, 27].

The plieotropic nature of type I IFNs is apparent by the broad scope of immunomodulatory properties they possess. The cytotoxic effects of natural killer cells are amplified by type IFNs [28-30]. Type I IFN stimulation enhances CD8+ T cell responsiveness by increasing the expression of major histocompatibity complex I (MHC I) on cell membranes [31]. Production and development of T helper 1 cells is stimulated [32]. In addition, the expression of cell adhesion molecules on the cell membrane is enhanced [33]. These immunomodulatory activities are in part responsible for the antiviral, antiproliferative and antitumor capabilities of type I IFNs. Type I IFNs also exert antiproliferative activities by arresting the cell cycle in cell lines such as Madin-Darby kidney cells, mouse L929 fibroblasts, and human WISH fibroblasts [8, 34]. Cell cycle arrest and apoptosis are also believed to be mechanisms by which type I IFNs exert their antitumor activities. Type I IFNs have been shown to down-regulate various cyclins of the cell cycle, inhibit c-myc expression, and inhibit phosphorylation of Rb [34, 35]. These cyclins and tumor suppressors have all been determined to play roles as causative agents and factors in various cancers. Various B-cell neoplasms, including hairy cell

leukemia and cryoglobulinemia, were sent into remission by IFNα treatment in some patients [36]. Human breast, kidney, and hematopoietic tumor cell growth has been inhibited by ovine IFNτ in vitro [8].

Despite structural and biochemical similarities with other type I IFNs, IFNτ is the only known type I IFN that serves as a pregnancy survival hormone [7]. Signalling from embryo to mother was found to occur simultaneously with the secretion of ovine IFNτ in pregnant ewes between days 13 and 21 of pregnancy. At day 16, high quantities, approximately 200 μg, of ovine IFNτ are secreted within 30 hours by a sheep conceptus. Ovine IFNτ is produced specifically by the trophectoderm, which is reflected by its original names, ovine trophoblast protein 1 (oTP-1), trophoblastin, and type I trophoblast interferon [37, 38].

The secretion of ovine IFNτ by trophoblasts results in down-regulation of oxytocin receptors in pregnant ewes [7]. Oxytocin induces the pulsing secretions of prostaglandin F2α (PGF2α) of cycling ewes and PGF2α, in turn, causes the corpus luteum to regress at the end of a non-pregnant ewe's cycle [38]. If the PGF2α pulses are blocked, the corpus luteum and therefore, pregnancy can be maintained. High concentrations of ovine IFNτ in sheep result in the inhibition of the expression of the oxytocin receptor [37].

The reproductive function of ovine IFNτ is considered to be luteostatic because it prevents the regression of the corpus luteum [7, 37].

Another marked difference between ovine IFNτ and other type I IFNs is the duration and quantity of protein release [38]. Ovine IFNτ secretion occurs for several continuous days in ruminants, whereas the release of IFNα in various species occurs only for a few hours in response to an immunological challenge. As mentioned earlier, approximately 200 μg, of ovine IFNτ will be secreted within 30 hours by a 16-day old sheep conceptus. This amount is approximately 300 times the quantities of IFNα released. Animal models have been shown to tolerate high quantities of ovine IFNτ; however, even in short durations, high doses of other type I IFNs result in apparent adverse effects (i.e. fever, flu-like symptoms etc.) [1]. Interestingly, ovine IFNτ retains the beneficial antiviral and cell inhibitory properties in tissue culture and animal models without the associated toxicity of the other type I IFNs [38, 39].

Functional Regions on the Ovine IFNτ Molecule

In previous studies, the function of ovine IFNτ could be blocked by peptides, but receptor binding could not be blocked [39]. Functional competition assays using ovine IFNτ peptides, identified as peptides oIFNτ(1-37), oIFNτ(62-92), oIFNτ(119-150), and

oIFNτ(139-172), as effective inhibitors of ovine IFNτ induced antiviral activity. Antiproliferative activity of ovine IFNτ was blocked by oIFNτ(119-150), oIFNτ(139-172), and to a lesser degree oIFNτ(90-122). Whole polyclonal antibodies to the peptides blocked ovine IFNτ biological activity with similar results to the competition assays using the ovine IFNτ peptides. All ovine IFNτ peptides, except oIFNτ(1-37), blocked human and bovine IFNα antiviral activity on MDBK cells, suggesting that the N-terminus of ovine IFNτ differentially recognizes the type I IFN receptor. Consistent with these studies, x-ray crystallography identified significant structural differences between the N-termini of human IFNα2 and ovine IFNτ, primarily involving residues 1-8 and 22-25 [9]. The crystal structure also showed that the functional peptides corresponded to regions that lie on the same face or side of the ovine IFNτ molecule. Multiple binding sites may be necessary for monomers of ovine IFNτ to bind to receptor with high affinity.

Previous studies using IFNα variants revealed that three regions within residues 10-35, 78-107, and 123-166 were necessary for growth inhibitory activity, antiviral activity, and receptor binding [39]. Another study using molecular variants of IFNα showed that truncated human IFNα2 consisting of amino acids 1-110, but not the fragment of human IFNα2 consisting of residues 111-153, blocked antiviral activity

of the intact molecule [40]. These studies combined suggest that N-terminal regions of human IFNα2 are important for receptor recognition and function.

Structural Characteristics of the Type I IFN Receptor

Type I IFNs initialize their biological properties by interacting with the type I IFN receptor complex, a plasma membrane-bound receptor [41]. This receptor is made up of at least two subunits, IFNAR1 and IFNAR2. IFNAR1 and IFNAR2 were previously referred to as the α and β subunits of the type I IFN receptor. IFNAR2 is expressed in cells in two alternative variant forms, IFNAR2b and IFNAR2c [42, 43]. Truncated IFNAR2 variant, IFNAR2b, was referred to as the β short subunit in older literature [42]. It is only 331 amino acids long and includes an extracellular, transmembrane, and truncated intracellular domain [44]. Although it does not allow cellular response to type I IFN stimulation, IFNAR2b is expressed in low levels in type I IFN responsive cell lines [42]. If over-expressed, it competes with the long IFNAR2c subunit for type I IFN binding and blocks its biological effects [42, 43]. IFNAR2c is the 515 amino acid membrane-bound form of IFNAR2 that upon ligand binding can initiate a cellular response [43, 44]. This 90 kD protein is generally identified as IFNAR2 unless otherwise specified. The ratio of expression of IFNAR2c/IFNAR2b in U-266 cells is 10-20/1 [42]. IFNAR2a is a

recombinant, soluble variant of IFNAR2c that is expressed without the hydrophobic transmembrane domain that is not typically present in cells [42, 45]. The α subunit of the receptor, IFNAR1, is 557 amino acids long and has a molecular weight of 110 kD [46, 47]. The extracellular domain of IFNAR1 is 457 amino acids long; however, only 100 residues of IFNAR1 construct the intracellular domain [48].

Binding and Biochemical Features of the Type I IFNs to the Type I IFN Receptor

Despite the substantial extracellular domain, IFNAR1 only serves as an accessory protein with respect to type I IFN binding [49]. Binding studies have shown that IFNAR2 alone binds type I IFNs with low/intermediate binding affinity, while IFNAR1 alone fails to bind type I IFNs [42, 49]. Human IFNα bound to IFNAR2 expressed on the membranes of mouse L929 fibroblasts with a dissociation equilibrium constant (K_d) of 0.5 to 1 nM, whereas binding to IFNAR1 was undetectable. When the receptor chains are complexed, ligand is bound with high affinity binding [42, 43, 44, 50-52]. Coexpression of IFNAR1 and IFNAR2 on mouse L929 fibroblasts result in high affinity receptor binding on the order of 10-100 pM [43]. On Madin-Darby kidney cells, the dissociation constant (K_d) for ovine IFNτ binding to the type I IFN receptor on MDBK cells was 3.9×10^{-10} M [53]. In competition assays, excess ovine IFNτ did not block receptor binding

or cell death induced by IFNαA [53]. It followed that the cytotoxicity associated with IFNαA was a result of type I IFN receptor saturation, whereas antiviral activity only required a small fractional occupancy of the receptors. In part, the higher binding affinity of IFNαA appeared to account for the differences in toxicities.

Interactions between the Type I IFN Receptor and Intracellular Signalling Molecules

Both receptor subunits contribute to the signaling required for cellular function [12, 54, 55]. IFNAR1 has a cytoplasmic binding site for the Janus kinase, Tyk2, and the signal transducer and activator of transcription 1 (STAT1) transcription factor [56-58]. Tyk2 constitutively associates with IFNAR1 and is believed to contribute structurally to IFNAR1 [57, 59, 60]. The JAKs and STATs are pre-associated with the receptor complex in unactivated, unphosphorylated forms [60, 61]. The STATs bind to the receptor subunits by their SH2 domains. However, without STAT2 complexed to IFNAR2, STAT1 will not bind IFNAR1 [42, 62]. In addition, unactivated STAT1 and STAT2 will complex in the cytoplasm without type I IFN stimulation; the biological significance remains to be determined [63]. In cells that do not express Tyk2, little IFNAR1 is expressed on the cell membrane [60]. Possibly Tyk2 is structurally important for IFNAR1. IFNAR2 is responsible for Janus kinase 1 (JAK 1) binding and interacts with both

STAT 1 and STAT2 [42]. JAK1 and STAT2 interaction with IFNAR2 is continuous; however, the structural relevance of these proteins with respect to IFNAR2 is unknown.

Signal Transduction and Biological Response to Ovine IFNτ

Type I IFN receptor binding results in signal transduction, primarily via the JAKs/STATs pathway [14, 64]. The type I IFN recognition and initial binding to the type I IFN receptor brings the receptor complex into close proximity, activating JAK1 and Tyk2 [57, 65, 66]. JAK1 and Tyk2 phosphorylate the receptor complex [14, 66]. Specifically, phosphorylation of tyrosine 466 of IFNAR1 results in a conformational change that creates a docking site for STAT2 [58, 67]. The substitution of a phenylalanine for the tyrosine at 466 abrogates the kinase cascade required for signaling [67]. Tyrosine 701 of STAT1 and tyrosine 690 STAT2 are subsequently activated by phosphorylation [68]. STAT2 must be phosphorylated before docking and phosphorylation of STAT1 can occur [61, 62]. STAT1 and STAT2 are then believed to heterodimerize and traffic to the nucleus to initiate the transcription of type I IFN inducible genes [14, 69]. For the vast array of cytokines, growth factors, and hormones that utilize this pathway, only six STATs and four JAKs have been identified [14]. However, despite the overlap in the use of JAKs and STATs, the cellular response to cytokines differs. This suggests that the specificity

of function elicited by cytokines, growth factors and hormones is only in part due to the differential roles of JAKs and STATs; differential receptor binding is probably responsible as well. Homologous type I IFN subtypes that have slightly different functional properties bind to the type I IFN receptor differentially [70-72]. These observations may stimulate more research on the structural differences at the receptor level that may be responsible for the varying functional abilities of the type I IFNs.

Cellular Internalization and Processing

The type I IFN receptor not only undergoes lateral movement on the cell membrane in response to type I IFN stimulation, but it is also internalized into the cell via receptor-mediated endocytosis (RME) [73, 74]. The effects of RME on the signal transduction of the type I IFNs are unknown. However, RME may serve as a means of attenuating the receptor population in response to continual or excessive type I IFN stimulation [75]. The dynamics of the receptor population expressed on the cell membranes reflect 1) continual de novo synthesis, 2) internalization, 3) degradation and/or 4) receptor recycling, especially after a cell interacts with ligand [77]. After ligand occupancy of a membrane-bound receptor that undergoes RME, the ligand-receptor complex is internalized via a clathrin-coated pit [77, 78]. The pits containing ligand-occupied receptors are engulfed to form clathrin-

coated vesicles [79]. Fusion of a vesicle with an acidic compartment and loss of the clathrin creates an early endosome (EE) [80-82]. Dissociation between the ligand and the receptor begins in the EE [83, 84]. The pH of the inside of an EE ranges from 6.0 to 6.8 [82]. Therefore, to allow receptor recycling, ligand and receptor sorting can occur without damaging the proteins [77]. Ligand starts to accumulate in the central region of the vesicle, while the receptor tends to gather in peripheral microtubules of the EEs [77, 81, 82, 84, 85]. The secretory pathway can meet the endocytotic pathway at this point [85, 86]. Receptor recycling has been shown to occur from microtubular extensions of the EE [84, 86]. The extensions can bud off into compartments separate from EEs called recycling vesicles (RVs) to return the dissociated receptors to the plasma membrane [84, 85]. Within the cytoplasm, microtubular “tracks” guide the EEs with free ligand into a perinuclear region, where they fuse with subsequent vesicles to create late endosomes (LEs) [80, 84]. The interior of LEs has an even lower pH (pH = 5) than that of EEs and degradation of the ligand often begins here [80]. Ligand degradation is completed in lysosomes, which have high quantities of degradative enzymes in addition to the acidic environment, to finish the breakdown of ligand [80, 85, 87]. If the receptor is not recycled, it may traffic to the LEs and lysosomes to undergo degradation [77, 80]. Alternatively,

it is believed that receptors may be transferred reversibly to the perinuclear trans-Golgi network (TGN) from endosomal or lysosomal compartments [88-90]. The TGN may be another connection to the secretory/recycling pathway [91-93]. Studies have suggested that the pH within the TGN is more basic (pH = 6.0 to 6.4) in comparison to LEs and lysosomal compartments (pH = 5) [82, 94, 95]. The mildly acidic environment would spare receptors from further degradation for recycling purposes [77, 88]. However, it is difficult task for researchers to distinguish between these vesicles morphologically [80, 96]. Many of the vesicles, especially the various types of endosomes, are microtubular in appearance [88, 96]. In addition, pH is not a good indicator because the pH of the endosomal compartments may be equivalent to that of the TGN [82, 94, 95]. Further, proteins that are found in various endosomal vesicles are also detected in the TGN [88]. Distinguishing lysosomes from the TGN is less difficult because lysosomes function as terminal degradative compartments for ligand and sometimes receptor [77, 97]. After degradation of the macromolecules occurs in the lysosomes, the contents are released from the cells [77].

Equilibrium Binding of Type I IFNs to the Type IFN Receptor

Biochemical techniques, such as 4^{o}C equilibrium-binding studies of whole cells, give insight into ligand:receptor binding on the cell

surface, allowing the comparison of how various ligands interact with their membrane-bound receptors [53, 74, 75, 77, 98]. The internalization of ligand is inhibited at 4^{o}C, so all ligand binding occurs only on the plasma membrane of cells [53, 77]. Cells are treated with radiolabeled ligand in increasing concentrations and then allowed to incubate at 4^{o}C to achieve equilibrium. Equilibrium is reached when nearly saturating amounts of added ligand binds to surface-bound receptor and no further changes in binding are observed. The unbound ligand is then separated from the bound ligand. A popular and effective method is using cell suspensions and centrifugation [77]. The cells are pelleted in microfuge tubes within 5 seconds leaving the unbound ligand in solution. The tip of the microfuge tube is cut off to count the radioactivity in the cell pellet. The slope of a Scatchard plot, a plot of bound ligand/free ligand versus bound ligand, reveals the equilibrium association constant (K_a), the equilibrium dissociation constant (K_d), and the maximum concentration of surface-bound receptors (B_{max}) [77].

To determine K_a, K_d, and B_{max}, the data can be transformed linearly to use Scatchard analysis; however, a graph of the concentration of bound ligand versus the concentration of free ligand can also reveal these values [77, 99]. The B_{max} is equivalent to the concentration on the y-axis when the receptor is saturated [77, 100].

The K_d is the $B_{max}/2$ and is the inverse of K_a. A graph in the latter form shows a criterion for equilibrium binding; ligand binding to its receptor must be saturable [75, 77]. Receptor binding is considered to be saturated when it reaches a plateau on a saturation binding curve. This plateau is represented by the hyperbolic relationship between bound and free ligand [77, 100-102]. Affinity is directly proportional to K_a and inversely proportional to K_d. Therefore, as the K_d value decreases, the affinity of a ligand for its receptor increases.

The total binding increases hyperbolically as a function of increasing amounts of free ligand, while nonspecific binding increases linearly [77, 102]. The linear nature of nonspecific binding is due to the inability of nonreceptor sites to be saturated in the same form as the specific receptor sites [77, 103]. Specific binding equals total binding minus nonspecific binding. Specific binding, therefore, also assumes the hyperbolic shape in a plot of bound versus unbound ligand. To determine non-specific binding in an equilibrium-binding assay, unlabeled ligand is added in excess to the free ligand [53, 54, 74, 75, 77, 104, 105]. Usually, an amount equivalent to 100 times the K_d is used [77, 104]. The unlabeled and labeled hormones should have similar biological activity [53, 74, 77]. The previously determined K_d values of human IFNαA and MDBK cells range from 2.5×10^{-10} M to 6.0×10^{-11}M [53, 54, 74, 75, 106].

Steady-state Models and Kinetics of the Type I IFNs and the Type I IFN Receptor in Whole Cells

Although equilibrium-binding studies give insight into surface binding, physiologically relevant ligand and receptor dynamics on and within cells must be studied at 37^{o}C [107-109]. Kinetic studies in which ligand-treated cells are placed at 37^{o}C for specified time intervals and then quickly placed at 4^{o}C allows the discrimination between surface-bound ligand, internalized ligand:receptor complexes, and degraded ligand [74-77, 104, 107-109]. Internalization of ligand-receptor complexes is prevented by reducing the temperature to 4^{o}C because RME is ATP dependent [77]. A temperature of 4^{o}C also slows further degradation, inhibits changes in surface receptor binding and prevents changes in receptor population [107,110]. Treating the supernatant with trichloroacetic acid (TCA) and coprecipitation with bovine serum albumin (BSA) separates degraded ligand from intact free ligand that is not associated with the cell [77, 111]. The TCA-soluble fraction has ligand degraded by the cells exogenously and endogenously and the TCA-insoluble fraction contains intact ligand. Surface-bound ligand is retrieved from cells at 4^{o}C by treating with an acidic buffer followed by centrifugation and removal of the supernatant [110, 112, 113]. Changes in surface binding over time are then compared to the optimal surface binding that occurs at 4^{o}C to reveal

the dissociation rate constant (k_d) [104, 110, 113, 114]. Internalization of ligand is inhibited at 4°C, so all ligand binding occurs only on the plasma membrane [77, 99, 106]. After surface-bound ligand is dissociated from the cells, internalized ligand can be released by cell solubilization [104, 106]. These kinetic studies have been performed on human IFNαA treated A549 cells to give insight into the binding, internalization, and cellular processing of human IFNαA and the type I IFN receptor [115]. The dissociation rate constant (k_d) of human IFNαA and membrane-bound type I IFN receptor was determined to be 7.2×10^{-2} min^{-1} using the kinetic experiments previously described and the following equation [77]:

k_d, (min^{-1}) = Slope of $ln[LR]_s/[LR]_o$ vs. time
$[LR]_s$ = Molar concentration of surface ligand:receptor complexes at 37°C
$[LR]_o$ = Molar concentration of surface ligand:receptor complexes at 4°C

A straight line indicates that the interaction between the ligand and its receptor is a first-order, bimolecular reaction that follows the law of mass action [77, 113]. Only one receptor population is specific for the ligand and changes in affinities do not occur while the ligand binds to various regions on the receptor [99, 113, 116].

Changes in affinities as the ligand binds, referred to as positive and negative cooperativity, result in curvilinear plots [99]. Positive cooperativity means that as ligand binds to receptor, the affinity for

additional ligand binding increases and does not readily dissociate. The slope becomes more steep over time. With negative cooperativity, the slope becomes more shallow because binding of ligand to receptor decreases subsequent binding. If more than one receptor is specific for the ligand and the independent forms of receptors have different binding affinities, a curvilinear plot will result [77]. The dissociation rate constant has been referred to as k_2 in some reports. The association rate constant (k_a), sometimes called k_1, is determined using the results from an equilibrium binding study, specifically the equilibrium dissociation constant (K_d) and the k_d. The equation is as follows:

$$k_a, (min^{-1}M^{-1}) = k_d, (min^{-1})/K_d, (M)$$

The k_a of human IFNαA to type I IFN receptors on MDBK cells was determined to be 3.3×10^8 $min^{-1}M^{-1}$ based on the K_d of human IFNαA to MDBK cells and time-concentration points of $[LR]_s$ [75].

Further analysis of receptor population turnover at 37°C is accomplished by using steady state models developed by Wiley and Cunningham [108-110]. Values for rate constants of endocytosis of ligand-receptor complexes (k_e), endocytosis of unoccupied receptors (k_t), degradation of internalized ligand (k_h), and the insertion of receptors into the plasma membrane (V_r) are some of the applications of steady state models [108-110, 116-118]. Before a cell is

stimulated by a ligand, it is in a steady state in which the rate of insertion of a receptor population equals the rate of removal of the unoccupied receptors [77, 110].

Therefore, $V_r = k_t\ [R]_s$
$[R]_s$ = the concentration of surface receptors, ([M])
V_r = rate of insertion of receptors into the cell membrane, ([M] min^{-1})
k_t = rate of endocytosis of unoccupied receptors, (min^{-1})

Ligand stimulation of the cells can then adjust these cellular dynamics. Ligand occupancy of the cell-surface receptors introduces another variable into the equation. Often the rate of internalization of the occupied receptors exceeds that of unoccupied receptors.

Therefore, $V_r = k_t[R]_s + k_e[LR]_s$
$[LR]_s$ = the concentration of surface ligand:receptor complexes, ([M])
k_e = endocytosis of ligand occupied receptors, (min^{-1})

If the procedures for a 4°C equilibrium binding experiment are performed at 37°C and the results are plotted linearly as in a Scatchard graph, the slope reveals not $-K_a$, but the negative steady state constant ($-K_{ss}$), and the x-intercept represents V_r/k_e instead of B_{max}. The determination of k_e and k_t is discussed later. The units for K_{ss} and V_r/k_e are the same as K_a and B_{max}, respectively. However, K_a is only the association constant of the ligand and its specific surface-bound receptor; K_{ss} represents cell dynamics internally and externally [110]. The K_{ss} of human IFNαA interaction with MDBK cells was

previously determined to be 1.9 x 10^{10} M^{-1} [76]. The equation K_{ss} for is as follows:

$K_{ss} = (k_e k_a)/k_t(k_d + k_e)$
K_{ss} = Steady state constant, (molar concentration^{-1} ([M^{-1}])

The internalization of ligand-receptor complexes can be expressed using the following equation:

$[LR]_i = k_e[LR]_s/k_h$
$[LR]_i$ = the concentration of internalized ligand:receptor complexes, ([M])
k_h = rate of hydrolysis of internalized ligand, (min^{-1})

When the rates of internalized ligand-receptor complexes and degradation of ligand internally remain unchanged (i.e. steady state is achieved), then k_e and k_h can be accurately determined. The degraded ligand is monitored by treating with TCA. The TCA soluble fraction reveals the degraded ligand [119]. If degradation is not occurring, internal ligand measurements are assumed to be solely dependent on internalized ligand from the cell surface, isolating a k_e measurement [110]. Therefore, the slope of $[LR]_i/[LR]_s$ versus time when degradation is not occurring equals k_e. A linear plot shows that degradation is not occurring and that the cell has reached a steady state. A change in the slope of the line reveals when degradation occurs. The k_e of human IFNαA into MDBK cells was 3.1 x 10^{-2} min^{-1} and the k_h was 1.4 x 10^{-2} min^{-1} [75]. The ratio of k_e/k_h was therefore

2.2. For every two human IFNαA molecules endocytosed, only one is hydrolyzed.

The rate of turnover of unoccupied receptors can be used to determine the relative change in internalization of receptors into cells when a ligand is associated with the receptor [110]. Initially, cells are allowed to reach steady state in the presence of a constant, subsaturating concentration of ligand, $[L]_x$. The bound and free ligand quantities are measured and cells with the same concentration of ligand are placed at 4°C. Therefore, the receptor population that was readjusted by adding subsaturating amounts of ligand is prevented from changing any further. An equilibrium-binding assay is then performed on these cells to reveal the new number of cell-surface receptors. The x-intercept equals $[LR]_x + [R]_x$ and the value for $[LR]_x$ was previously determined at 37°C. So, k_t is then determined by the following equation:

$$k_t = (V_r - k_e[LR]_x)/[R]_x$$

Zoon et al. determined the k_t of the type I IFN receptors of MDBK cells in response to human IFNαA stimulation to be 2.3×10^{-2} min^{-1} [75]. However, a computer modeling program that calculates steady state parameters k_a, k_d, k_e, k_h, and k_t using the time-concentration pairs of $[LR]_s$ and $[LR]_i$ in Zoon's studies contended that a k_t, of

3.3 x 10^{-3} min^{-1} was a better fit [74]. The ratio of k_e/k_t reported by Zoon for IFNαA treated MDBK cells was 1.4. When using the best fit as determined by the computer modeling program, the ratio increased to 9.7, suggesting that in MDBK cells, ligand-occupied type I IFN receptors are internalized 10 times faster than unoccupied type I IFN receptors.

Elucidating the specific structural/functional sites on ovine IFNτ and the type I IFN receptor and determining the cellular binding, internalization and processing of this ligand and its receptor are very significant, especially in view of its potent biological activities without type I IFN associated toxicity. Most importantly, determining the sites involved in binding and function of ovine IFNτ and IFNAR2 may serve as groundwork for the future design of less toxic and more specific therapeutics. Further, determination of the specific binding sites and cellular processing necessary for the ovine IFNτ:type I IFN receptor interaction will also provide important insight into receptor recognition and signal transduction initialized by type I IFNs.

CHAPTER 2
MATERIALS AND METHODS

Cell Lines

Madin-Darby Bovine Kidney (MDBK) cells, a cell line responsive to ovine IFNτ, were used for all assays involving viable cells. Cells were grown in a 37°C, 5% CO_2, 100% humidity incubator. Eagle minimum essential media (EMEM) supplemented with antibiotics, 12 U/mL of penecillin and 125 μg/mL streptomycin, and 10% fetal bovine serum (FBS) nourished the cells.

Recombinant Ovine IFNτ

Recombinant ovine IFNτ was expressed in Pichia pastoris. The specific antiviral activity of the purified ovine IFNτ was determined to be 1 x 10^8 antiviral units/mg. The FDA approved IFN, Roferon, was used as the standard in the antiviral assay. Recombinant ovine IFNτ was received as a gift from two independent sources, Dr. Howard M. Johnson and Dr. Fuller W. Bazer.

Peptide Synthesis and Purification

Using solid-phase 9-fluorenylmethylcarbonyl (Fmoc) chemistry, overlapping peptides corresponding to the primary sequence of ovine IFNτ and IFNAR2, the binding subunit of the type I IFN receptor were

synthesized on a PE Biosystems 9050 Peptide Synthesizer [121]. Completed peptides were removed from the resin by adding 2.5:44:1 phenol: trifluoroacetic acid (TFA): triispropylsilane. Resin-conjugated peptides in this solution were placed on a nutator for two hours to separate the peptides from the resin. The peptides remain in solution; the resin is insoluble. The TFA solution containing the soluble peptides was then treated with ethyl ether at a 10 to 1 ratio to precipitate the peptide product. The peptides were then resolubilized with deionized water and lyophilized to remove moisture. Molecular weight and purity of the synthesized peptides were analyzed using mass spectrometry (Alfred Chung, Protein Core, University of Florida). Amino acid analysis was used to determine if the amino acid composition of the peptide product was as expected (Alfred Chung, Protein Core, University of Florida).

Biotin Labeling of IFNτ Peptides and Ovine IFNτ for Synthetic Peptide Studies

Ovine IFNτ and ovine IFNτ peptides were biotinylated by using a biotin-bound, reactive N-hydroxysuccinimide ester [122]. The N-hydroxysulfosuccinimide (NHS) ester cross-links biotin to lysine epsilon-amino groups. Ovine IFNτ (2 mg) or ovine IFNτ peptides (4.5 mg) were dissolved in 500 μL of pH 7.2 phosphate buffered saline (PBS). NHS-LC-Biotin (Pierce, Rockford, IL) (2 mg) was dissolved in 1

mL of DMF and then 20 μL were added to either the ovine IFNτ or ovine IFNτ peptide solution. The reaction mixture was then placed on ice for 2 hours and agitated every 30 minutes to maximize biotinylation. Free biotin was removed from the biotinylated ovine IFNτ by centrifugation for at least 15 minutes in a 3000 molecular weight cut-off (MWCO) Amicon microconcentrator. This process was performed three times. Biotinylated ovine IFNτ peptides were removed from the free biotin by gel filtration using either a pre-packed 1800 MWCO column (Pierce, Rockford, IL) or a column packed with Sephadex G-10, whichever was more appropriate for the mass of the peptide. The protein concentration was then determined using a bicinchoninic acid (BCA) protein assay (Pierce, Rockford, IL) [123].

Radioiodination of Ovine IFNτ for Synthetic Peptide Studies

Ovine IFNτ was radiolabeled with ^{125}-Iodine using the Bolton and Hunter monoiodoester and the Bolton and Hunter protocol [124]. The solvent on the monoiodoester was removed by a gentle stream of nitrogen gas transferred by a 22-gauge needle inserted into the cap of the vial. Ovine IFNτ (5 μg) in 10 μl of 0.1 M borate buffer, pH 8.5, was added to the 500 μCi of monoiodoester in the solid-phase, agitated, and placed on ice for 15 minutes. Further reactions between ovine IFNτ and the monoiodoester were stopped by a 5-minute incubation at 0^{o}C with 500 μl of 0.2 M glycine in 0.1 M borate buffer. Ovine ^{125}I-

IFNτ was separated from unwanted radiolabeled products by a gel filtration column. A Sephadex G-10 packed column was equilibrated and eluted using 0.05 M phosphate buffer with 0.25% gelatin w/v. Specific activity of the ovine ^{125}I-IFNτ was determined by placing 5 μl of the radiolabeled proteins in a 1275 Minigamma gamma counter (LBK Wallac).

Direct Binding Assays

Synthetic IFNAR2 peptides (1.5 μg) were bound to 96-microwell plates using a pH 9.6, 0.1 M bicarbonate binding buffer [125]. Solvent was removed by evaporation using a gentle stream of warm air. Nonspecific binding was inhibited by the addition of 1% bovine serum albumin (BSA) in phosphate buffered saline (PBS), pH 7.5, to the solid-phase IFNAR2 peptides for 2 hours. The BSA solution was then removed and the IFNAR2 peptides were treated with biotinylated-intact ovine IFNτ or biotinylated-synthetic ovine IFNτ peptides at a final concentration of 0.5 μM. The peptides were then incubated with anti-biotin antibodies conjugated to alkaline phosphatase (1:5000 dilution) for 1 hour. At a volume of 50 μL/well, p-Nitrophenyl phosphate (PNP) (1 mg/mL) was added. Receptor peptide binding was determined colormetrically by measuring the alkaline phosphatase activity at a wavelength of 405 nM (Bio-Rad, Hercules, CA).

Competitive Binding Assays on Viable Cells

Viable MDBK cells were grown to near confluency on microwell plates. The cells were treated with a final concentration of 1 nM of ^{125}I-ovine IFNτ in the presence of increasing concentrations of synthetic ovine IFNτ or IFNAR2 peptide competitors [125, 126]. Radioiodine counts from bound ^{125}I-ovine IFNτ were measured after a 2-hour incubation at room temperature. Wells were removed from the microwell strip plates and placed in the 1275 Minigamma gamma counter (LBK Wallac).

Solid-phase Competition Assays

Synthetic IFNAR2 peptides (1.5 μg) were bound to 96-microwell plates using a pH 9.6, 0.1 M bicarbonate binding buffer [125]. Solvent was removed by evaporation using a gentle stream of warm air. Solid-phase peptides were treated with a final concentration of 5 nM of ^{125}I-ovine IFNτ in the presence of increasing concentrations of synthetic ovine IFNτ or IFNAR2 peptide competitors. Radioiodine counts from bound ^{125}I-ovine IFNτ were measured after a two-hour incubation at room temperature. Wells were removed from the microwell strip plates and placed in the 1275 Minigamma gamma counter (LBK Wallac).

Vesicular Stomatis Virus (VSV) Propagation

MDBK cells were grown to confluency in 75-cm^2 tissue culture-treated flasks in EMEM supplemented with antibiotics, 12 U/mL of penecillin and 125 μg/mL streptomycin, and 10% FBS, respectively, in a 37°C, 5% carbon dioxide, 100% humidified incubator. To increase the yield of VSV and increase specificity of the virus for each cell line, confluent monolayers were infected with approximately 3 x 10^5 plaque forming units of VSV in 3 mL of 37°C of EMEM. The VSV was supplied by Dr. Janet K. Yamamoto at the University of Florida. The flasks were incubated at 37°C for a total of 1 hour. Every 15 minutes the flasks were gently rocked for approximately 30 seconds to maximize viral absorption to cells. The maintenance medium, EMEM supplemented with 2% FBS, was warmed to 37°C and added to the virally infected flasks at a volume of 30 mL. The flasks were placed back in the 37°C, 5% CO_2, humidified incubator until greater than 50% cytopathic effect (CPE) occurred, requiring at least a 24-hour incubation time. The supernatants, which contained the virus, were then removed and centrifuged at approximately 1000 rpm for 5 minutes to remove residual cellular material. The supernatants of the centrifugation step were then placed on ice, 10% DMSO was added, and virus was stored at –70°C in 1 mL aliquots.

Antiviral Cytopathic Effect Inhibition Assay

MDBK cells in microwell plates at near confluency were incubated with 10 U/mL of ovine IFNτ in the presence of extracellular competitor receptor peptides for 18 hours [8, 39]. Ovine IFNτ reaches optimum antiviral activity by 18 hours. The MDBK cells monolayers were then infected with VSV. After 36 hours the remaining fixed cells were stained with crystal violet, washed, and air-dried. The dye was extracted from each well with 2-methoxyethanol [53]. The absorbance of dye was then measured at 570 nM to reveal the ability of the receptor peptides to inhibit the antiviral activity of ovine IFNτ.

Localization of IFNAR2 in MDBK Cells Using Immunofluorescence

MDBK cells (2.5×10^5/ slide) were grown overnight in chambered glass slides (Lab-Tek). Cells were stimulated with 5000 U/mL of ovine IFNτ and incubated at 4^oC for 2 hours. Cells were then transferred to a 37^oC incubator for the time intervals, 0, 8, 16, 32, 60, and 120 minutes. Cells were fixed immediately after the completion of each time interval with 2% paraformaldehyde at 4^oC for 30 minutes. Polyclonal rabbit antibody against IFNAR2 (Santa Cruz, Santa Cruz, CA) in 0.1% saponin (Sigma, St. Louis, MO) was placed on the cells for 1 hour at room temperature. Saponin, derived from quillaja bark, permeabilizes the cells. After three vigorous washings with the saponin:1% BSA: PBS solution, cells were treated with goat anti-rabbit

secondary antibodies conjugated to Texas Red (Molecular Probes, Eugene, OR), for 1 hour at room temperature, also in the presence of saponin as the permeabilization is temporary. The goat anti-rabbit secondary immunoglobulin G (IgG) antibodies were highly cross-absorbed against bovine, goat, human, mouse, and rat IgG serum. Cells were viewed using a Zeiss fluorescent microscope at a 40X magnification. Pictures of the cells were taken using a Spot digital camera (Diagnostic Instrumental, Inc.) and the Spot version 3.0 digital imaging software.

Localization of Ovine IFNτ with respect to the Lysosomes in MDBK Cells Using Immunofluorescence

MDBK cells (2.5 x 10^5/slide) were grown overnight in chambered glass slides (Lab-Tek). Cells were stimulated with 5000 U/mL of ovine IFNτ and incubated at 4^{o}C for 2 hours; the units per milliliter were standardized by the antiviral activity of the FDA approved human IFNα, Roferon. Cells were then transferred to a 37^{o}C incubator for various time intervals. After fixation with 2% paraformaldehyde at 4^{o}C for 30 minutes, cells were treated with a mouse monoclonal antibody against ovine IFNτ and a highly cross-absorbed rabbit polyclonal antibody against the lysosomal associated matrix protein 1 (LAMP-1) (Santa Cruz, Santa Cruz, CA) in 0.1% saponin to permeabilize the cells. After three vigorous washings with the saponin:BSA:PBS

solution, cells were treated with a highly cross-absorbed polyclonal goat anti-mouse secondary antibody coupled to Alexa Green (Molecular Probes, Eugene, OR) and highly cross-absorbed polyclonal goat anti-rabbit secondary antibody coupled to Texas Red (Molecular Probes, Eugene, OR), also in the presence of saponin as the permeabilization is temporary. The goat anti-rabbit secondary immunoglobulin G (IgG) antibodies were highly cross-absorbed against bovine, goat, human, mouse, and rat IgG serum; the goat anti-mouse secondary IgG antibodies were highly cross-absorbed against bovine, goat, human, rabbit, and rat IgG serum. The anti-mouse antibody: Alexa Green conjugate allows the detection of ovine IFNτ and the anti-rabbit: Texas Red conjugate allows the detection of LAMP-1. Cells were viewed using a Zeiss fluorescent microscope at 40X and 63X magnification. Pictures of the cells were taken using a Spot digital camera (Diagnostic Instrumental, Inc.) and the Spot version 3.0 digital imaging software.

Assays to Determine Lysosomal Degradation

MDBK cells grown to near confluency in 150 cm^2 flasks were treated with a final concentration of 100 μM chloroquine in 10 mL of 10% FBS MEM or 10 mL of 10% FBS MEM with no chloroquine and incubated for 4 hours at 37°C [77, 109, 119]. Cells were scraped from the flasks and resuspended in 35 mLs of MEM. The cells were then

treated with a final concentration of 0.5 nM of ovine ^{125}I-IFNτ. Cells were incubated on a rocker for 7 hours at 4°C to allow ovine ^{125}I-IFNτ to bind. Cells were aliquoted at a quantity of 2.7 x 10^6 cells/mL to represent the time intervals of 37°C incubation. The specific time intervals were 0, 15, 60, and 120 minutes. The sets of cells were then placed into a 37°C water bath for the specified times. Cells were then removed from the water bath at appropriate times and were pelleted using centrifugation. Following centrifugation the supernatant fluids from each 1 mL replicate were aspirated and treated with 200 μg of BSA followed by a 10% final volume of TCA to precipitate intact ligand, leaving degraded ligand in solution [109]. The TCA treated supernatants were incubated overnight at 4°C to ensure proper separation of degraded and intact ligand.

Iodogen Radioiodination of Ovine IFNτ and Human IFNαA for Equilibrium Binding and Kinetic Assays

Iodogen (75 μL) was placed in a glass vial under a gentle stream of air to evaporate the chloroform solvent from the solid-phase [127]. Foil was placed over the apparatus to protect iodogen from exposure to light, as it is light sensitive. Evaporation time was approximately 15 minutes. Ovine IFNτ or human IFNαA (10 μL of 1 mg/mL) in 65 μL of 0.05 phosphate buffer pH 7.5 was then placed on the solid-phase iodogen [129, 130]. Free ^{125}Iodine (0.5 μCi) was added to the vial and

incubated at room temperature for 5 minutes. Radiolabeling of the interferon molecules was slowed with the addition of excess 0.25% gelatin in 0.05 M phosphate buffer, pH 7.5, which dilutes the reaction mixture. The reaction was stopped when this solution was aspirated from the solid phase Iodogen. The solution was then placed on a column packed with Sephadex G-25. The Sephadex G-25 was previously equilibrated and eluted with 0.25% gelatin in 0.05 M phosphate buffer, pH 7.5. One milliliter fractions were removed and counted on the gamma counter to determine fractions containing radiolabeled ligand. Radiolabeled ligand fractions were then tested for their biological potency using an antiviral cytopathic assay.

Cellular Binding and Internalization Kinetic Assays

MDBK cells grown to near confluency were rinsed 2 times with 4^{o}C FBS-free EMEM in the cold room. FBS-free EMEM (5 mL) was then added to flasks, to allow the manual removal of cells. Cells were spun down and resuspended in 35 mLs of MEM with 0.1% BSA to reduce non-specific binding in the experiment. The viable cells population was determined with a hemocytometer and trypan blue treatment to detect dead cells. The cells were then split into two sets. Set one, the experimental set, was treated with a final concentration of 0.5 nM of either ^{125}I- ovine IFNτ or ^{125}I-human IFNαA [105]. In addition to the final concentration of 0.5 nM of either ^{125}I-ovine IFNτ or ^{125}I-human

IFNαA, set two was treated with a 100 nM final concentration of unlabeled ovine IFNτ or human IFNαA, respectively [77, 105]. Still in the cold room, the tubes were placed on a rocker to increase homogeneity and cellular contact and binding with ligand. Cells were incubated on the nutator for 7 hours. Duplicates of the experimental and control cell sets were then agitated and aliquoted at a quantity of 2.7×10^6 cells/mL into 5 sets of 3 mLs to represent the 5 time intervals of 37°C incubation. Triplicate one mL aliquots of the radiolabeled IFN treated cells were then placed into microcentrifuge tubes for each time point. The specific time intervals were 0, 16, 32, 60, and 120 minutes. The sets of cells were then placed into a 37°C water bath for the specified times. The cells were agitated while in the water bath to maintain homogeneity. Cells were then removed from the bath at appropriate times and transferred to the cold room where the surface bound ligand could be separated from the internalized ligand by centrifugation for 10 seconds [77]. Following centrifugation, the supernatant was aspirated and 200 μg of BSA was added per mL of supernatant followed by a 10% final volume of TCA, which precipitated intact ligand, leaving degraded ligand in solution [77, 111]. The TCA treated supernatants were incubated overnight at 4°C. The cell pellets were treated with a glycine buffer (100 mM NaCl/ 50 mM glycine) to remove surface-bound ligand [105]. The cells were solubilized in 0.1

M NaOH at room temperature for 10 minutes to release internalized ligand [75, 105]. The specific activities of the radiolabeled human IFNαA and ovine IFNτ ranged from 157 to 161 μCi/μg and 122 to 129 μCi/μg, respectively. Radioiodinations were performed using solid-phase iodogen as previously described.

Equilibrium Binding Assay

MDBK cells grown to near confluency were rinsed 2 times with 4°C FBS-free MEM in the cold room. Fetal bovine serum-free MEM was then added to flasks, so flasks could be scraped to collect cells. Cells were pelleted and resuspended in MEM with 0.1% BSA to reduce non-specific binding in the experiment. The viable cells population was determined with a hemocytometer and trypan blue treatment to detect dead cells. The cells were aliquoted at a quantity of 2.5×10^6 cells/mL into 5 duplicate sets of 3 mLs, one experimental set and one control set. At 4°C, the duplicate sets of cells were treated with increasing concentrations of ^{125}I-ovine IFNτ or ^{125}I-human IFNαA [75, 77]. The control sets were treated with the same concentrations of radiolabeled ligand and 100 nM of unlabeled ovine IFNτ or human IFNαA to reveal non-specific binding. Still in the cold room, the tubes were placed on a nutator to increase homogeneity and cellular contact and binding with ligand. Cells were incubated on a rocker for 9 hours to ensure equilibrium was reached. The cells were then transferred to microfuge

tubes and surface bound ligand was separated from the free ligand by centrifugation for 10 seconds. The supernatant was removed to determine $[L]_f$. The tips of the microfuge tubes were cut off at the 0.1 mL mark to measure $[LR]_s$ [77]. Non-specific binding was subtracted from total binding to reveal specific binding. The specific activities of the radiolabeled human IFNαA and ovine IFNτ ranged from 157 to 161 μCi/μg and 122 to 129 μCi/μg, respectively. Radioiodinations were performed using solid-phase iodogen as previously described [127]. Linear regressions of the Scatchard plots used to determine the equilibrium constants and total concentrations of surface receptor were derived using the Sigmaplot version 2000 scientific graphing software. GraphPad Prism software version 3.0, a program specifically designed for ligand:receptor binding analysis, calculated the binding constants and receptor concentrations using nonlinear regression analysis.

Steady State Binding Assays

MDBK cells grown to near confluency were rinsed 2 times with 4°C FBS-free MEM. Flasks were scraped to collect cells. Cells were pelleted and resuspended in MEM with 0.1% BSA to reduce non-specific binding in the experiment. The viable cell population was determined with a hemocytometer. Trypan blue was added to the suspension for the detection of dead cells. The cells were aliquoted at a quantity of 2.0×10^6 cells/mL into 5 duplicate sets of 3 mL volumes,

one experimental set and one control set. The duplicate sets of cells were treated with increasing concentrations of ^{125}I-ovine IFNτ or ^{125}I-human IFNαA [77, 105, 110]. The control sets were treated with the same concentrations of radioligand and 100 nM of unlabeled ovine IFNτ or human IFNαA to reveal non-specific binding. The cells were incubated for 8 hours at 37^{o}C to achieve steady state conditions [75, 110]. The cells were then transferred to microfuge tubes in one mL aliquots and surface bound ligand was separated from the free ligand by centrifugation. The supernatant was removed to determine $[L]_f$. Using a hot scalpel, the tips of the microfuge tubes were cut off at the 0.1 mL mark to measure $[LR]_T$ [77]. Non-specific binding was subtracted from total binding to reveal specific binding. The specific activities of the radiolabeled human IFNαA and ovine IFNτ ranged from 157 to 161 μCi/μg and 122 to 129 μCi/μg, respectively. Radioiodinations were performed using solid-phase iodogen as previously described [127]. Sigmaplot version 2000 scientific graphing software derived the steady state constants and total receptor concentrations by calculating the slope and x-intercept of the Scatchard graphs modified for steady state assays. GraphPad Prism software version 3.0 eliminated the need of the linear transformation of nonlinear raw data by calculating the binding constants and receptor concentrations using nonlinear regression analysis.

Unoccupied Receptor Turnover Binding Assays

MDBK cells grown to near confluency were rinsed two times with 4°C FBS-free MEM. FBS-free MEM was then added to flasks, so flasks could be scraped to collect cells. Cells were pelleted and resuspended in MEM with 0.1% BSA to reduce non-specific binding in the experiment. The viable cells population was determined with a hemocytometer and trypan blue treatment to detect dead cells. Human ^{125}I-IFNαA (6 x 10^5 CPM) or ovine ^{125}I-IFNτ (6 x 10^5 CPM) was added to each 3 mL aliquot of 1.0 x 10^6 cells/mL in one experimental group and one control group [77, 110]. Concentrations of unlabeled human IFNαA or ovine IFNτ that were equivalent to the amounts of radiolabeled IFN were added to 3 mL aliquots of 1.0 x 10^6 cells/mL in 5 experimental group and 5 control sets of cells. Each set of cells represented a concentration point for the equilibrium-binding assay that was performed after these cells reached steady state. The cells were incubated for 8 hours at 37°C for steady state to be achieved. Cells with ^{125}I-human IFNαA of ^{125}I-ovine IFNτ were then immediately pelleted by centrifugation to separate free ligand from receptor bound ligand. The tips of the microfuge tubes were cut off with a hot scalpel to reveal $[LR]_x$ [77, 110]. The constant subsaturating concentration of ligand added is represented by the subscript, x. The concentration of free ligand was determined by counting the supernatant in the gamma

counter. The remaining cells, which were previously treated with unlabeled ligand, were transferred to the cold room. The duplicate sets of cells were treated with increasing concentrations of ^{125}I-ovine IFNτ or ^{125}I-human IFNαA. The control sets were treated with the same concentration of radiolabeled ligand and 100nM of unlabeled ovine IFNτ or human IFNαA to reveal non-specific binding [77]. The cells were incubated at 4^{o}C on a rocker for 9 hours to ensure that equilibrium was reached. The cells were then transferred to microfuge tubes in one mL aliquots and surface bound ligand was separated from free ligand by centrifugation. The supernatant fluid was removed to determine $[L]_f$. Using a hot scalpel, the tips of the microfuge tubes were cut off at the 0.1 mL mark to measure $[LR]_T$ [77]. Non-specific binding was subtracted from total binding to reveal specific binding. The specific activities of the radiolabeled human IFNαA and ovine IFNτ ranged from 157 to 161 μCi/μg and 122 to 129 μCi/μg, respectively. Radioiodinations were performed using solid-phase iodogen as previously described [127]. The total receptor concentrations were determined as the x-intercept of the Scatchard plots as revealed by Sigmaplot version 2000 scientific graphing software. GraphPad Prism software version 3.0, a program specifically designed for ligand:receptor binding analysis, calculated the total receptor concentrations using nonlinear regression analysis.

CHAPTER 3
DETERMINATION OF STRUCTURAL AND FUNCTIONAL REGIONS OF OVINE IFNτ AND THE TYPE I IFN RECEPTOR

Direct Binding of Biotinylated Ovine IFNτ to IFNAR2 Extracellular Domain Peptides

To determine the major ligand binding sites on IFNAR2 for ovine IFNτ, long overlapping peptides of the extracellular domain of IFNAR2 were synthesized [134]. The sequences of the synthesized IFNAR2 peptides are shown in Table 3-1. As an initial approach, direct binding studies entailed treating immobilized extracellular domain IFNAR2 peptides with biotin-labeled ovine IFNτ. The biotinylated, biologically active ovine IFNτ bound directly and most significantly to peptides IFNAR2(1-38) and IFNAR2(34-67) of the 7 synthetic peptides of the extracellular domain (Figure 3-1). Direct binding of biotinylated ovine IFNτ to overlapping synthetic peptides of the extracellular domain of IFNAR2. Biotinylated ovine IFNτ was used at a final concentration of 0.5 μM. Receptor peptide binding was determined colormetrically by alkaline phosphatase activity. Bars represent the standard significantly to peptides IFNAR2(1-38) and IFNAR2(34-67) of the 7 synthetic peptides of the extracellular domain (Figure 3-1).

Table 3-1. Sequences and secondary structure predictions of the synthetic extracellular domain peptides of IFNAR2. Secondary structure predictions were formulated by comparing Chou-Fasman (CF) secondary prediction results to those obtained using the Garnier-Osguthorpe-Robson (GOR) secondary structure prediction method. Chou-Fasman and GOR predictions were calculated using the PeptideStructure computer program (Genetics Computer Group, Inc.) [129-131]. Lower case letters denote regions where the structure prediction models did not coincide or predictions were weak.

Peptide Name	Peptide Sequence	Secondary Structure
IFNAR2(1-38)	ISYDSPDYTDES CTFKISLRNFRSI LSWELKNHSIVP T	TURN/BETA/ helix/BETA
IFNAR2(34-67)	SIVPTHYTLLYTI MSKPEDLKVVK NCANTTRSFC	BETA/turn/ BETA/turn
IFNAR2(63-99)	TRSFCDLTDEW RSTHEAYVTVLE GFSGNTTLFSCS	turn/helix/ turn/BETA/ TURN/BETA
IFNAR2(95-133)	LFSCSHNFWLAI DMSFEPPEFEIV GFTNHINVMVK FPSI	BETA/TURN/ HELIX/TURN/ BETA
IFNAR2(129-164)	FPSIVEEELQFD LSLVIEEQSEGI VKKHKPEIKGN	BETA/HELIX/ turn
IFNAR2(160-196)	EIKGNMSGNFT YIIDKLIPNTNYC VSVYLEHSDEQ A	turn/BETA/ TURN/BETA/ TURN
IFNAR2(186-217)	LEHSDEQAVIKS PLKCTLLPPGQE SESAESAK	TURN/HELIX/ BETA/TURN/ HELIX

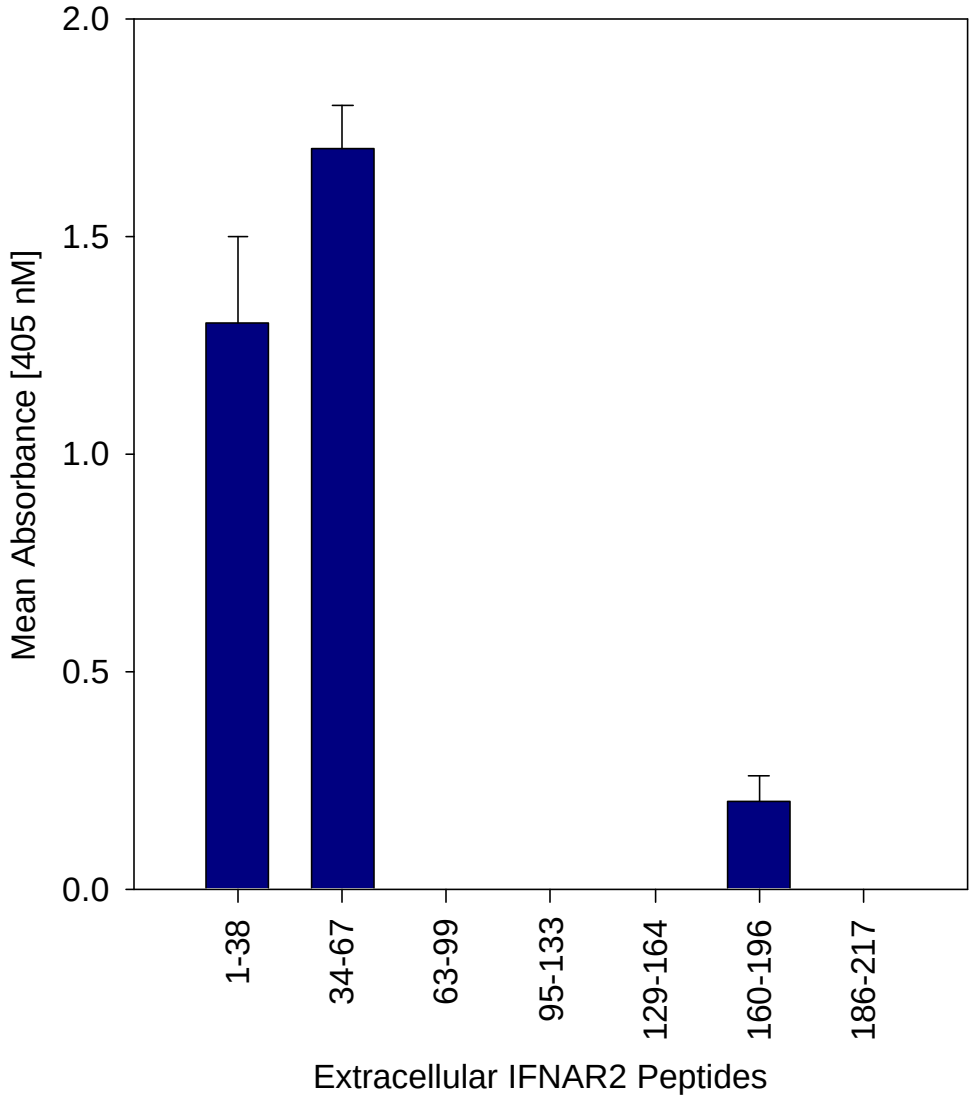

Figure 3-1. Direct binding of biotinylated ovine IFNτ to overlapping synthetic peptides of the extracellular domain of IFNAR2. Biotinylated ovine IFNτ was used at a final concentration of 0.5 μM. Receptor peptide binding was determined colormetrically by alkaline phosphatase activity. Bars represent the standard error. All assays were performed in triplicate.

The remaining five receptor peptides were not recognized by the biotinylated ovine IFNτ (Figure 3-1). These results suggest that the first 67 amino acids of the N-terminus of IFNAR2 may play an important role in the recognition of ovine IFNτ.

Extracellular Domain Receptor Peptides Block Ovine ^{125}I-IFNτ Binding to Viable MDBK Cells

Specificity of bindings was established using the IFNAR2 peptides as competitors against type I IFN receptors on MDBK cells for biologically active ovine ^{125}I-IFNτ. On viable and intact MDBK cells, *N*-terminal peptides IFNAR2(1-38) and IFNAR2(34-67) were dose-dependent inhibitors of type I IFN receptor binding of ovine ^{125}I-IFNτ at a final concentration of 5 nM (Figure 3-2). Peptide IFNAR2(34-67) consistently appeared to be a more effective inhibitor at higher concentrations, which suggests that a region within 34-67 may be more structurally important for ovine IFNτ binding (Figure 3-2). The failure of IFNAR2(186-217) to block binding is representative of those receptor peptides that did not recognize ovine IFNτ (Figure 3-2). In addition, the combination of IFNAR2(1-38) and IFNAR2(34-67), in which each peptide made up 50% of the total concentration of each dose, inhibited ovine ^{125}I-IFNτ binding by a factor greater than the additive effect of the individual peptides (Figure 3-2). Therefore, the binding of ovine IFNτ with the distinct ligand binding regions within

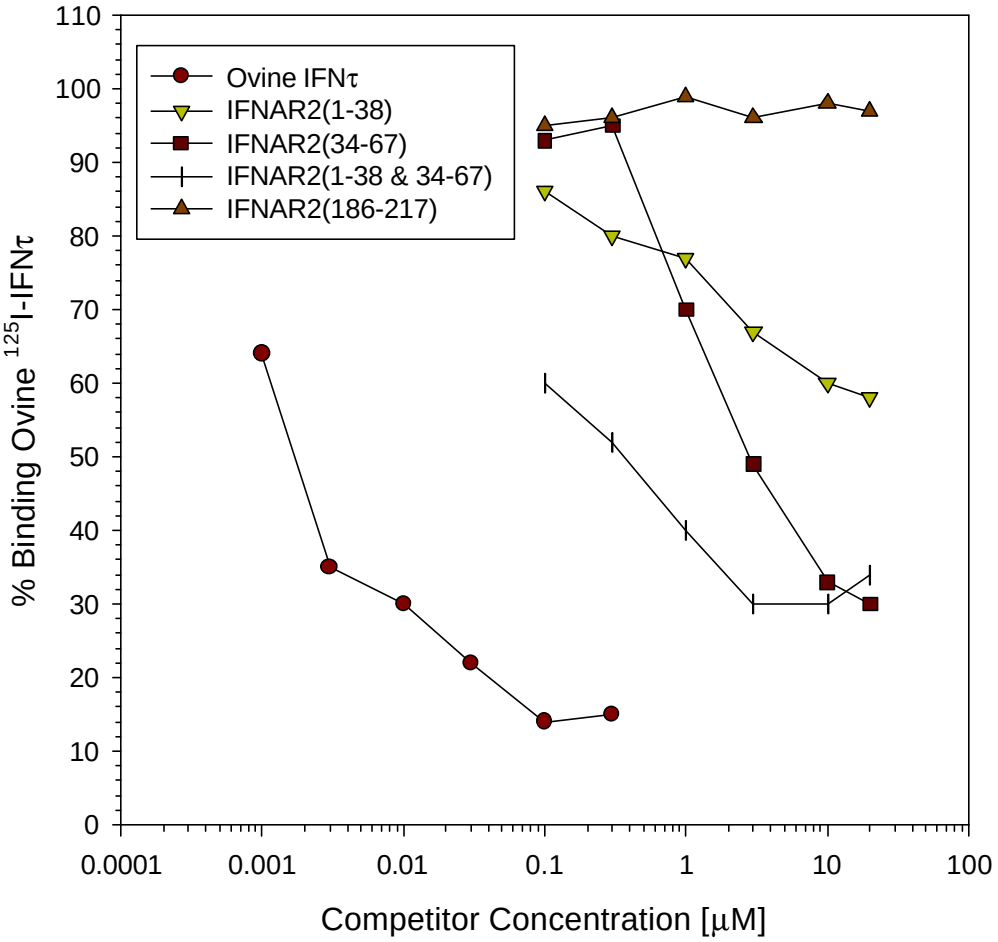

Figure 3-2. Dose-response of unlabeled ovine IFNτ and extracellular IFNAR2 peptide competitors on ovine IFNτ binding to the type I IFN receptor on viable MDBK cells. Ovine ^{125}I-IFNτ was used at a final concentration of 5 nM. Radioiodine counts from bound ovine ^{125}I-IFNτ were measured after a 2-hour incubation at room temperature. All assays were performed in triplicate with coefficients of variation not greater than 10%. IFNAR2(186-217) represents receptor peptides that did not bind to ovine IFNτ.

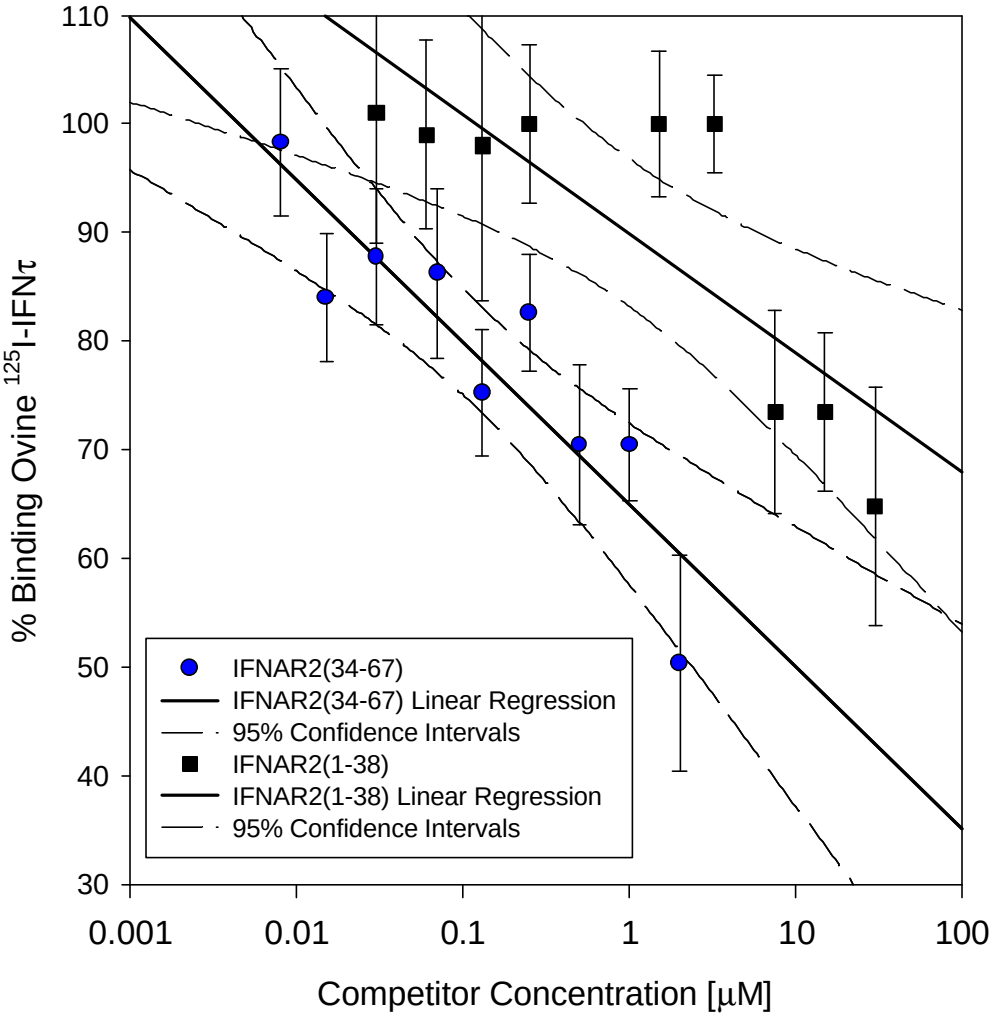

Figure 3-3. Dose-response of extracellular IFNAR2 peptide competitors, IFNAR2(1-38) and IFNAR2(34-67) on ovine ^{125}I-IFNτ binding to the type I IFN receptor on MDBK cells. Ovine ^{125}I-IFNτ was used at a final concentration of 1 nM. Radioiodine counts from bound ovine ^{125}I-IFNτ were measured after a 2-hour incubation at room temperature. Bars represent the standard error. All assays were performed using at least four replicates to increase accuracy.

residues 1-67 in combination appears to establish the property of avidity, thereby strengthening the interaction.

Differential Binding Affinities of IFNAR2(1-38) AND IFNAR2(34-67) for Ovine ^{125}I-IFNτ

The more effective inhibition of ovine ^{125}I-IFNτ binding to MDBK cells by IFNAR2(34-67) than IFNAR2(1-38) at concentrations above 1 μM indicates that the affinity of ovine IFNτ for these independent binding regions may differ. Therefore, to further elucidate the differential affinities of ovine ^{125}I-IFNτ for IFNAR2(1-38) and IFNAR2(34-67), IFNAR2(1-38) and IFNAR2(34-67) served as competitors against receptor on MDBK cells for a reduced, subsaturating concentration of ovine ^{125}I-IFNτ (Figure 3-3). When concentrations of radioligand approach saturation, low affinity binding sometimes cannot be distinguished from that of high affinity because of the shear quantity of radioligand that binds to low affinity sites. Therefore, the final concentration of ovine ^{125}I-IFNτ to 1 nM was based on previous K_d determinations for ovine IFNτ binding to MDBK cells [53]. The concentration of IFNAR2(1-38) required to block just 25% of receptor binding was approximately 100-fold more than the necessary concentration of IFNAR2(34-67) (Figure 3-3). This further suggests that the sequence of the extracellular domain that corresponds to peptide IFNAR2(1-38) may contain a low affinity

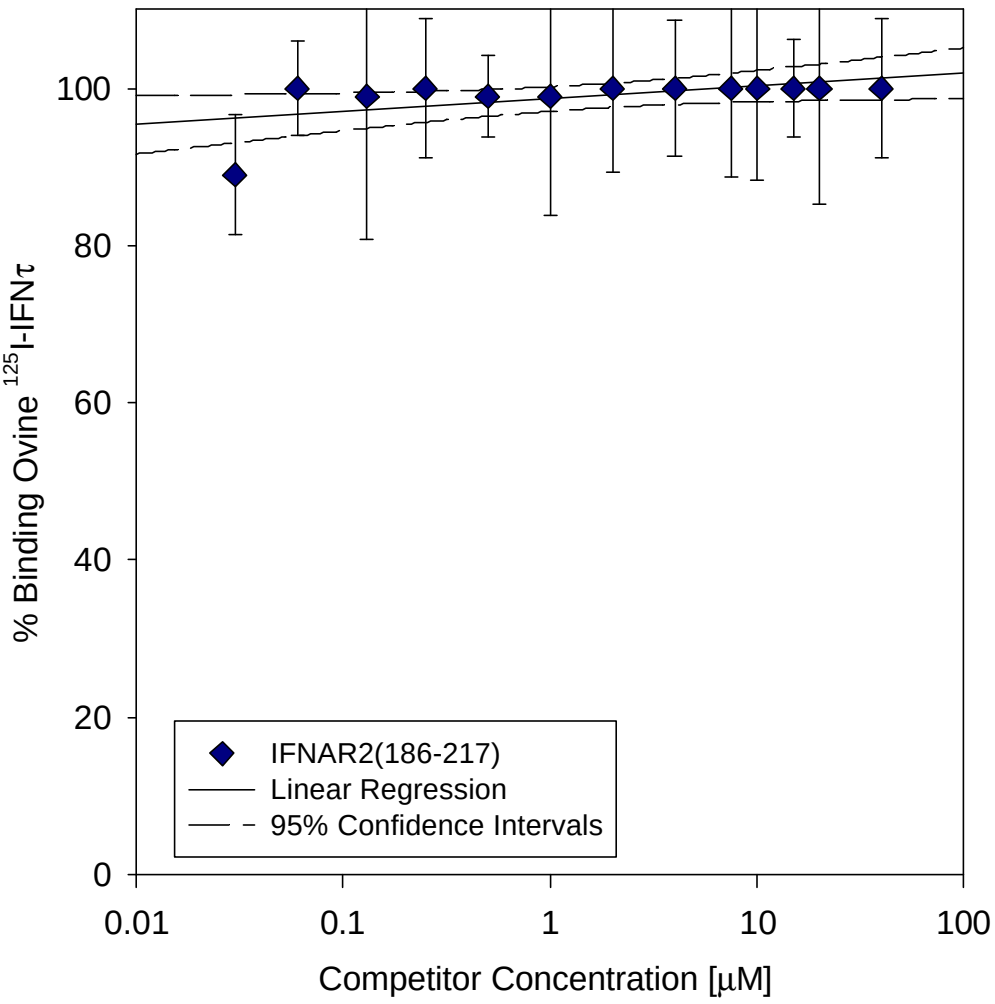

Figure 3-4. Extracellular IFNAR2 peptide, IFNAR2(186-217), does not effect ovine ^{125}I-IFNτ binding to the type I IFN receptor on MDBK cells. Ovine ^{125}I-IFNτ was used at a final concentration of 1 nM. Radioiodine counts from bound ovine ^{125}I-IFNτ were measured after a 2-hour incubation at room temperature. Bars represent the standard error. All assays were performed using at least four replicates to increase accuracy.

binding site, whereas amino acids 34-67 may contain a site more significant for ovine IFNτ recognition. As observed in previous experiments using a final concentration of 5 nM ovine ^{125}I-IFNτ, extracellular IFNAR2(186-217) showed no dose-dependent inhibition of receptor binding, indicating that this region is not crucial for direct interactions between ovine IFNτ and the type I IFN receptor (Figure 3-4).

Structurally Important Extracellular IFNAR2 Peptides Block Antiviral Activity of Ovine IFNτ

The physiological importance of the structurally required peptides of the extracellular domain of IFNAR2 was examined using an antiviral cytopathic effect inhibition assay. Consistent with the competition binding assays, the structurally important IFNAR2 peptides also blocked antiviral activity of ovine IFNτ (Figure 3-5). Again, IFNAR2(34-67) was the more potent inhibitor of antiviral activity when compared to IFNAR2(1-38) (Figure 3-5). In addition, IFNAR2(1-38) and IFNAR2(34-67) in combination enhanced the inhibition of function when compared to the individual performance of either peptide (Figure 3-5). Peptide IFNAR2(186-217), previously shown not to block binding of ovine ^{125}I-IFNτ, failed to block function (Figure 3-5). Collectively, the dose-dependent inhibition of function as well as inhibition of receptor binding by extracellular IFNAR2 peptides

IFNAR2(1-38) and IFNAR2(34-67) indicate that amino acids 1-67 of the type I IFN receptor β subunit comprise a region or regions that are structurally and functionally important.

Human IFNαD Antagonizes Biotinylated Ovine IFNτ Binding to IFNAR2(34-67)

Solid phase competition assays revealed that human IFNαD, like ovine IFNτ, specifically recognizes peptide IFNAR2(34-67) (Figure 3-6). Unlabeled human IFNαD appeared to bind slightly more effectively than unlabeled ovine IFNτ to IFNAR2(34-67). These data further demonstrate that ovine IFNτ specifically binds IFNAR2(34-67) and may require a region within amino acids 34-67 of IFNAR2 to bind to the type I IFN receptor. However, it also suggests that the residues corresponding to IFNAR2(34-67) do not recognize ovine IFNτ exclusively, but may interact with more than one type I IFN.

Direct Binding of Biotinylated Ovine IFNτ to IFNAR2 Intracellular Domain Peptides

To determine if possible ligand binding sites for ovine IFNτ on the intracellular IFNAR2 existed, long overlapping peptides of the intracellular domain of IFNAR2 were synthesized. The sequences of the synthesized intracellular domain IFNAR2 peptides are presented in Table 3-2. A potential intracellular ligand binding site on the receptor was revealed when biotinylated and biologically active ovine IFNτ

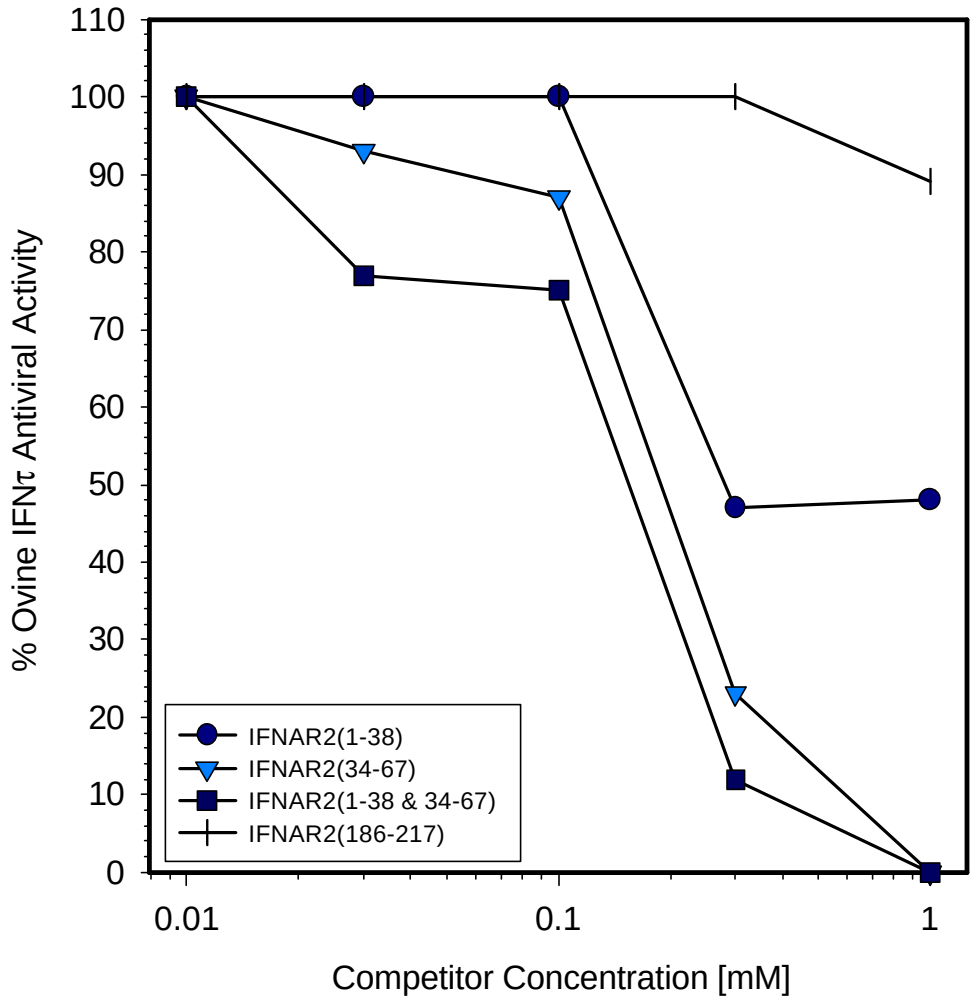

Figure 3-5. Extracellular IFNAR2 peptides inhibition of ovine IFNτ antiviral activity. After an 18-hour incubation of 10 U/mL ovine IFNτ in the presence of extracellular competitor receptor peptides, MDBK cell monolayers were infected with VSV. After 36 hours, cells were stained with crystal violet, washed, and air-dried. The remaining dye was extracted with 2-methoxyethanol [53]. The absorbance was measured at 570 nM. All assays were performed in triplicate.

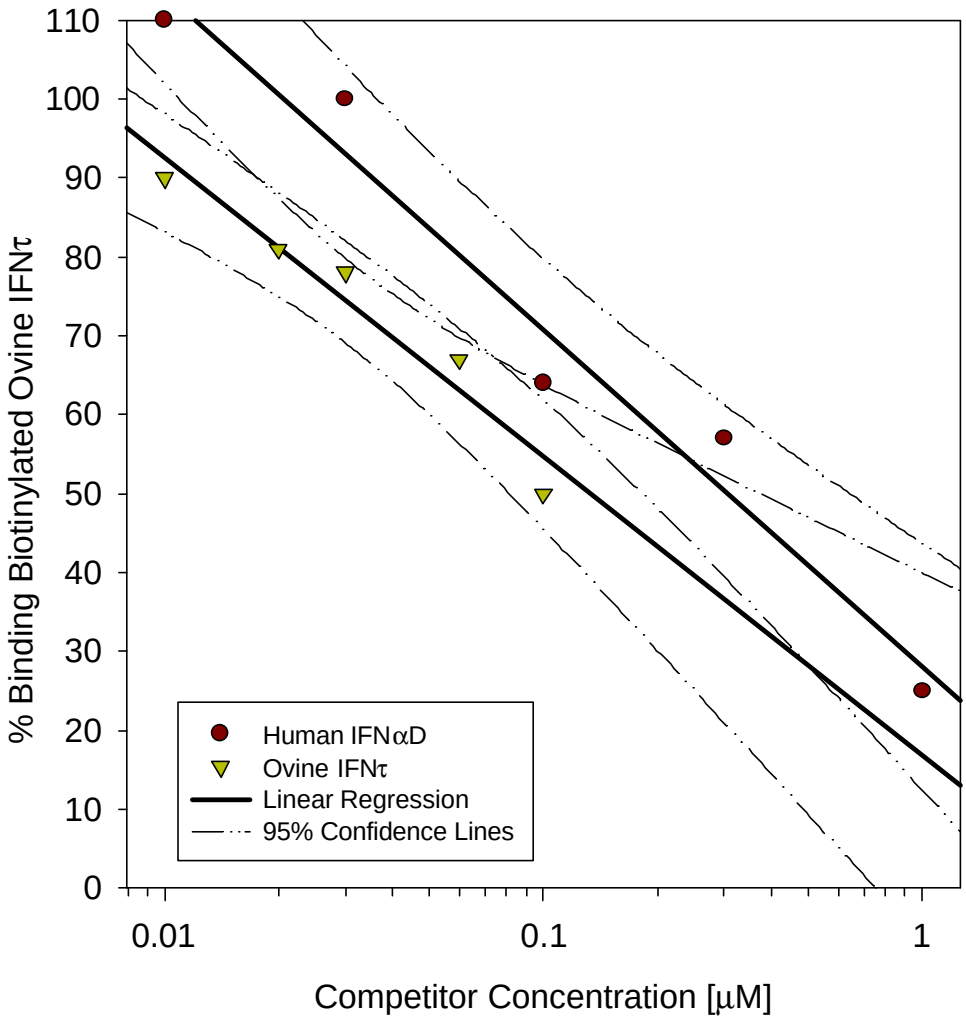

Figure 3-6. Dose-dependent inhibition of biotinylated ovine IFNτ binding to IFNAR2(34-67) by unlabeled ovine IFNτ and human IFNαD. Biotinylated ovine IFNτ was used at a final concentration of 0.5 μM. All assays were performed in triplicate with coefficients of variation not greater than 10%.

Table 3-2. Sequences and secondary structure predictions of the synthetic intracellular domain peptides of IFNAR2. Secondary structure predictions were formulated by comparing Chou-Fasman (CF) secondary prediction results to those obtained using the Garnier-Osguthorpe-Robson (GOR) secondary structure prediction method [129-131]. Chou-Fasman and GOR predictions were calculated using the PeptideStructure computer program (Genetics Computer Group, Inc.). Lower case letters denote regions where the structure prediction models did not coincide or predictions were weak.

Peptide Name	Peptide Sequence	Secondary Structure
IFNAR2(265-300)	KWIGYICLRNSLPKVLNFA WPFPNLPPLEAMDM	BETA/turn/BETA/turn/ HELIX
IFNAR2(287-315)	AWPFPNLPPLEAMDMVVE VIYINRKKKVWD	turn/HELIX/beta
IFNAR2(313-338)	VWDYNYDDESDSDTEAA PRTSGGGYT	beta/TURN/BETA
IFNAR2(335-368)	GGYTMHGLTVRPLGQASA TSTESQLIDPESEEEP	BETA/HELIX
IFNAR2(366-395)	EEPDLPEVDVELPTMPKDS PQQLELLSGPC	HELIX/TURN/HELIX/TUR N
IFNAR2(393-423)	GPCERRKSPLQDPFPEED YSSTEGSGGRITF	TURN/BETA
IFNAR2(421-445)	ITFNVDLNSVFLRVLDDED SDDLEA	BETA/TURN/HELIX
IFNAR2(442-470)	DLEAPLMLSSHLEEMVDP EDPDNVQSNHL	HELIX/TURN/helix
IFNAR2(467-498)	SNHLLASGEGTQPTFPSP SSEGLWSEDAPSDQ	helix/beta/TURN/HELIX/ TURN
IFNAR2(495-515)	PSDQSDTSESDVDLGDG YIMR	TURN/helix/TURN/beta

bound to the intracellular IFNAR2 peptide, IFNAR2(287-315) (Figure 3-7). IFNAR2(265-300), an overlapping receptor peptide that lacks the *C*-terminal 15 amino acids of IFNAR2(287-315), was not recognized by biotinylated ovine IFNτ, suggesting that these 15 residues may be particularly important for ovine IFNτ binding (Figure 3-7). Peptides corresponding to residues 313-515 of IFNAR2 were not significantly recognized by biotinylated ovine IFNτ (Figure 3-7). Therefore, similar to results found for IFNγ, ovine IFNτ appears to recognize a region localized on the intracellular domain of the binding subunit of the receptor [126].

An Intracellular Peptide Inhibits Ovine ^{125}I-IFNτ Binding to IFNAR2 on Viable and Intact MDBK Cells

As the concentration of IFNAR2(287-315) was increased, binding of ovine ^{125}I-IFNτ to MDBK cells decreased, revealing that this synthetic peptide specifically recognized ovine ^{125}I-IFNτ (Figure 3-8). When the final concentration of ovine ^{125}I-IFNτ was reduced to 1 nM in the competition binding studies, IFNAR2(287-315) still effectively competed with receptors on MDBK cells for ovine ^{125}I-IFNτ in a dose-dependent manner (Figure 3-9). This further implicates the sequence of the intracellular domain that corresponds to peptide IFNAR2(287-315) as a potential binding site for ovine IFNτ.

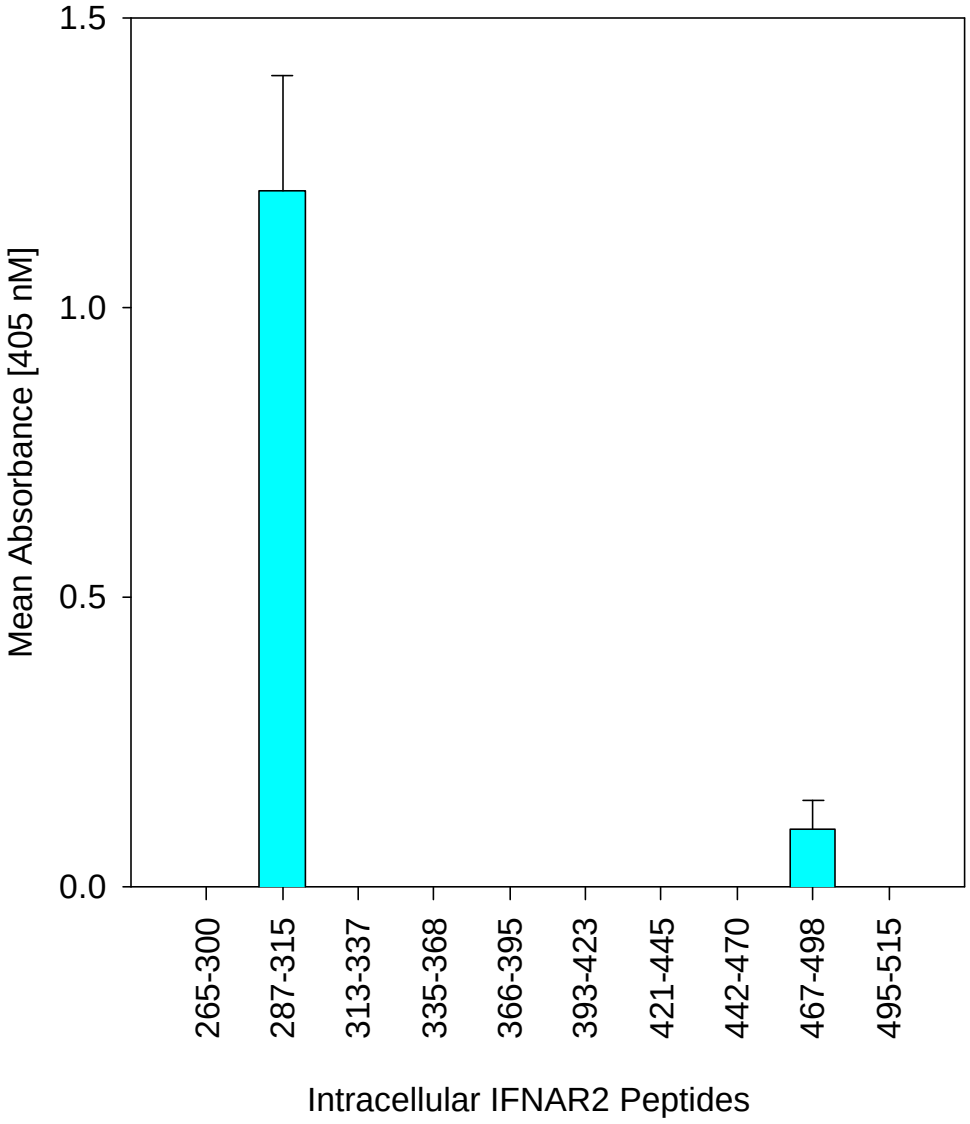

Figure 3-7. Direct binding of biotinylated ovine IFNτ to overlapping synthetic peptides of the intracellular domain of IFNAR2. Biotinylated ovine IFNτ was used at a final concentration of 0.5 μM. Receptor peptide binding was determined colormetrically by alkaline phosphatase activity. Bars represent the standard error. All assays were performed in triplicate.

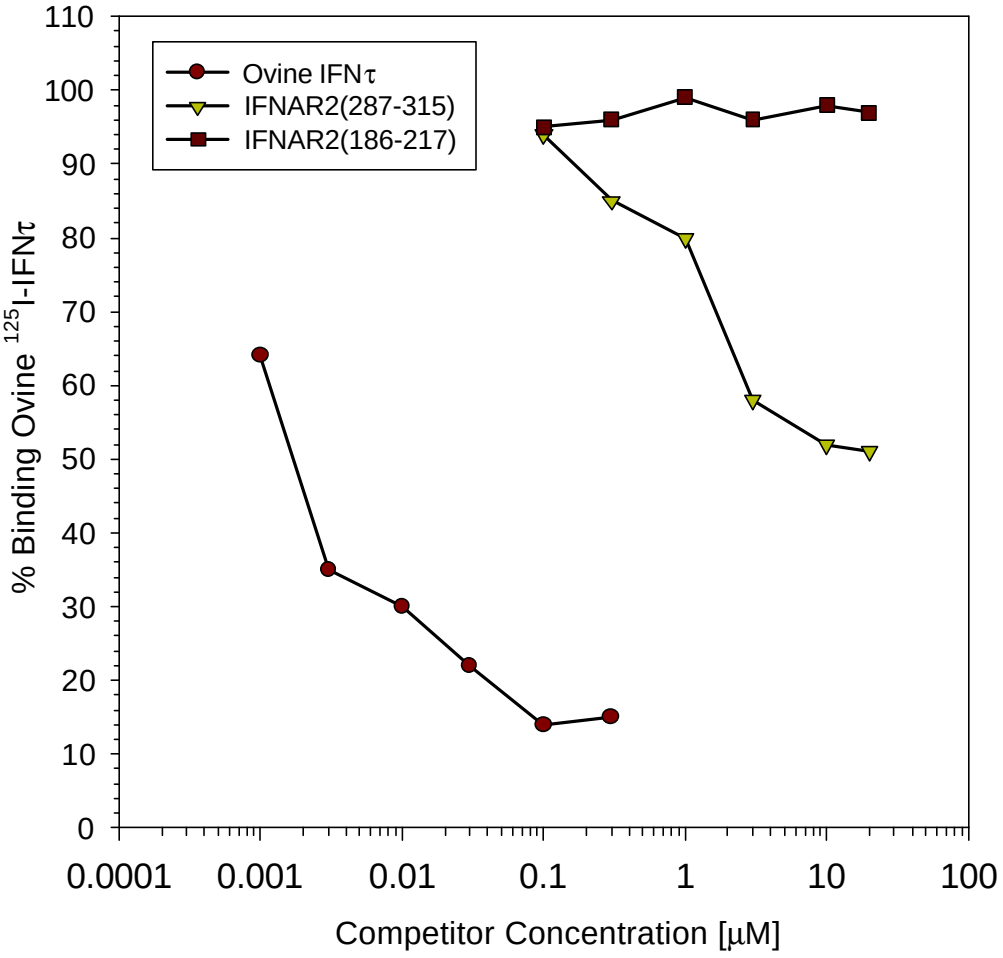

Figure 3-8. Dose-response of unlabeled ovine IFNτ and extracellular IFNAR2 peptide competitors on ovine IFNτ binding to the type I IFN receptor on MDBK cells. Ovine ^{125}I-IFNτ was used at a final concentration of 5 nM. Radioiodine counts from bound ovine ^{125}I-IFNτ were measured after a 2-hour incubation at room temperature. All assays were performed in triplicate with coefficients of variation not greater than 10%. IFNAR2(186-217) represents receptor peptides that did not bind to ovine IFNτ.

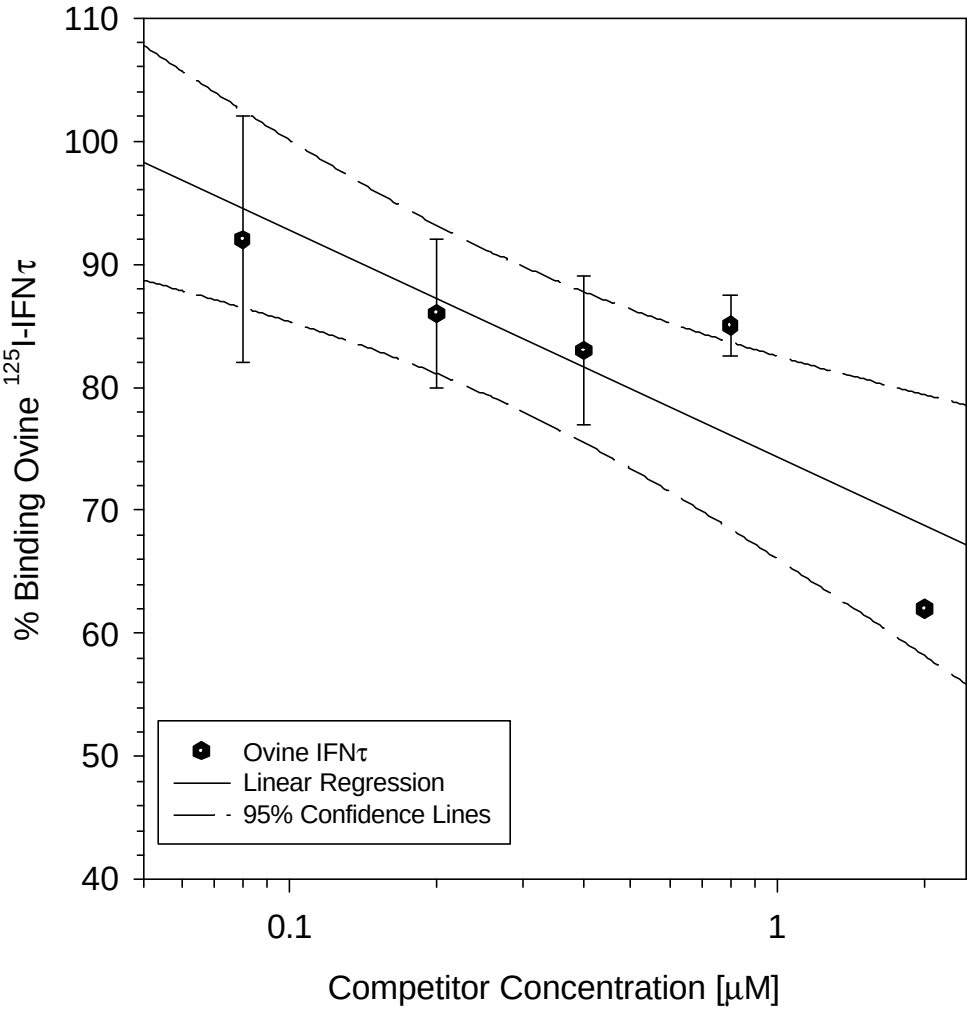

Figure 3-9. Dose-response of intracellular IFNAR2 peptide competitor, IFNAR2(287-315) on ovine ^{125}I-IFNτ binding to the type I IFN receptor on MDBK cells. Ovine ^{125}I-IFNτ was used at a final concentration of 1 nM. Radioiodine counts from bound ovine ^{125}I-IFNτ were measured after a 2-hour incubation at room temperature. All assays were performed using at least four replicates to increase accuracy.

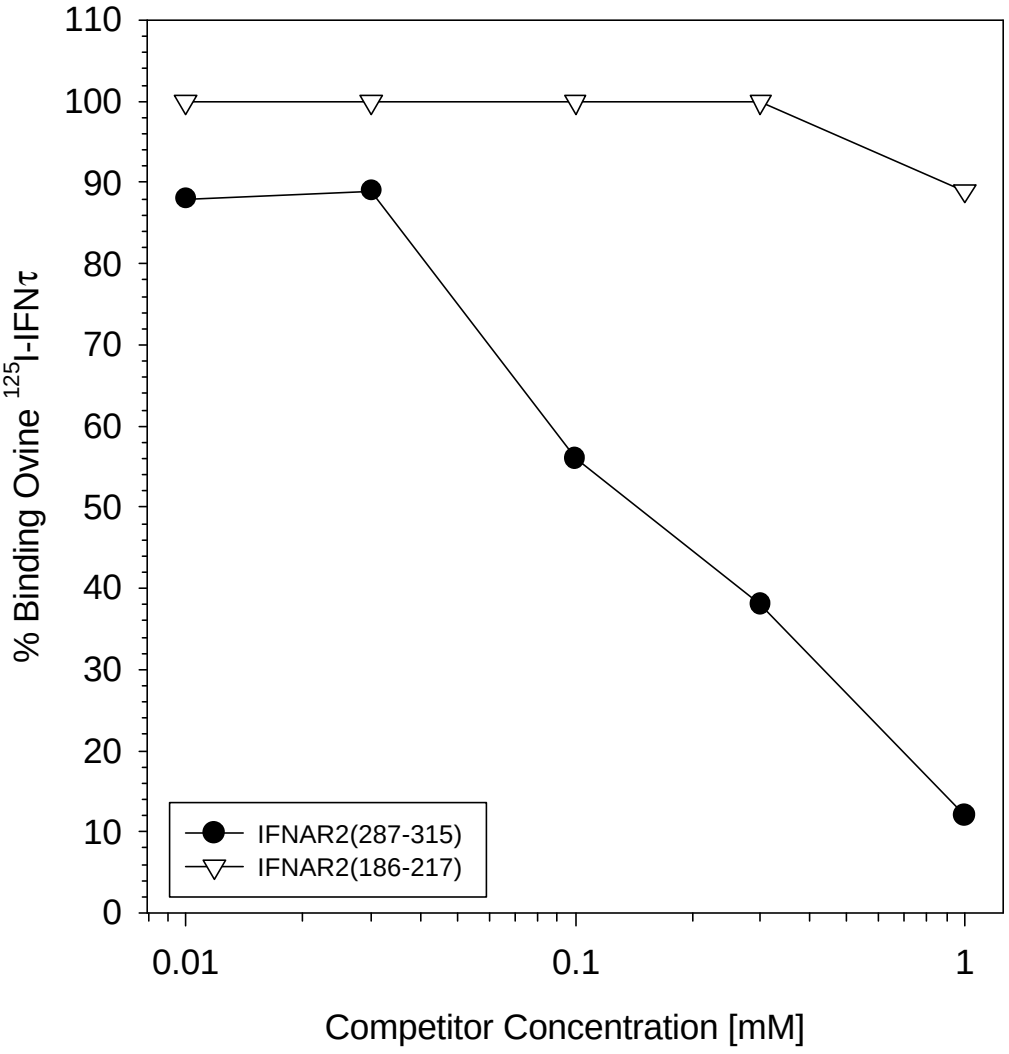

Figure 3-10. Intracellular IFNAR2 peptide inhibition of ovine IFNτ antiviral activity. After an 18 hour incubation of 10 U/mL ovine IFNτ in the presence of varying concentrations of IFNAR2(287-315), MDBK cell monolayers were infected with VSV. After 36 hours, cells were stained with crystal violet, washed, and air-dried. The remaining dye was extracted with 2-methoxyethanol [53]. The absorbance was measured at 570 nM. All assays were performed in triplicate.

An Intracellular Peptide Inhibits Ovine IFNτ Antiviral Activity

Like the structurally important extracellular receptor peptides IFNAR2(34-67) and IFNAR2(1-38), the intracellular receptor peptide IFNAR2(287-315) significantly inhibited ovine IFNτ function in a cytopathic antiviral assay (Figure 3-10). The potency of IFNAR2(287-315) was most comparable to that of IFNAR2(34-67) and more effective as an inhibitor than IFNAR2(1-38). This study suggests that IFNAR2(287-315) represents a functionally important region on IFNAR2.

Direct Binding of Biotin-conjugated Ovine IFNτ Peptides to Extracellular IFNAR2 Peptides

Three ovine IFNτ peptides, IFNτ(1-38), IFNτ(118-138), and IFNτ(153-168), were labeled with biotin and used to reveal potential sites of interaction between regions on ovine IFNτ and IFNAR2. Immobilized extracellular and intracellular domain IFNAR2 peptides were treated with these biotinylated ovine IFNτ peptides. In general, on the extracellular domain IFNAR2 peptides, the biotin-labeled ovine IFNτ peptides bound to IFNAR2(1-38) and IFNAR2(34-67) (Figure 3-11). However, the recognition of the receptor peptides was not as strong as that of ovine IFNτ. IFNτ(1-38) bound approximately as strongly as ovine IFNτ to IFNAR2(1-38) and one third as strongly as ovine IFNτ to IFNAR2(34-67) (Figure 3-11). Ovine IFNτ peptide,

IFNτ(118-138), bound significantly to IFNAR2(1-38) (Figure 3-11). IFNAR2(34-67) was highly recognized by IFNτ(118-138) (Figure 3-11). The *C*-terminal ovine IFNτ peptide, IFNτ(153-168) did not significantly bind IFNAR2(1-38); however, it did have some recognition of IFNAR2(34-67) (Figure 3-11). The lack of recognition of IFNτ(153-168) concurs with the findings that the *C*-terminus of ovine IFNτ is not largely responsible, if at all, for extracellular receptor recognition of the ovine IFNτ molecule. It appears that the internal amino acids of the ovine IFNτ sequence, and possibly the N-terminus of ovine IFNτ, may play the pivotal role in ovine IFNτ receptor recognition. These results also further suggest that the first 67 amino acids of the N-terminus of IFNAR2 recognize regions on ovine IFNτ.

Direct Binding of Biotin-conjugated Ovine IFNτ Peptides to Intracellular IFNAR2 Peptides

Interestingly, IFNτ(153-168) was attracted to the intracellular receptor peptide IFNAR2(287-315) (Figure 3-12). IFNτ(118-138) significantly recognized IFNAR2(287-315) and IFNτ(1-38) also bound IFNAR2(287-315), although less effectively. These results suggest that sites within the internal and C-terminal regions of ovine IFNτ may be recognizing an intracellular, transmembrane proximal region of IFNAR2. These results are similar to those in studies that have

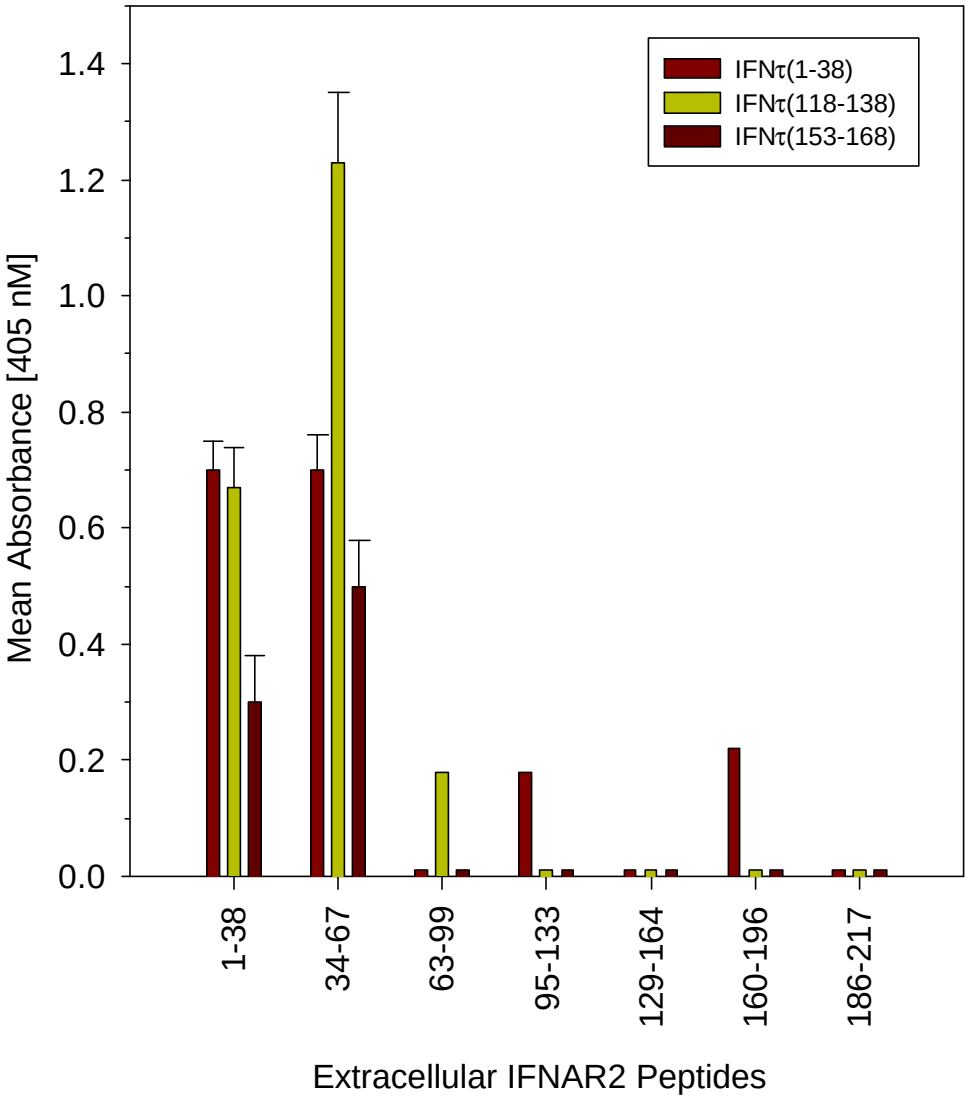

Figure 3-11. Binding of biotinylated ovine IFNτ, and ovine IFNτ peptides, IFNτ(1-38), IFNτ(118-138), and IFNτ(153-168) to overlapping synthetic peptides corresponding to the extracellular domain of IFNAR2. Biotinylated ovine IFNτ and ovine IFNτ peptides are at a final concentration of 0.5 μM. Receptor peptide binding was determined colormetrically by alkaline phosphatase activity. Bars represent the standard deviations. All assays were performed in triplicate.

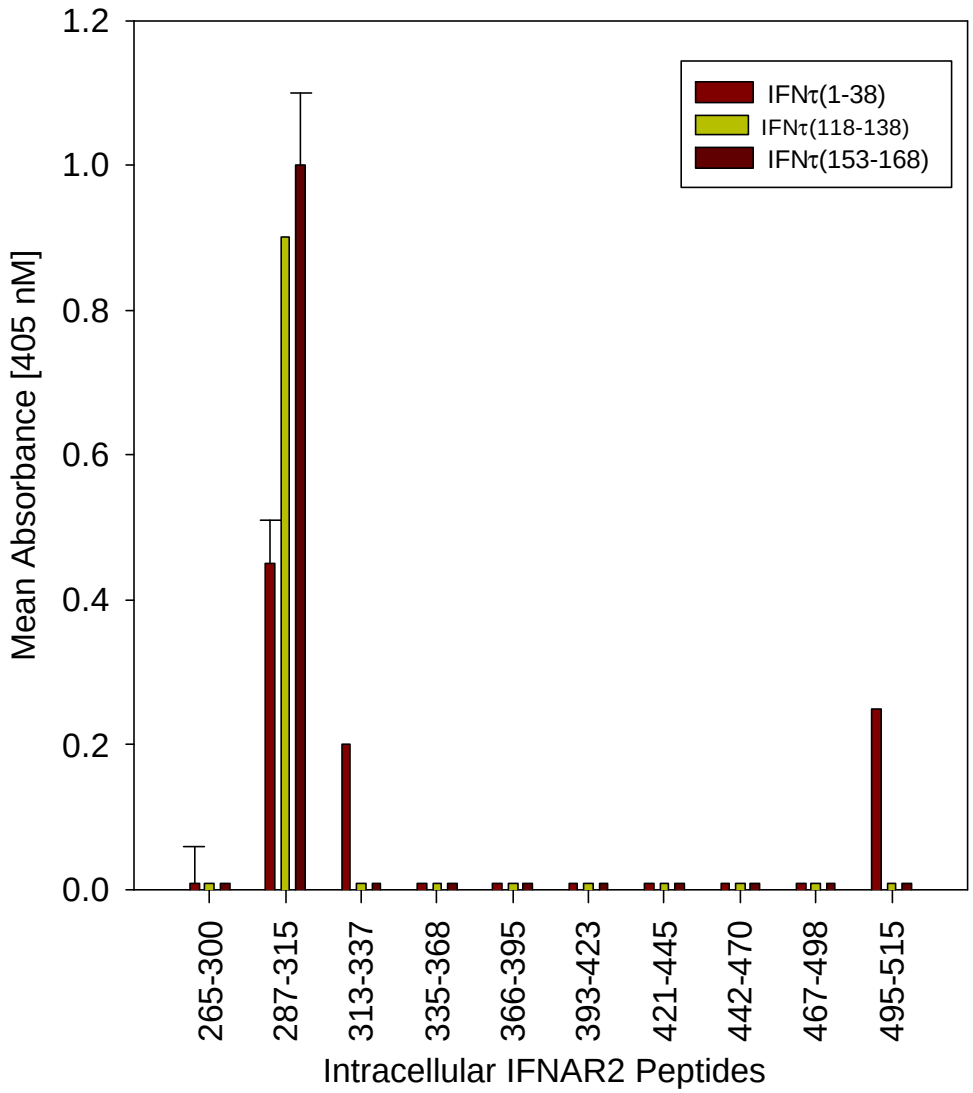

Figure 3-12. Binding of biotinylated ovine IFNτ, and ovine IFNτ peptides, IFNτ(1-38), IFNτ(118-138), and IFNτ(153-168) to overlapping synthetic peptides corresponding to the intracellular domain of IFNAR2. Biotinylated ovine IFNτ and ovine IFNτ peptides are at a final concentration of 0.5 μM. Receptor peptide binding was determined colormetrically by alkaline phosphatase activity. Bars represent the standard deviations. All assays were performed in triplicate.

determined that the C-terminus of IFNγ is recognizing an intracellular receptor site [128].

Ovine IFNτ Peptides Compete with Ovine ^{125}I-IFNτ for IFNAR2(1-38)

The remaining ovine IFNτ peptides to complete the molecule were synthesized. Each of the five helices inclusive of surrounding turns and structurally random regions were represented, as recently determined by x-ray crystallography are shown in Table 3-3. The ovine IFNτ peptides were initially used as competitors against ovine ^{125}I-IFNτ for immobilized extracellular receptor peptide IFNAR2(1-38) in solid-phase competition assays. Five of the six ovine IFNτ peptides blocked ovine ^{125}I-IFNτ binding to IFNAR2(1-38) in a concentration-dependent manner; only IFNτ(136-158) did not compete (Figure 3-13A-F). However, although some dose-dependent inhibition of binding of ovine ^{125}I-IFNτ to IFNAR2(1-38) was evident in the saturation experiments, ovine IFNτ did not appear to interact strongly with this receptor peptide (Figure 3-14). The structural integrity of the immobilized IFNAR2(1-38) was ensured by the competition between soluble IFNAR2(1-38) and ovine ^{125}I-IFNτ (Figure 3-15). Receptor peptide IFNAR2(186-217), a receptor peptide that did not bind ovine IFNτ in previous experiments, served as a negative control and did not compete with ovine ^{125}I-IFNτ for immobilized IFNAR2(1-38).

Table 3-3. Sequences and secondary structure of the synthetic ovine IFNτ peptides. Secondary structure of ovine IFNτ was determined with x-ray crystallography [9].

Peptide Name	Peptide Sequence	Secondary Structure
IFNτ(1-38)	CYLSRKLMLDAREKLLDRM NRSPHSCLQDRKDFGL	HELIX A, AB LOOP (cys 29 bound to cys 139 of helix e), AB LOOP 2 (note: loops are turns that connect the helices.)
IFNτ(36-79)	KDFGLPQEMVEGDQLQKD QAFPVLYEMLQQSFNLFYT EHSSAADT	AB LOOP 2, AB LOOP 3, HELIX B, BC LOOP
IFNτ(77-119)	WDTTLLEQLCTGLQQQLD HLDTCRGQGMGEEDSELG NMDPIVT	BC LOOP, HELIX C, CD LOOP
IFNτ(118-138)	LFSCSHNFWLAIDMSFEPP EFEIVGFTNHINVMVKFPSI	HELIX D, DE LOOP
IFNτ(136-158)	FPSIVEEELQFDLSLVIEEQ SEGIVKKHKPEIKGN	HELIX E
IFNτ(153-168)	EIKGNMSGNFTYIIDKLIPN TNYCVSVYLEHSDEQA	HELIX E, RANDOM REGION (i.e. little electron density)

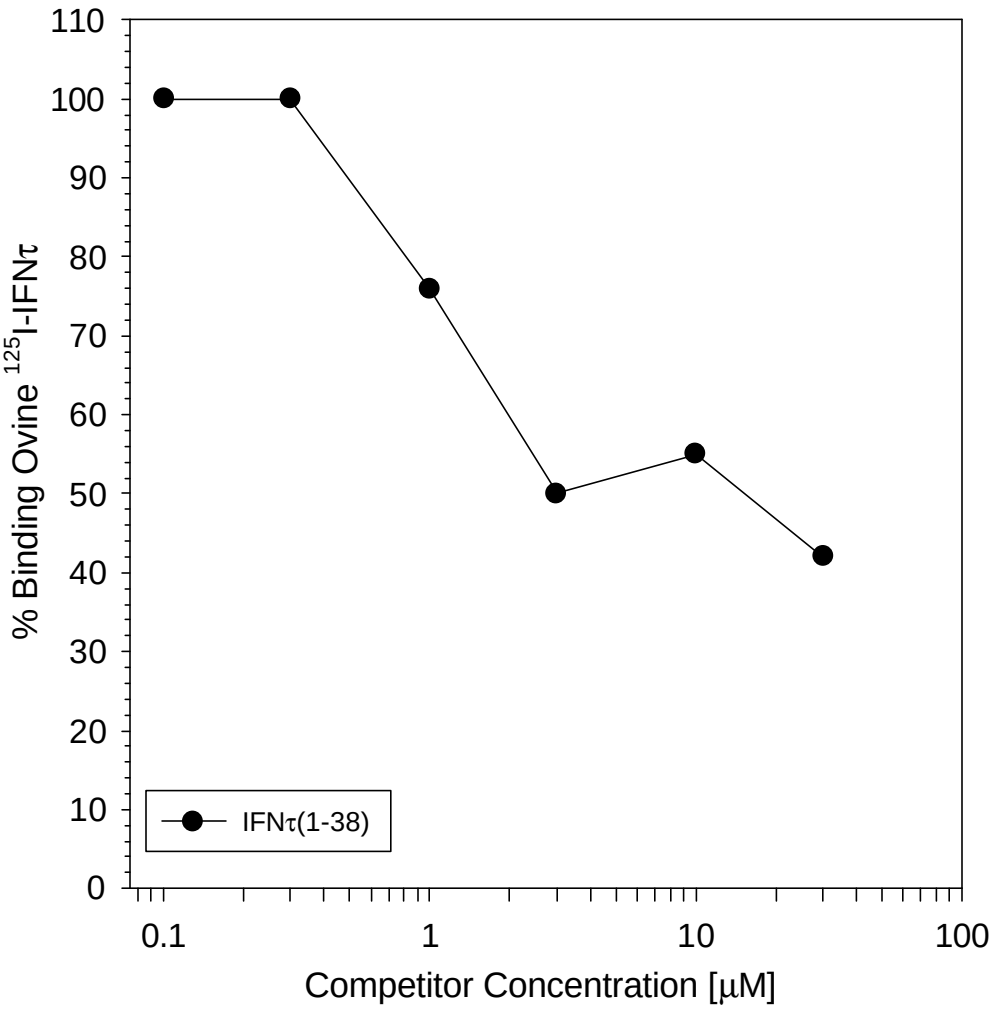

Figure 3-13. Dose-dependent binding of ovine ^{125}I-IFNτ to IFNAR2(1-38) in the presence of unlabeled ovine IFNτ peptides, (A) IFNτ(1-38), (B) IFNτ(36-79), (C) IFNτ(77-119), (D) IFNτ(118-138), (E) IFNτ(136-158) and (F) IFNτ(153-168). Ovine ^{125}I-IFNτ was used at a final concentration of 5 nM. All assays were performed in triplicate with coefficients of variation not greater than 10%.

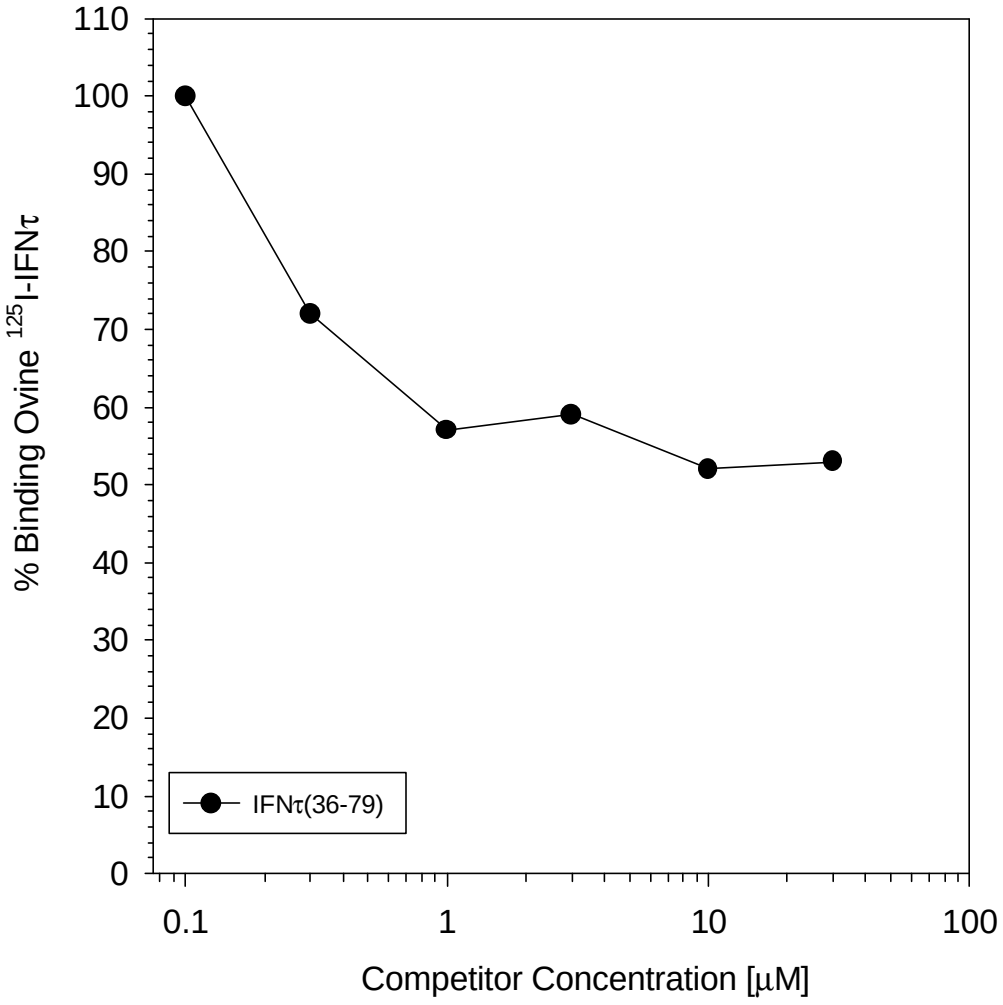
110
100
90
80
70
60
50
40
30
20
10
0
% Binding Ovine 125I-IFNτ
IFNτ(36-79)
0.1
1
10
100
Competitor Concentration [μM]

Figure 3-13B.

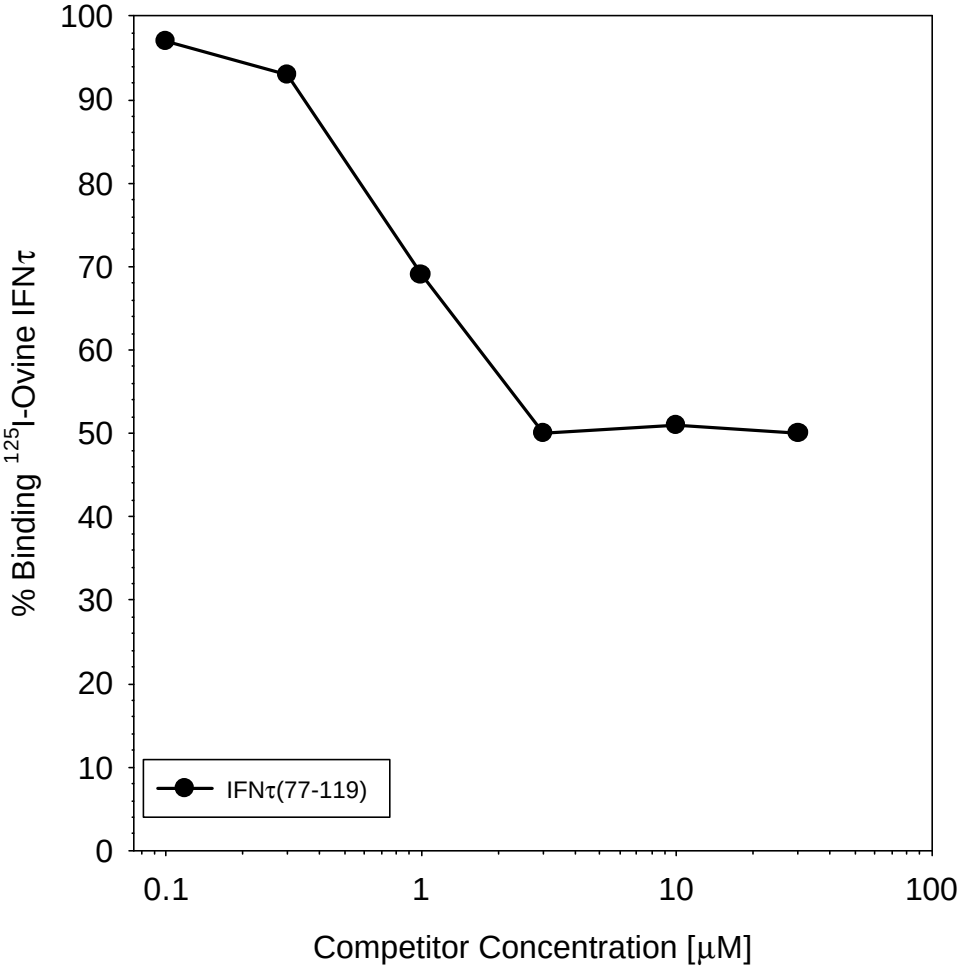
100
90
80
70
60
50
40
30
20
10
0
% Binding ^{125}I-Ovine IFNτ
IFNτ(77-119)
0.1
1
10
100
Competitor Concentration [μM]

Figure 3-13C.

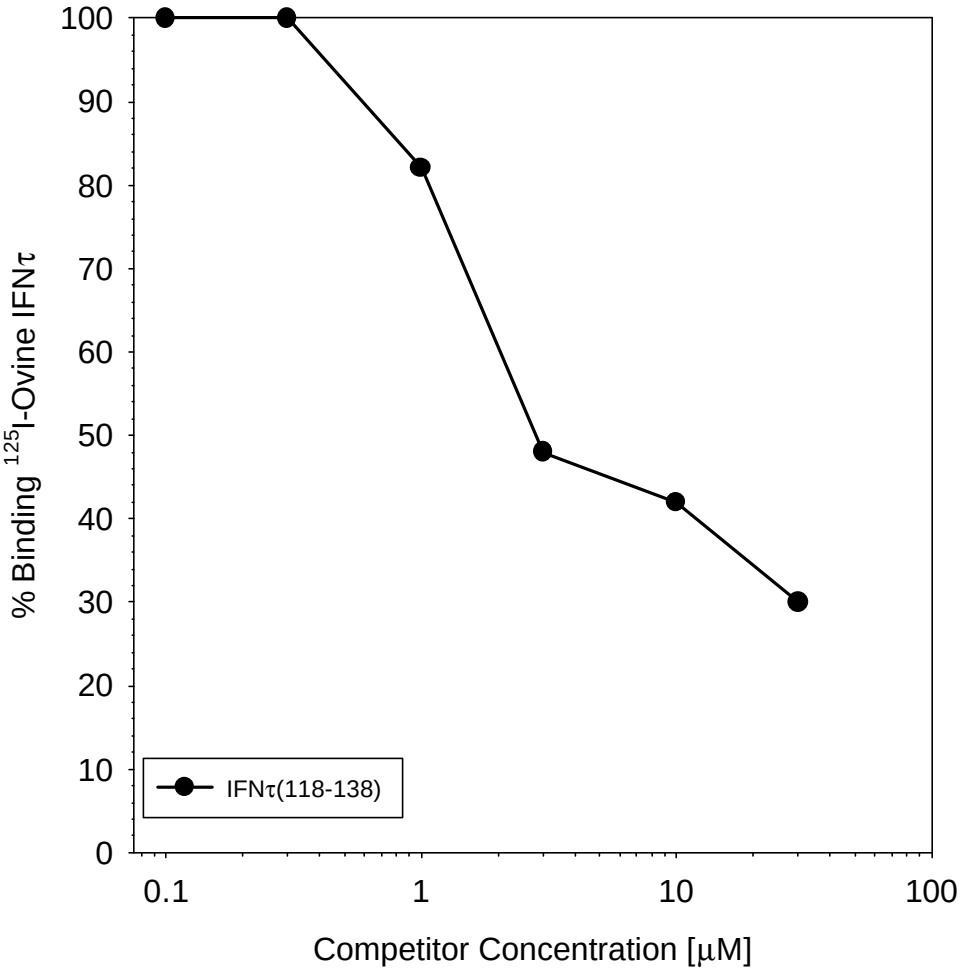
100
90
80
70
60
50
40
30
20
10
0
% Binding ^{125}I-Ovine IFNτ
IFNτ(118-138)
0.1
1
10
100
Competitor Concentration [μM]

Figure 3-13D.

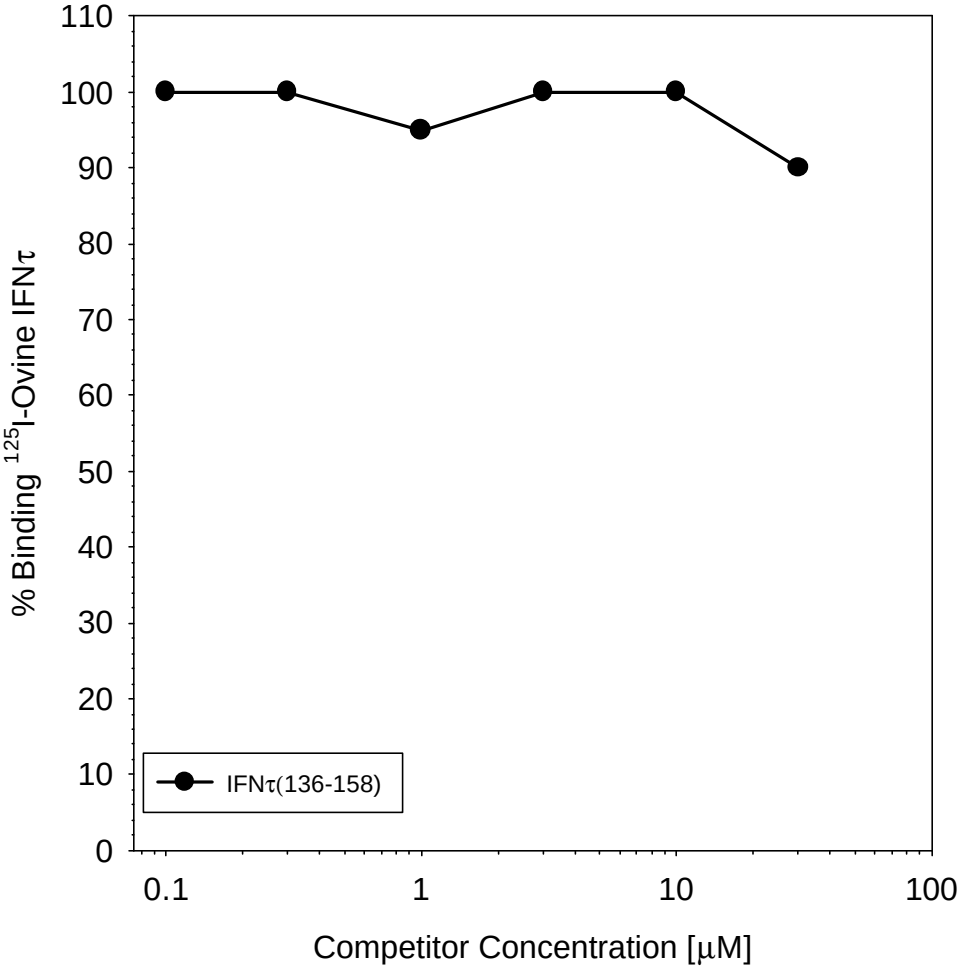
110
100
90
80
70
60
50
40
30
20
10
0
% Binding ^{125}I-Ovine IFNτ
IFNτ(136-158)
0.1
1
10
100
Competitor Concentration [μM]

Figure 3-13E.

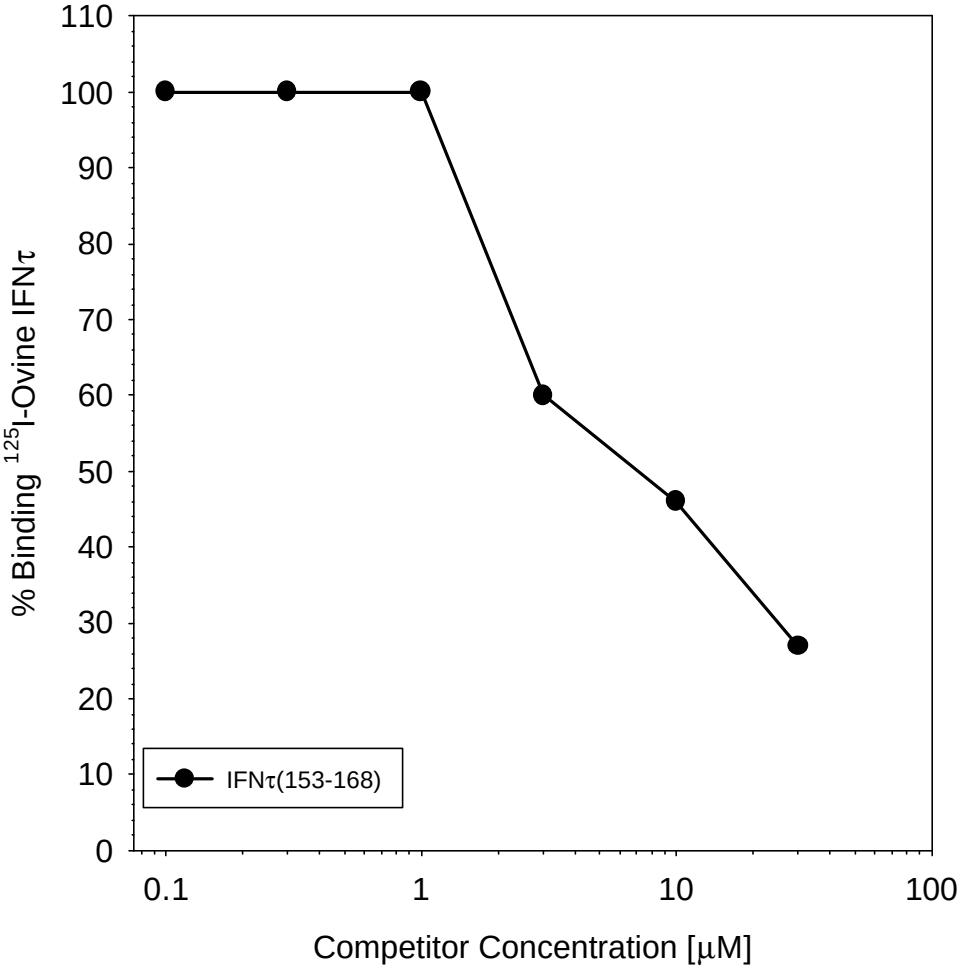
110
100
90
80
70
60
50
40
30
20
10
0
% Binding ^{125}I-Ovine IFNτ
IFNτ(153-168)
0.1
1
10
100
Competitor Concentration [μM]

Figure 3-13F.

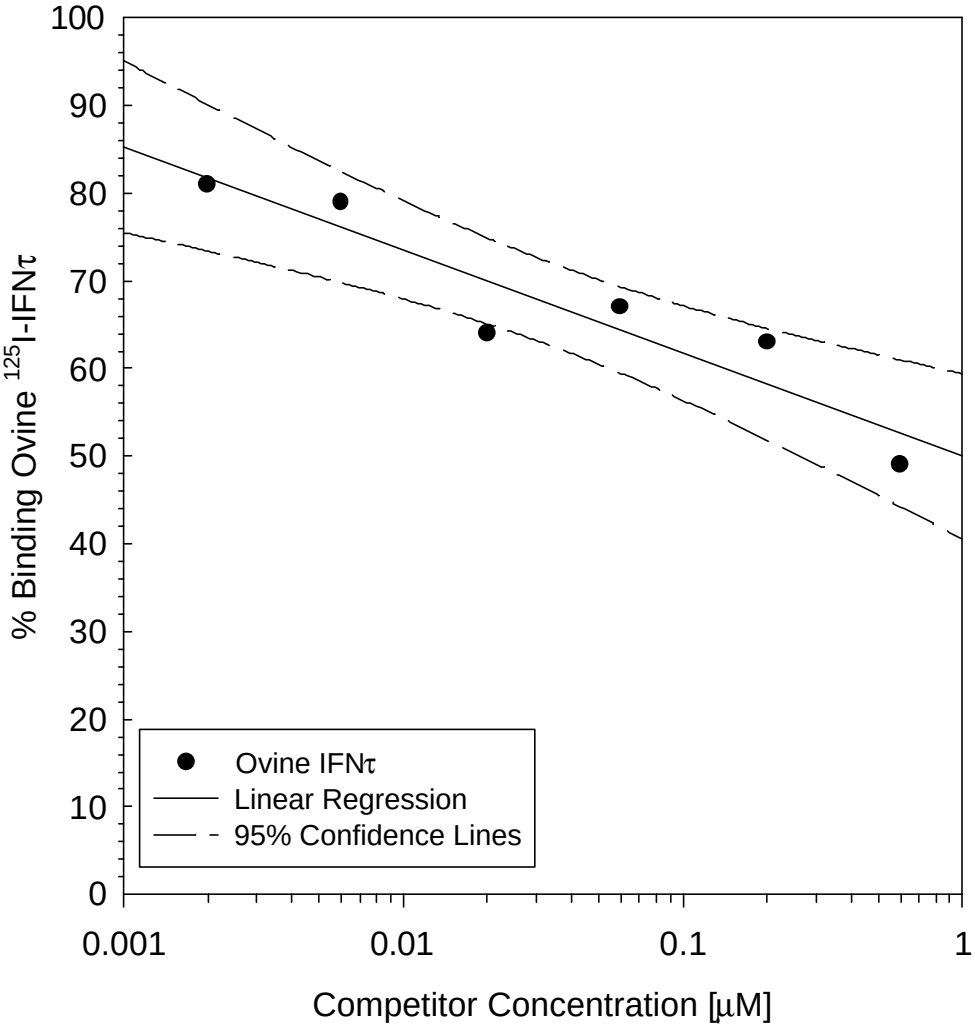

Figure 3-14. Dose-dependent binding of ovine ^{125}I-IFNτ to IFNAR2(1-38) in the presence of unlabeled ovine IFNτ. Ovine ^{125}I-IFNτ was used at a final concentration of 5 nM. Radioiodine counts from bound ovine ^{125}I-IFNτ were measured after a 2-hour incubation at room temperature. All assays were performed in triplicate with coefficients of variation not greater than 10%.

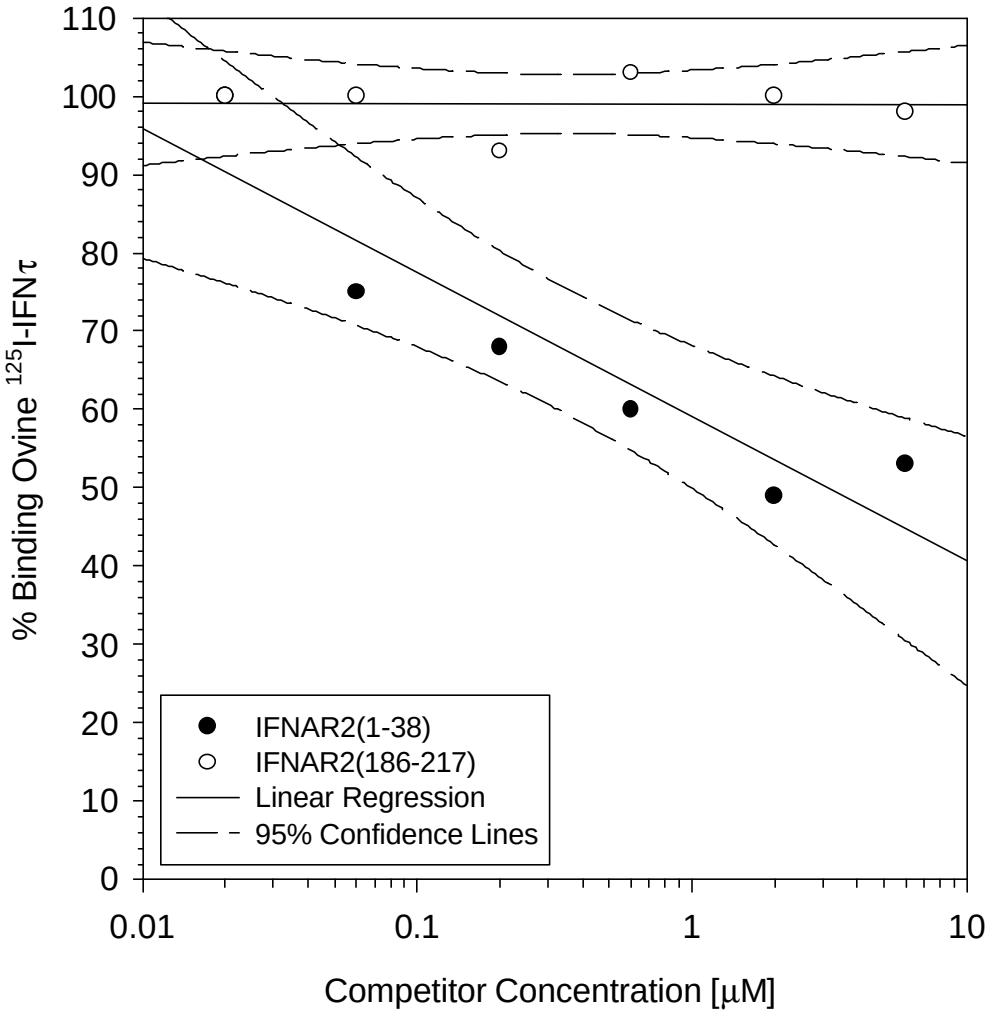

Figure 3-15. Dose-response of extracellular IFNAR2 peptide competitors, IFNAR2(1-38) and IFNAR2(186-217), on ovine ^{125}I-IFNτ binding to the type I IFN receptor on MDBK cells. Ovine ^{125}I-IFNτ was used at a final concentration of 5 nM. Radioiodine counts from bound ovine ^{125}I-IFNτ were measured after a 2-hour incubation at room temperature. All assays were performed using at least four replicates to increase accuracy.

Ovine IFNτ Peptides Compete with Ovine ^{125}I-IFNτ for IFNAR2(34-67)

In solid-phase competition assays, ovine ^{125}I-IFNτ binding to IFNAR2(34-67) was displaced by three of the six unlabeled ovine IFNτ peptides, IFNτ(1-38), IFNτ(77-119), and IFNτ(118-138) (Figure 3-16A, C, and D). Therefore, both IFNAR2(1-38) and IFNAR2(34-67) were specifically recognized by ovine IFNτ peptides IFNτ(1-38), IFNτ(77-119), and IFNτ(118-138), suggesting that the N-terminal extracellular domain of IFNAR2 recognizes multiple sites on ovine IFNτ (Figures 3-13A, C, and D and 3-16A, C, and D). Although previously shown to be functionally important [39], the C-terminus of ovine IFNτ, does not appear to be important for ovine IFNτ interactions with the structurally and functionally important extracellular regions of IFNAR2 (Figure 3-16F). It appears that the N-terminus of IFNAR2 specifically recognizes sites within amino acids 1-38 of the N-terminus of ovine IFNτ and regions corresponding to residues 77-138. Unlabeled ovine IFNτ strongly inhibited ovine ^{125}I-IFNτ interaction with IFNAR2(34-67) (Figure 3-17). These results provide further evidence for the interaction of ovine IFNτ and a region within residues 34-67 on IFNAR2. Soluble IFNAR2(34-67) competitor inhibited ovine ^{125}I-IFNτ binding to immobilized IFNAR2(34-67), suggesting that immobilization

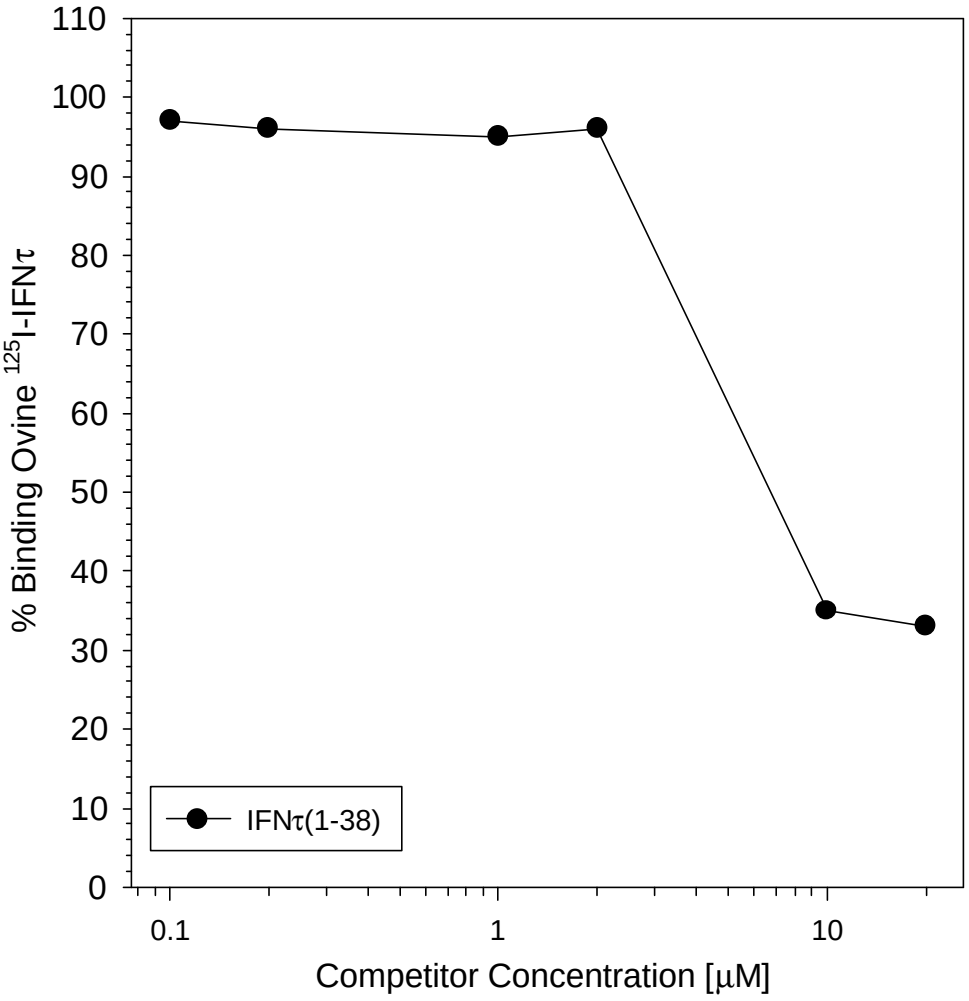

Figure 3-16. Dose-dependent binding of ovine ^{125}I-IFNτ to IFNAR2(34-67) in the presence of unlabeled ovine IFNτ peptides, (A) IFNτ(1-38), (B) IFNτ(36-79), (C) IFNτ(77-119), (D) IFNτ(118-138), (E) IFNτ(136-158) and (F) IFNτ(153-168). Ovine ^{125}I-IFNτ was used at a final concentration of 5 nM. Radioiodine counts from bound ovine ^{125}I-IFNτ were measured after a 2-hour incubation at room temperature. All assays were performed in triplicate with coefficients of variation not greater than 10%.

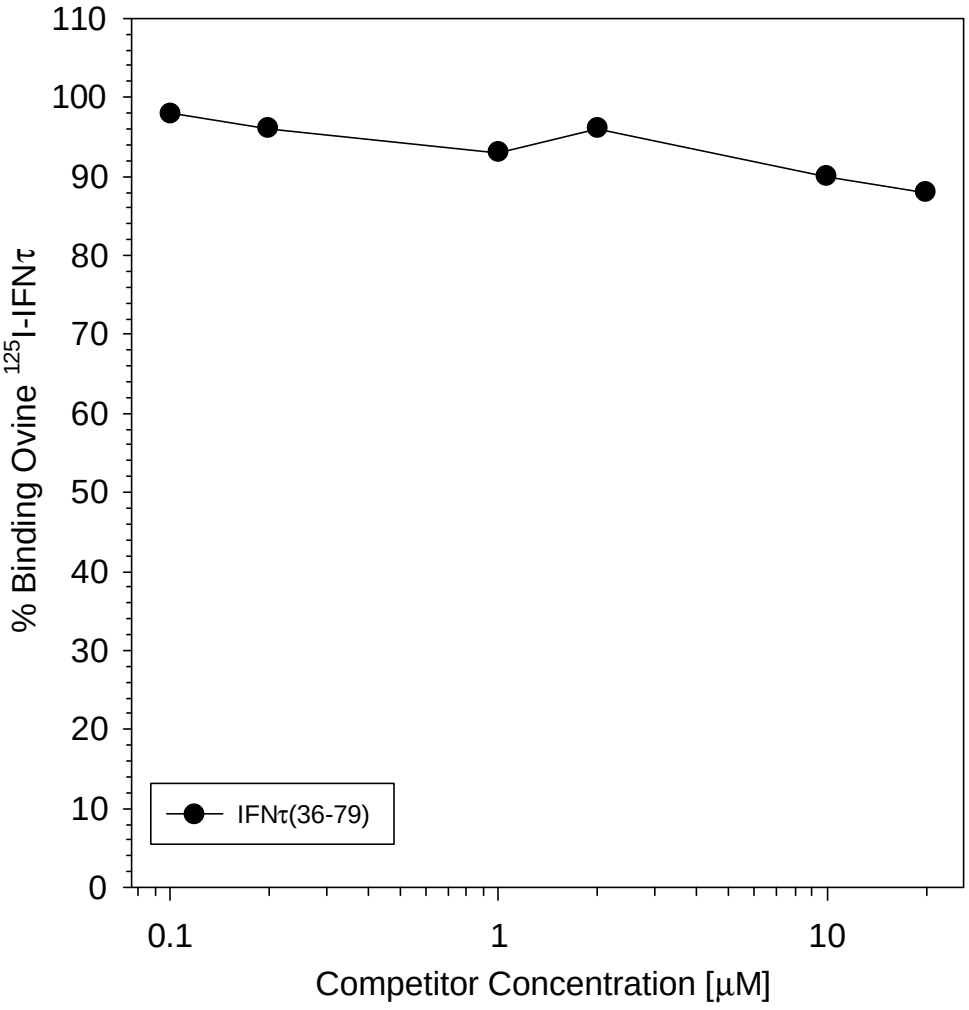
110
100
90
80
70
60
50
40
30
20
10
0
% Binding Ovine 125I-IFNτ
IFNτ(36-79)
0.1
1
10
Competitor Concentration [μM]

Figure 3-16B.

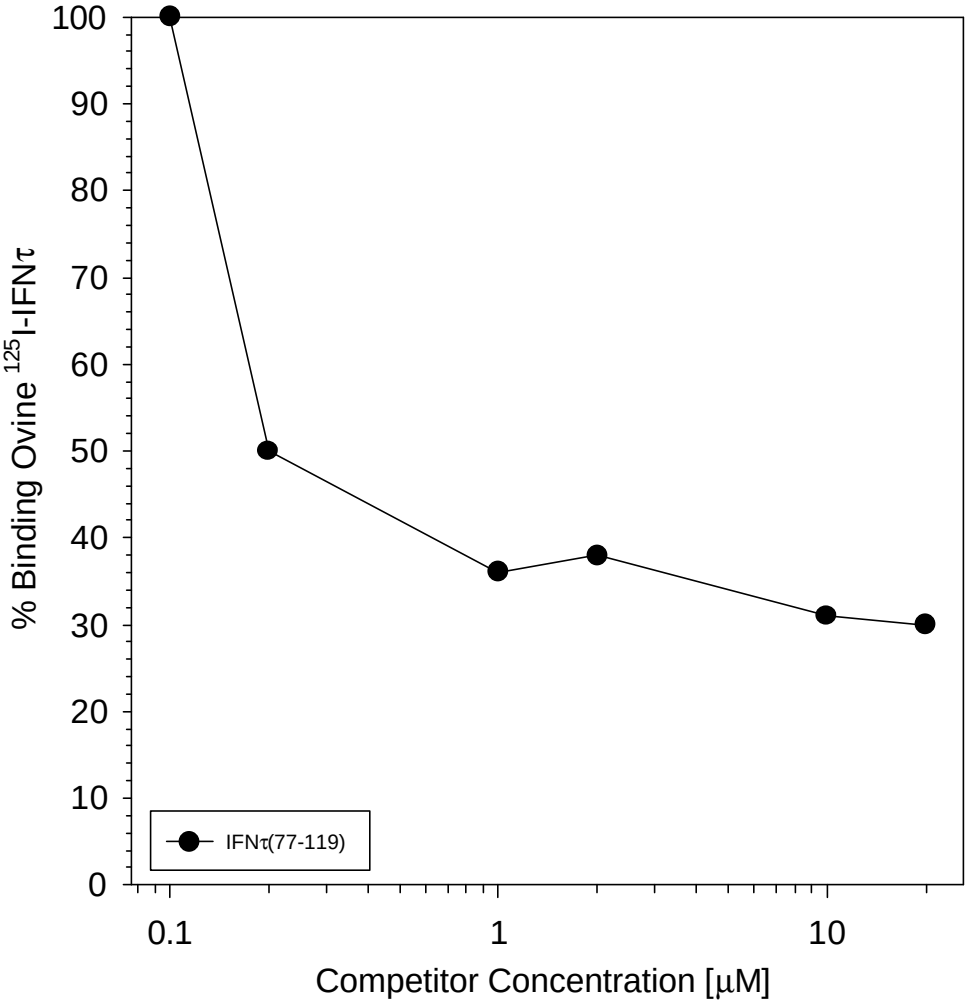
100
90
80
70
60
50
40
30
20
10
0
% Binding Ovine 125I-IFNτ
IFNτ(77-119)
0.1
1
10
Competitor Concentration [μM]

Figure 3-16C.

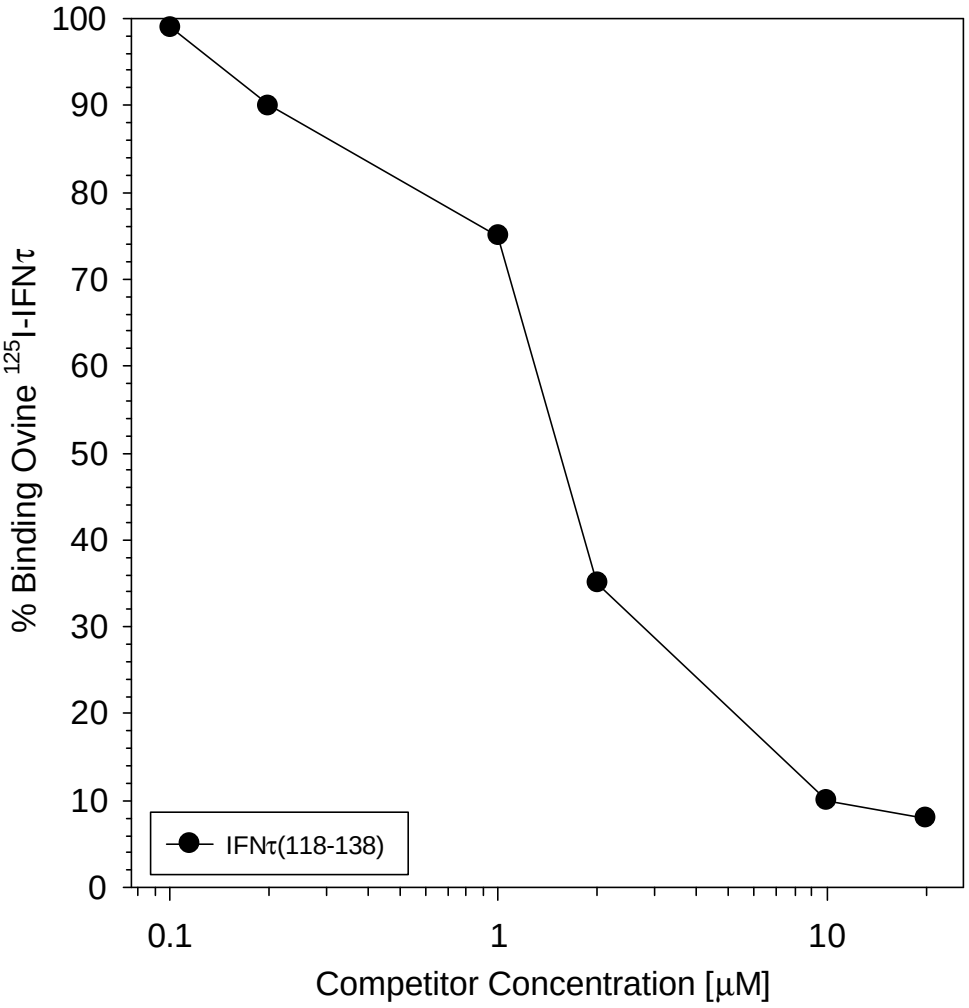
100
90
80
70
60
50
40
30
20
10
0
% Binding Ovine 125I-IFNτ
IFNτ(118-138)
0.1
1
10
Competitor Concentration [μM]

Figure 3-16D.

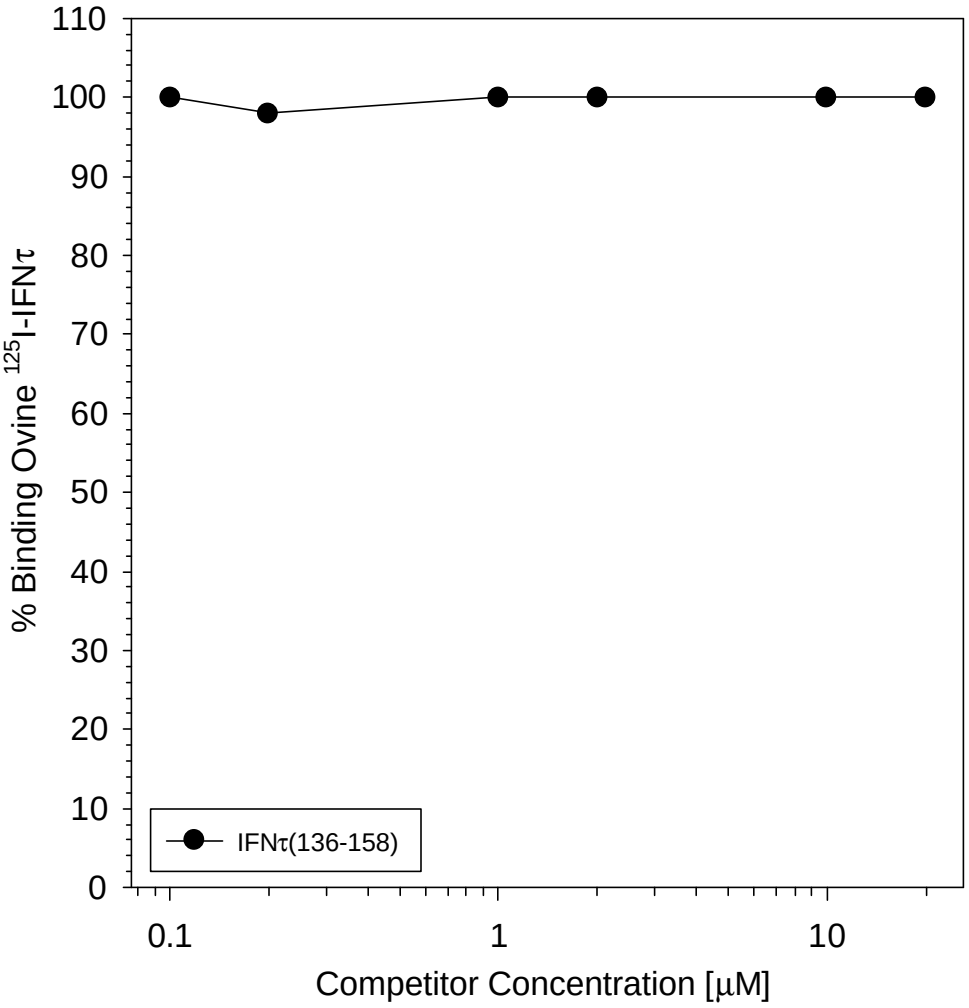
110
100
90
80
70
60
50
40
30
20
10
0
% Binding Ovine 125I-IFNτ
IFNτ(136-158)
0.1
1
10
Competitor Concentration [μM]

Figure 3-16E.

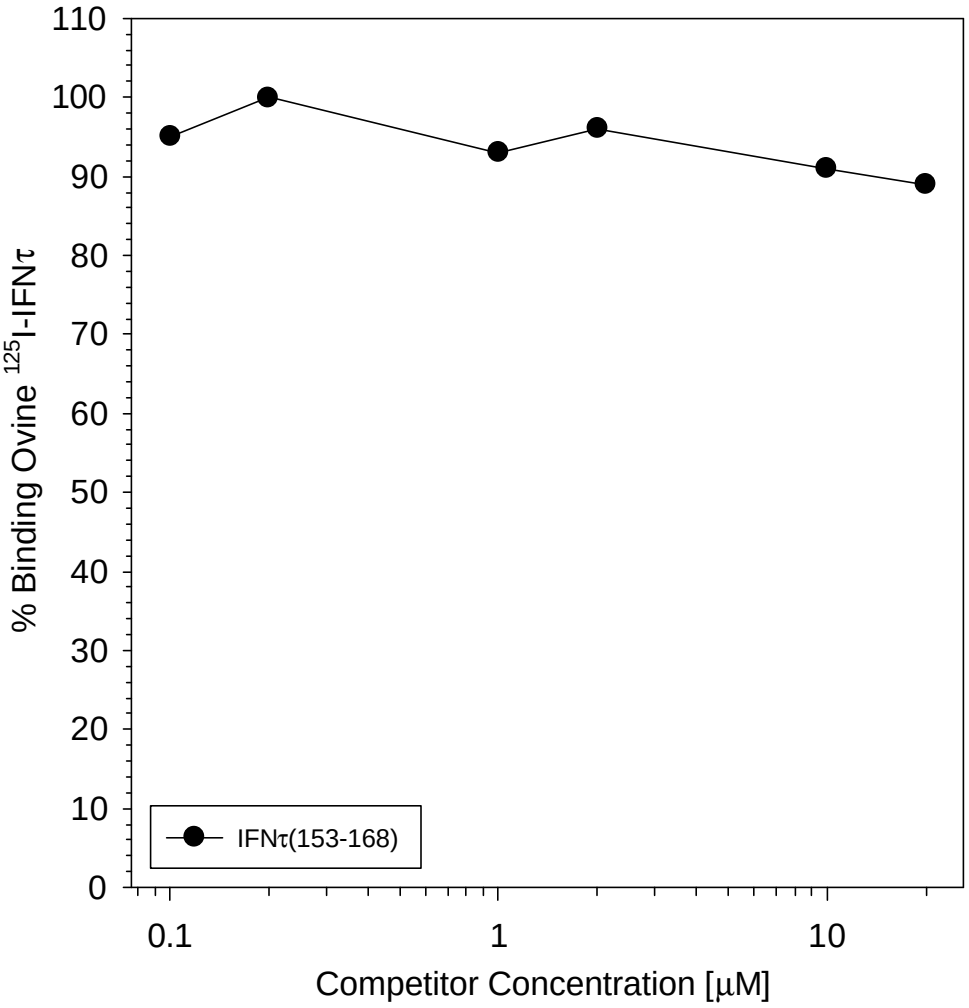
110
100
90
80
70
60
50
40
30
20
10
0
% Binding Ovine 125I-IFNτ
IFNτ(153-168)
0.1
1
10
Competitor Concentration [μM]

Figure 3-16F.

of the receptor peptide did not significantly alter the structure of IFNAR2(34-67) (Figure 3-18). In addition, the competition between ovine ^{125}I-IFNτ and IFNAR2(34-67) complements other results showing that ovine IFNτ specifically interacts with sites within extracellular IFNAR2 residues 34-67 (Figure 3-18). IFNAR2(186-217), an extracellular IFNAR2 peptide that does not interact with ovine IFNτ, did not compete effectively for IFNAR2(34-67) (Figure 3-18).

Ovine IFNτ and Ovine IFNτ Peptides Specifically Recognize IFNAR2(287-315)

Biotinylated ovine IFNτ binding to immobilized intracellular receptor peptide IFNAR2(287-315) was inhibited dose-dependently by ovine IFNτ peptide IFNτ(118-138) (Figure 3-19B). Although IFNτ(153-168) recognized IFNAR2(287-315) in direct binding assays, IFNτ(153-168) did not effectively inhibit biotin-labeled ovine IFNτ binding in the competition assays, suggesting that the C-terminus of ovine IFNτ does not bind to an intracellular region of IFNAR2 (Figure 3-19C). Therefore, it appears that IFNAR2(287-315) may interact with an internal region of ovine IFNτ, but not regions on the N- or C-terminus. The binding of intact, biotinylated ovine IFNτ to IFNAR2(287-315) was effectively inhibited by unlabeled ovine IFNτ (Figure 3-20). This suggests that ovine IFNτ specifically recognizes IFNAR2(287-315). Competition binding assays in which soluble IFNAR2(287-315)

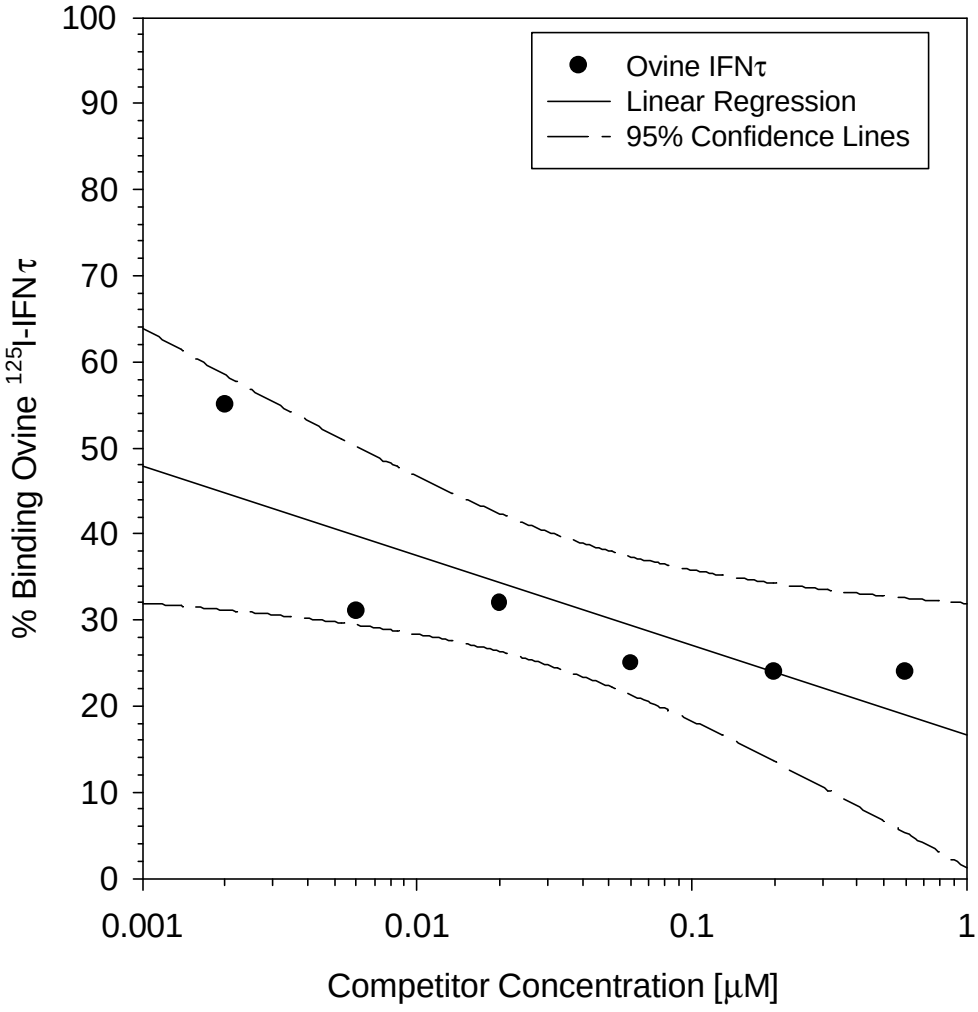

Figure 3-17. Dose-dependent binding of ovine ^{125}I-IFNτ to IFNAR2(34-67) in the presence of unlabeled ovine IFNτ. Ovine ^{125}I-IFNτ was used at a final concentration of 5 nM. Radioiodine counts from bound ovine ^{125}I-IFNτ were measured after a 2-hour incubation at room temperature. All assays were performed in triplicate with coefficients of variation not greater than 10%.

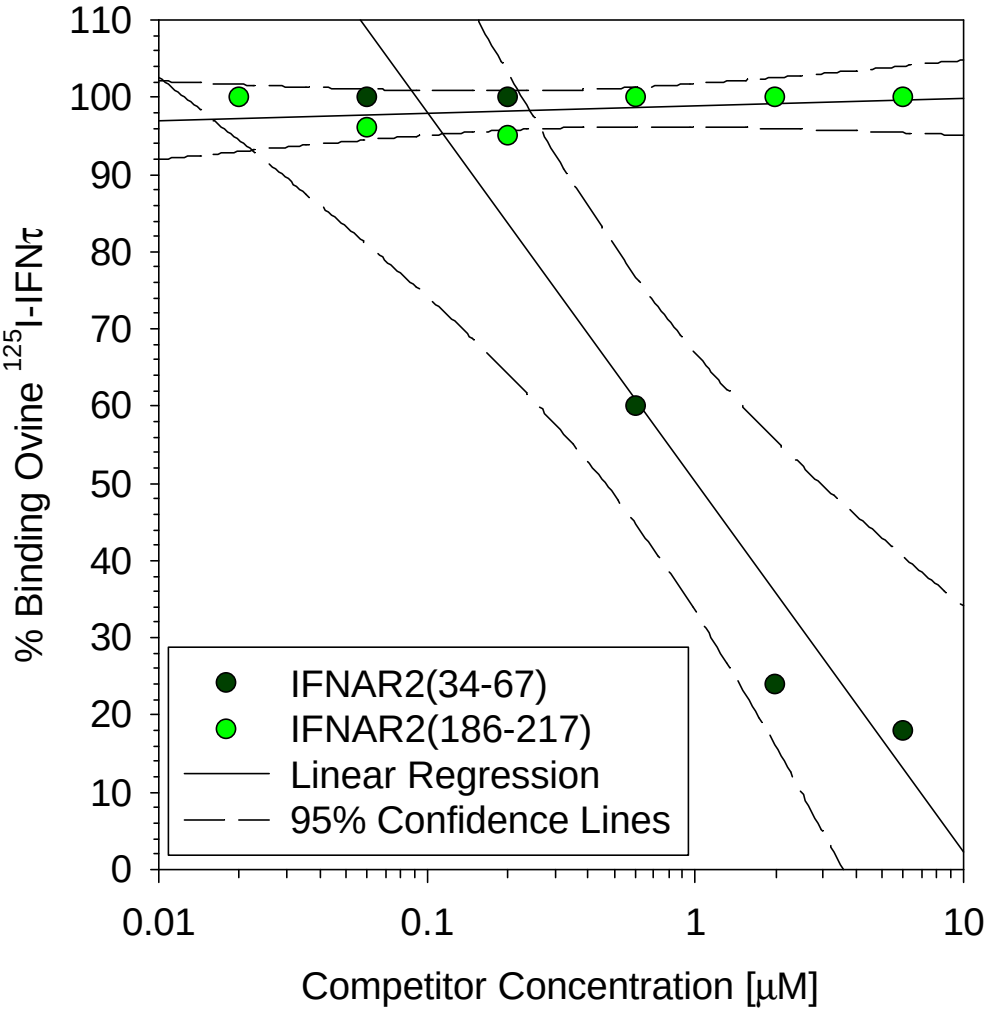

Figure 3-18. Dose-response of extracellular IFNAR2 peptide competitors, IFNAR2(34-67) and IFNAR2(186-217), on ovine ^{125}I-IFNτ binding to IFNAR2(34-67). Ovine ^{125}I-IFNτ was used at a final concentration of 5 nM. Radioiodine counts from bound ovine ^{125}I-IFNτ were measured after a 2-hour incubation at room temperature. All assays were performed using at least four replicates to increase accuracy.

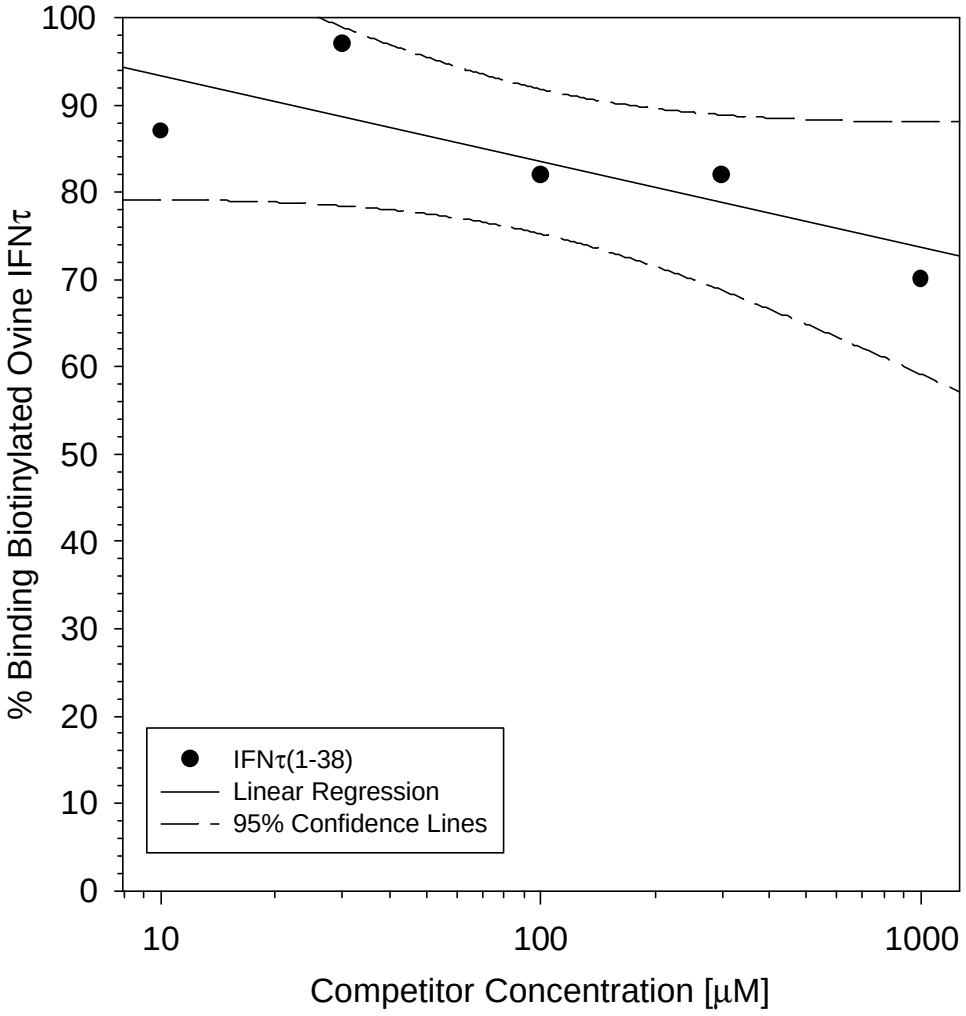

Figure 3-19. Dose-dependent binding of biotinylated ovine IFNτ peptides, IFNτ(1-38), IFNτ(118-138), and IFNτ(153-168) to IFNAR2(287-315) in the presence of unlabeled ovine IFNτ peptides. Biotinylated ovine IFNτ was used at a final concentration of 0.5 μM. Receptor peptide binding was determined colormetrically by alkaline phosphatase activity. Bars represent the standard deviations. All assays were performed in triplicate with coefficients of variation less than 10%.

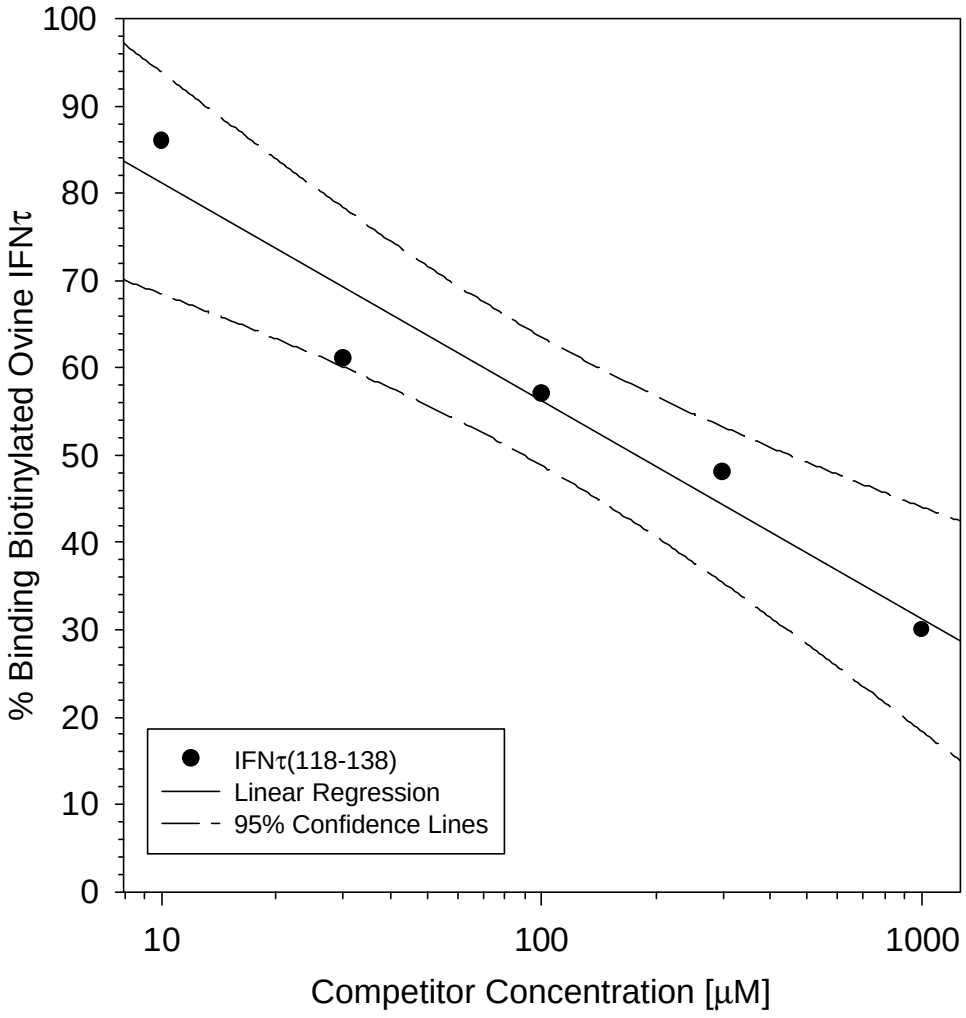
100
90
80
70
60
50
40
30
20
10
0
% Binding Biotinylated Ovine IFNτ
10
100
1000
Competitor Concentration [μM]
IFNτ(118-138)
Linear Regression
95% Confidence Lines

Figure 3-19B.

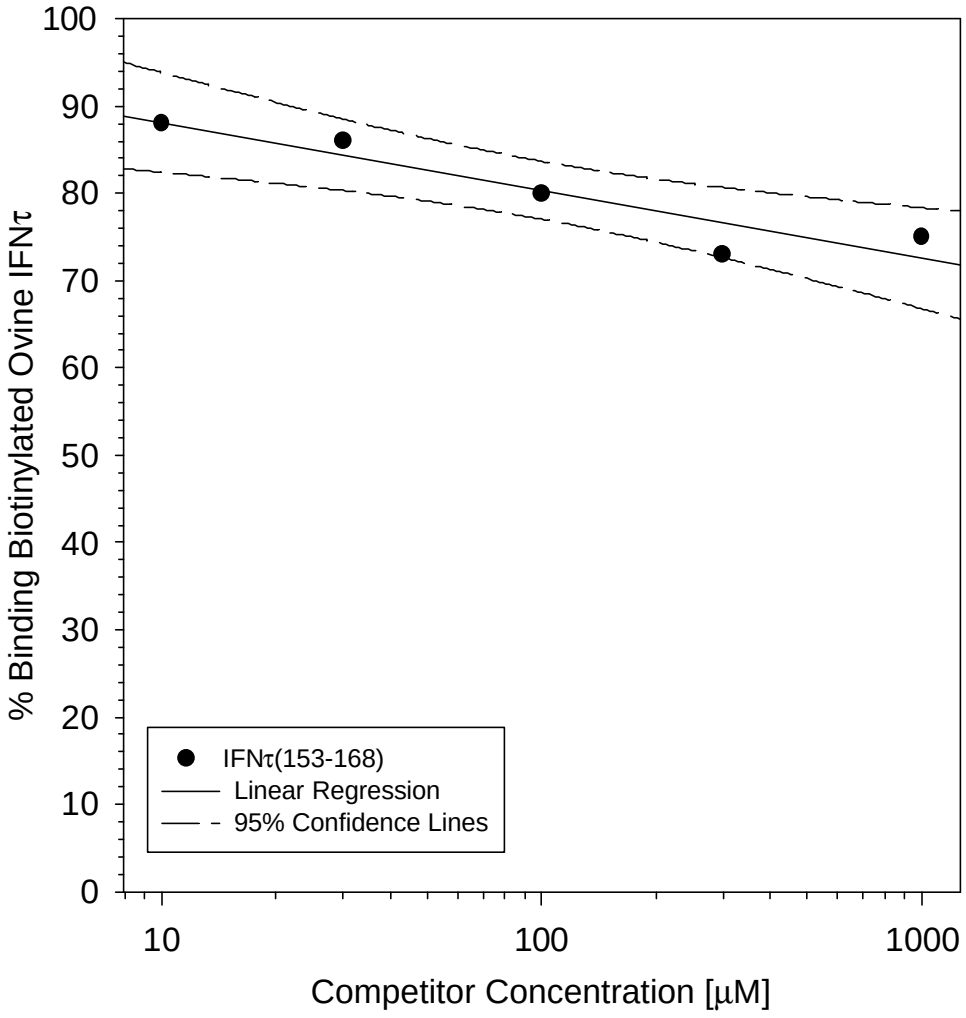
100
90
80
70
60
50
40
30
20
10
0
% Binding Biotinylated Ovine IFNτ
IFNτ(153-168)
Linear Regression
95% Confidence Lines
10
100
1000
Competitor Concentration [μM]

Figure 3-19C.

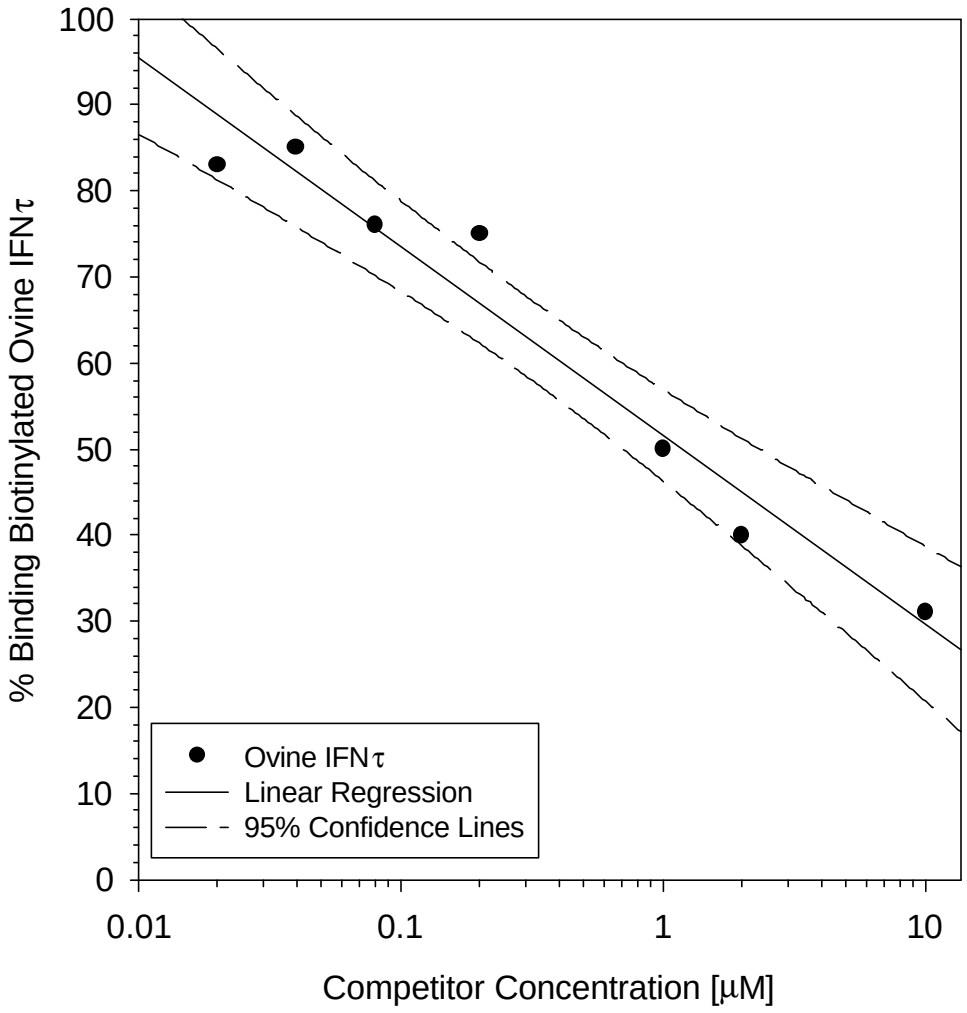

Figure 3-20. Binding of biotinylated ovine IFNτ to IFNAR2(287-315) in the presence of unlabeled ovine IFNτ. Radioiodinated ovine IFNτ was at a final concentration of 0.5 μM. Receptor peptide binding was determined colormetrically by alkaline phosphatase activity. Bars represent the standard deviations. All assays were performed in triplicate.

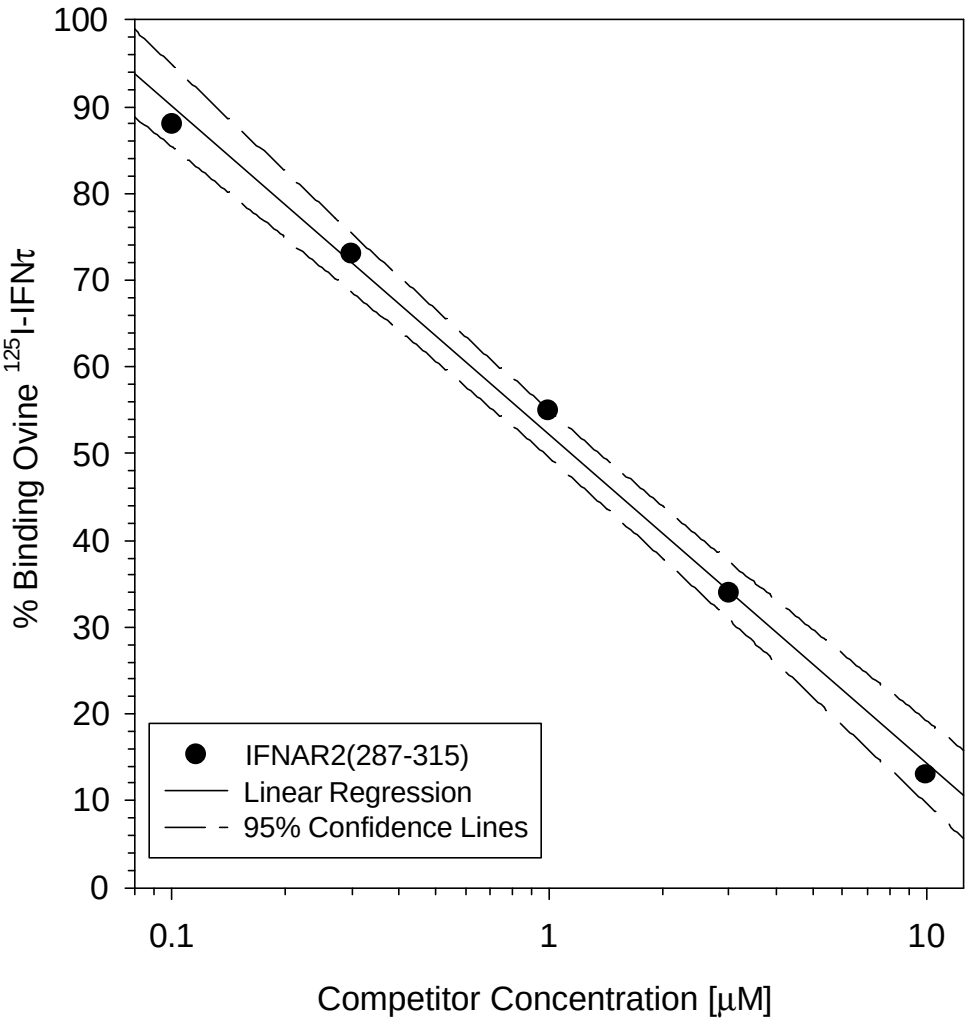

Figure 3-21. Dose-dependent binding of biotinylated ovine IFNτ to IFNAR2(287-315) in the presence of IFNAR2(287-315). Biotinylated ovine IFNτ was used at a final concentration of 0.5 μM. Receptor peptide binding was determined colormetrically by alkaline phosphatase activity. Bars represent the standard deviations. All assays were performed in triplicate with coefficients of variation less than 10%.

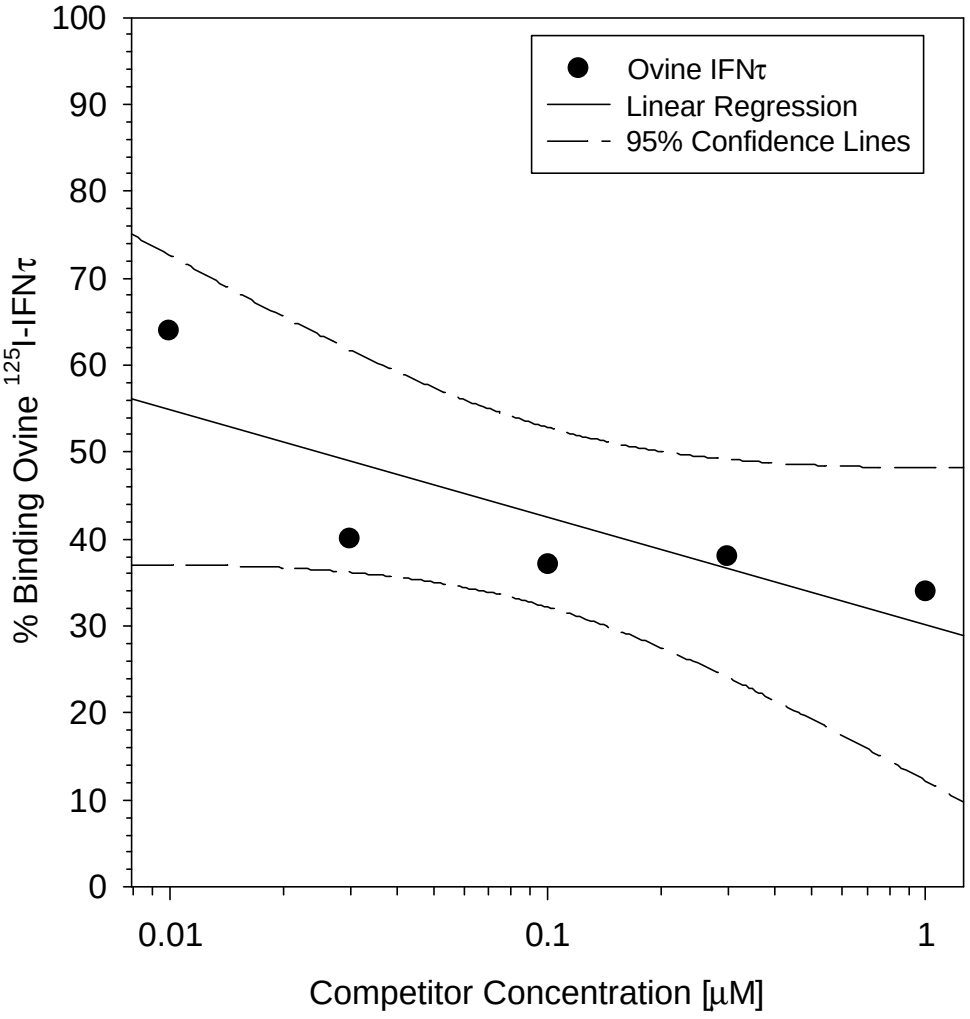

Figure 3-22. Dose-dependent binding of ovine ^{125}I-IFNτ to IFNAR2(287-315) in the presence of unlabeled ovine IFNτ. Ovine ^{125}I-IFNτ was used at a final concentration of 5 nM. Radioiodine counts from bound ovine ^{125}I-IFNτ were measured after a 2-hour incubation at room temperature. All assays were performed in triplicate.

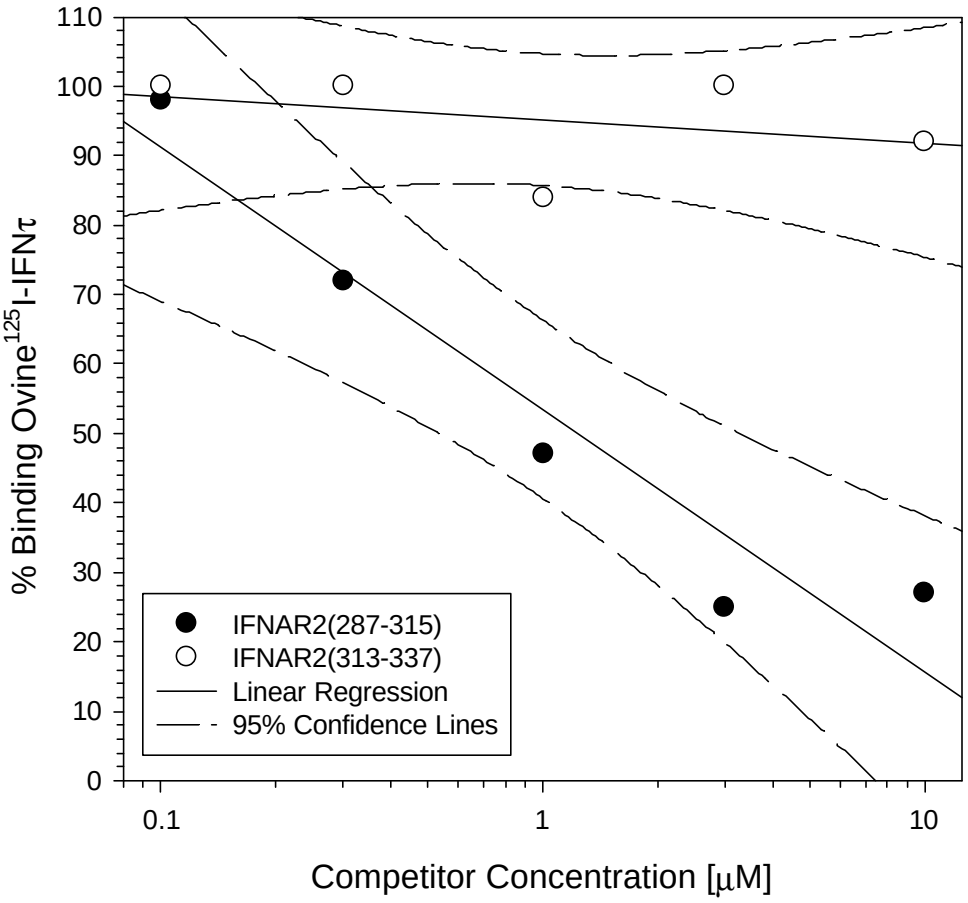

Figure 3-23. Dose-response of intracellular IFNAR2 peptide competitor, IFNAR2(287-315), on ovine ^{125}I-IFNτ binding to IFNAR2(287-315). Ovine ^{125}I-IFNτ was used at a final concentration of 5 nM. Radioiodine counts from bound ovine ^{125}I-IFNτ were measured after a 2-hour incubation at room temperature. All assays were performed with in triplicate with coefficients of variation not greater than 10%.

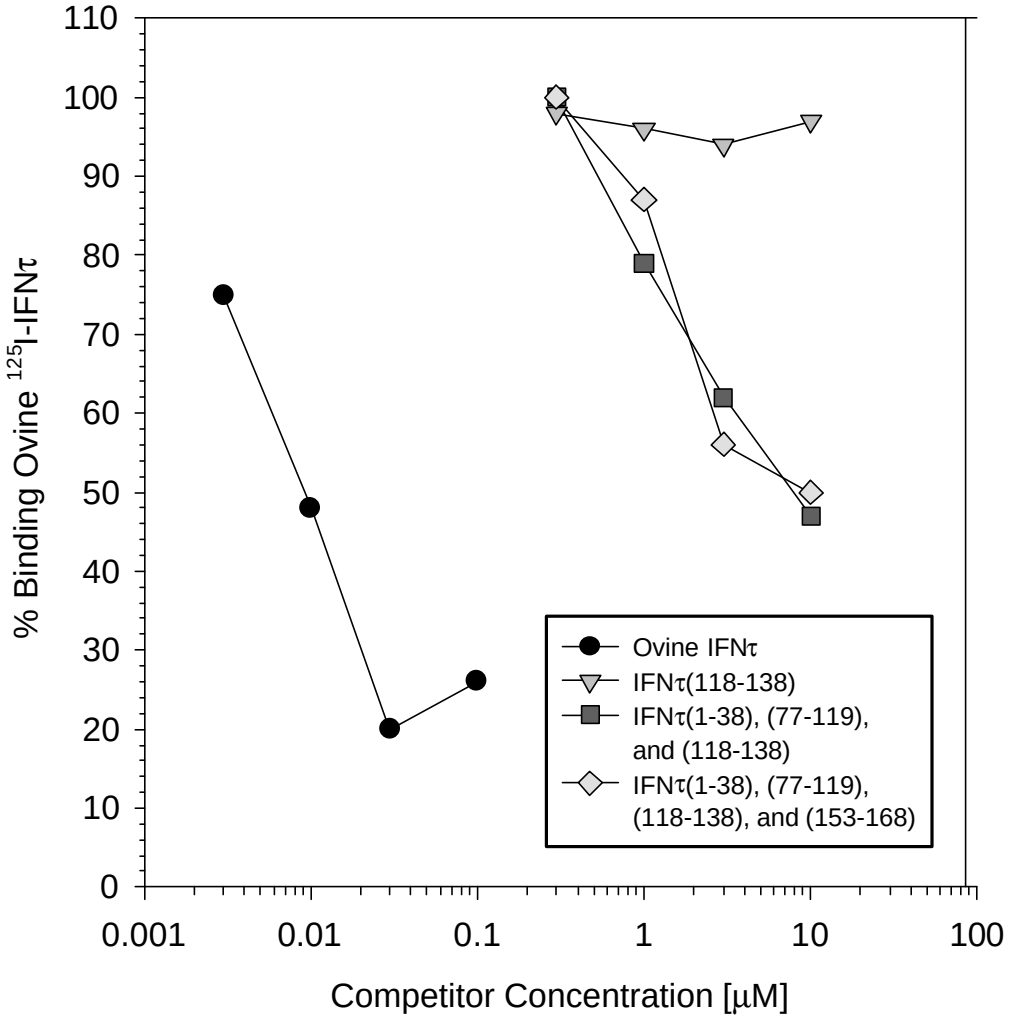

Figure 3-24. Dose-response of unlabeled ovine IFNτ and extracellular IFNAR2 peptide competitors on ovine IFNτ binding to the type I IFN receptor on MDBK cells. Ovine ^{125}I-IFNτ was used at a final concentration of 5 nM. Radioiodine counts from bound ovine ^{125}I-IFNτ were measured after a 2 hour incubation at room temperature. All assays were performed in triplicate with coefficients of variation not greater than 10%. IFNAR2(186-217) represents receptor peptides that did not bind to ovine IFNτ.

was used as a competitor against biotinylated ovine IFNτ, further implicate that ovine IFNτ specifically interacts with the intracellular IFNAR2 peptide IFNAR2(287-315) (Figure 3-21). The dose-dependent inhibition of biotinylated ovine IFNτ binding to immobilized IFNAR2(287-315) by soluble IFNAR2(287-315) also ensures that IFNAR2(287-315) is not significantly altered when in the solid-phase.

Saturation Binding Studies with ^{125}I-Ovine IFNτ Further Reveal Specific Recognition of IFNAR2(287-315)

Saturation binding studies showed that unlabeled ovine IFNτ inhibited ovine ^{125}I-IFNτ binding to IFNAR2(287-315) in a dose-dependent manner (Figure 3-22). The effectiveness of the inhibition of binding of ovine ^{125}I-IFNτ to IFNAR2(287-315) by unlabeled ovine IFNτ was similar to the inhibition of binding to IFNAR2(34-67) (Figure 3-17 and 3-22). Soluble IFNAR2(287-315) potently inhibits ovine IFNτ binding to immobilized IFNAR2(287-315) in a dose-dependent manner, further suggesting that IFNAR2(287-315) is specifically recognized by ovine IFNτ (Figure 3-23). IFNAR2(313-337), an intracellular receptor peptide that was not recognized by ovine IFNτ, had no effect on ovine ^{125}I-IFNτ binding to IFNAR2(287-315) (Figure 3-23).

Determination of Binding Regions on Ovine IFNτ for the Type I IFN Receptor

In previous studies, ovine IFNτ function could be dose-dependently inhibited by ovine IFNτ synthetic peptides; however, receptor binding could not be effectively inhibited [39]. The blocking of function by peptides probably reflected a partial competition; however, it was not sufficient to be detected by binding experiments. The inability of individual ovine IFNτ peptides to block binding of MDBK cells was confirmed using a competition-binding assay on MDBK cells. However, in combination ovine IFNτ peptides IFNτ(1-38), IFNτ(77-119), and IFNτ(118-138) significantly inhibited ^{125}I-IFNτ binding to MDBK cells (Figure 3-24). The addition of IFNτ(153-168) did not increase the efficacy of the combination competitor peptides, further suggesting that IFNτ(153-168) is not essential for receptor interactions (Figure 3-24). It appears that multiple interactions between ovine IFNτ and the type I IFN receptor are necessary.

DISCUSSION

Although the IFNα subtypes elicit biological properties by interacting with the same receptor complex, these subtypes have been shown to vary in antiviral activity [45]. Ovine IFNτ, which also initiates a cellular response through the type I IFN receptor, has been shown to be less toxic to cells when compared to other type I IFNs [1].

Binding studies have shown that the IFNAR2 subunit of the type I IFN receptor directly interacts with the type I IFNs, but IFNAR1 does not bind to the type I IFNs [42]. The data presented here provide insight into sites on IFNAR2 required for ovine IFNτ recognition. Ovine IFNτ bound directly to IFNAR2 extracellular domain peptides IFNAR2(1-38) and IFNAR2(34-67). Consistent with the direct binding studies, the only extracellular domain peptides that dose-dependently blocked ovine IFNτ binding to MDBK cells were IFNAR2(1-38) and IFNAR2(34-67). Together, peptides IFNAR2(1-38) and IFNAR2(34-67) showed synergism in inhibiting ovine IFNτ binding to cells. Consistent with the competitive binding, the receptor peptides alone and in combination inhibited ovine IFNτ antiviral activity with specificity. Therefore, the data suggest that the N-terminus of IFNAR2 is important in the extracellular recognition and antiviral function of ovine IFNτ. The results obtained here should be of considerable value in mutagenic studies of IFNAR2.

The intracellular domain of IFNAR2 was examined for a potential intracellular binding site for ovine IFNτ based on the following rationale. The IFNγ receptor, which belongs to the same class II cytokine receptor family as the type I IFN receptor, has been shown to possess a binding site for IFNγ in the N-terminal region of the cytoplasmic domain of the IFNγR α chain [126]. Analogous to the IFNγ

system, a peptide that correlated to the N-terminus of the cytoplasmic domain of IFNAR2, IFNAR2(287-315), specifically interacted with ovine IFNτ. IFNAR2(287-315) inhibited ovine IFNτ induced antiviral activity and blocked ovine IFNτ binding to the receptor on MDBK cells. Based on this evidence, ovine IFNτ may have an intracellular binding site. IFNAR2(287-315) represents a sequence proximal to the transmembrane region that is inclusive of the JAK1 Box domain and other regions important for JAK1 binding and activation [44]. IFNAR2(265-300), a receptor peptide that lacks the C-terminal 15 amino acids of IFNAR2(287-315), was not recognized by biotinylated ovine IFNτ, suggesting that these 15 residues may be particularly important for ovine IFNτ binding. The competition binding assays performed at 4^{o}C, revealed that IFNAR2(287-315) was blocking binding to extracellular regions of the type I IFN receptor. This suggests that regions within IFNAR2(287-315) may be structurally similar to the extracellular binding domain without being necessary for ovine IFNτ receptor recognition and activity.

In a previous study, functional sites on ovine IFNτ were identified by blocking antiviral and antiproliferative activites [39]. This study identified the N-terminus of type I IFNs as the determinant of toxicity. Paradoxically, although the function of ovine IFNτ could be blocked with ovine IFNτ peptides, receptor binding of ovine IFNτ could not be

inhibited in the previous or the present studies. Based on the previous functional studies, ovine IFNτ appeared to have multiple binding sites for receptor. Peptide binding of an ovine IFNτ binding site on IFNAR2, although blocking function, is not sufficient to inhibit ovine IFNτ interactions with other receptor binding sites. The ability of individual ovine IFNτ peptides to block ovine IFNτ binding to extracellular receptor peptides IFNAR2(1-38) and IFNAR2(34-67), but not binding to whole cells, is consistent with this hypothesis. However, ovine IFNτ binding to receptor on cells was inhibited by the presence of several ovine IFNτ peptides. In combination ovine IFNτ(1-38), IFNτ(77-119), and IFNτ(118-138) dose-dependently blocked ovine IFNτ cell binding; however, none of the peptides blocked binding separately. This probably reflects the role of avidity in ovine IFNτ binding to its receptor on MDBK cells. Most importantly, the ovine IFNτ peptides and competitions in ovine IFNτ binding to receptor peptides and intact receptor on MDBK cells is consistent with previous identification of functional sites on ovine IFNτ through peptide competition functional assays.

Multiple binding regions were also mapped for human IFNα2 to IFNAR2. Residues 26-34, 133, and 144-153, located on the A-B loop, helix D, and helix E, respectively, were shown to be structurally and functionally important [132]. These residues correlate to structurally

and functionally important regions on ovine IFNτ. Residues on helix D, specifically amino acids 135 and 136, appeared to also contribute significantly to the interactions between human IFNβ and IFNAR2; these residues were required for antiproliferative activity on the WISH cell line [133]. In contrast, helix E is not required for the function of human IFNβ on WISH cells. Interestingly, although helix E did not appear to be important for receptor binding by ovine IFNτ on the MDBK cell line, this region contributed to the antiproliferative activity of ovine IFNτ on WISH cells [39]. Interferonα2b was shown to require amino acids within 29-35 and 103-136 for receptor binding [39, 132, 134]. These results correlate with the regions that appear to be necessary for the association of ovine IFNτ with the type I IFN receptor.

Type I IFNs are widely used in therapy or treatment of viral hepatitis, cancer, and autoimmune diseases such as multiple sclerosis. Currently the limiting factors in more extensive and effective use of IFNs in treating the above diseases are the undesirable side effects of the required doses. The structure/function data here may help address this problem. For example, the ovine IFNτ/human IFNαD chimeric based on previous and current peptide studies has only 15 ovine IFNτ residues and is predominantly human IFNαD [135]. This strongly suggests the possibility of novel hybrid type I IFNs for

improved human therapy designed based on data presented here and previous studies.

CHAPTER 4
TOPOGRAPHICAL FATE OF OVINE IFNτ AND THE TYPE I IFN RECEPTOR AS DETERMINED BY INDIRECT FLUORESCENT MICROSCOPY

Ovine IFNτ Colocalizes with the Lysosomal Associated Matrix Protein 1 (LAMP1)

Differential indirect immunofluorescent microscopy was used to illustrate the time course of ovine IFNτ localization in respect to endogenous LAMP-1 in MDBK cells. Because LAMP-1 is exclusive to the lysosomes, the spatial localizations of ovine IFNτ relative to the lysosomal vesicles can be determined. MDBK cells pre-incubated with ovine IFNτ at 4^{o}C were warmed to 37^{o}C for various time intervals. At each time point, the cells were immediately fixed. Ovine IFNτ was indirectly labeled with Alexa Green, a fluorescein derivative, and LAMP-1 was labeled with Texas Red. Therefore, the lysosomes were denoted by the red emissions of LAMP-1 and ovine IFNτ by the green emissions. The overlap of the red and green signals resulted in a yellow coloration, which indicated that ovine IFNτ was proximal to LAMP-1 (Figure 4-1). This suggests that ovine IFNτ trafficked to the lysosomes in MDBK cells. Green emissions diffusely distributed on the cells at Time 0 indicated that ovine IFNτ was initially associated with the cell surface (Figure 4-2A). Ovine IFNτ colocalized with LAMP-1

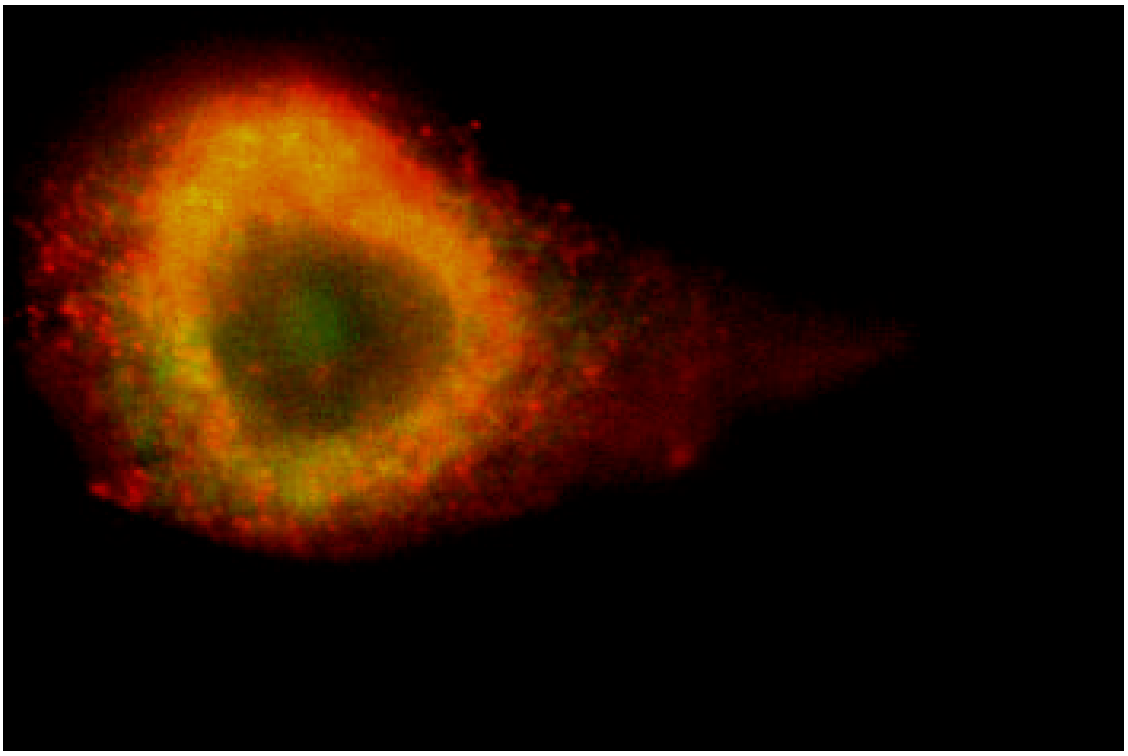

Figure 4-1. Translocation of ovine IFNτ in respect to LAMP-1, a lysosomal protein, at 32 minutes. MDBK cells were grown overnight in chambered glass slides (Lab-Tek). Cells were stimulated with 5000 U/mL of ovine IFNτ and incubated at 4°C for 2 hours; the units per milliliter were standardized by the antiviral activity of the FDA approved human IFNα, Roferon. Cells were then transferred to a 37°C incubator for the indicated time intervals. After fixation with 2% paraformaldehyde, cells were treated with antibodies against ovine IFNτ and LAMP-1 in 0.1% saponin to permeabilize the cells. After three vigorous washings with the saponin:BSA:PBS solution, cells were treated with secondary antibodies to ovine IFNτ (Alexa Green) and LAMP-1 (Texas Red), also in the presence of saponin as the permeabilization is temporary. The cell was viewed using a Zeiss fluorescent microscope at a 63X magnification.

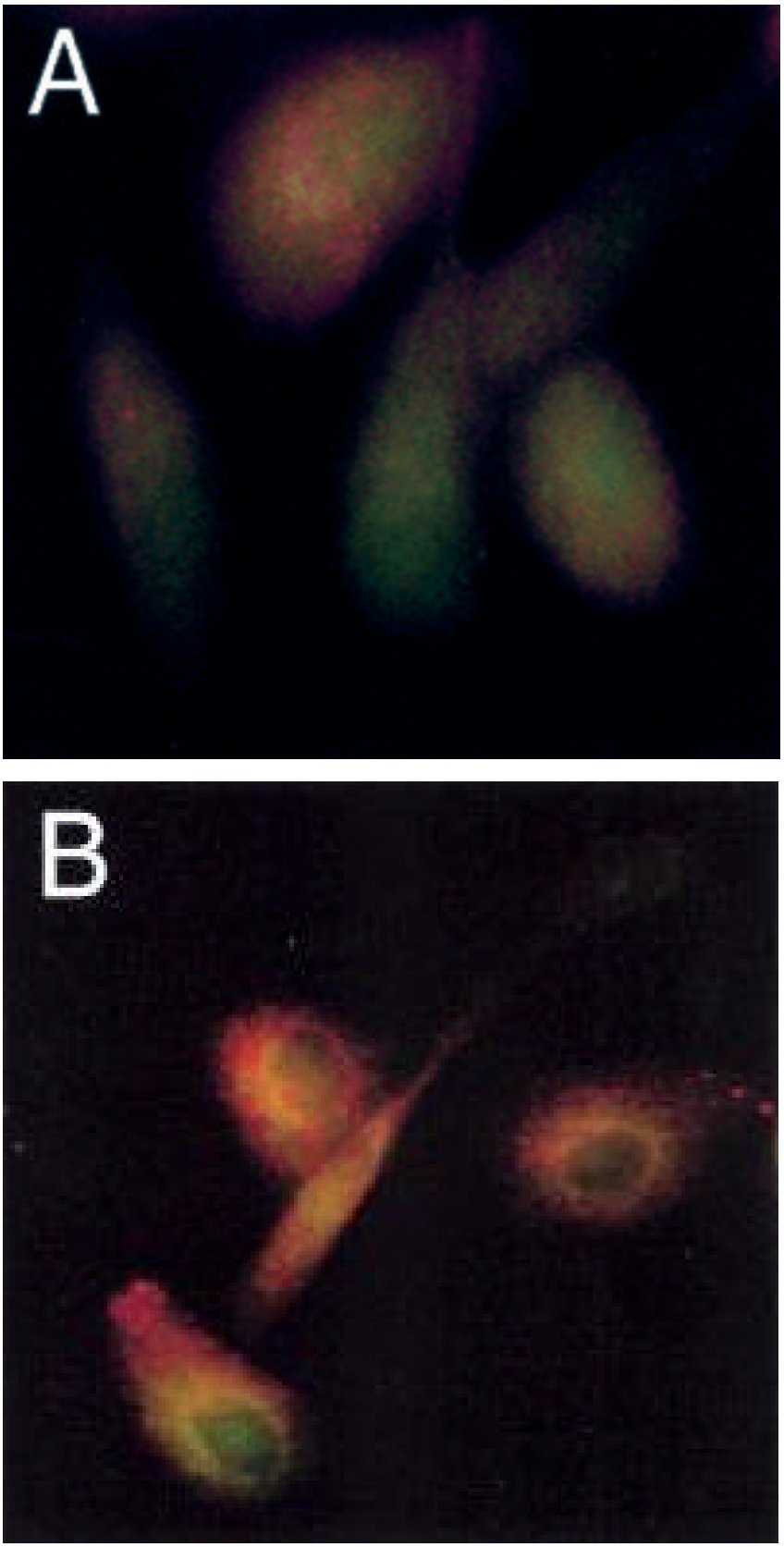
A
B

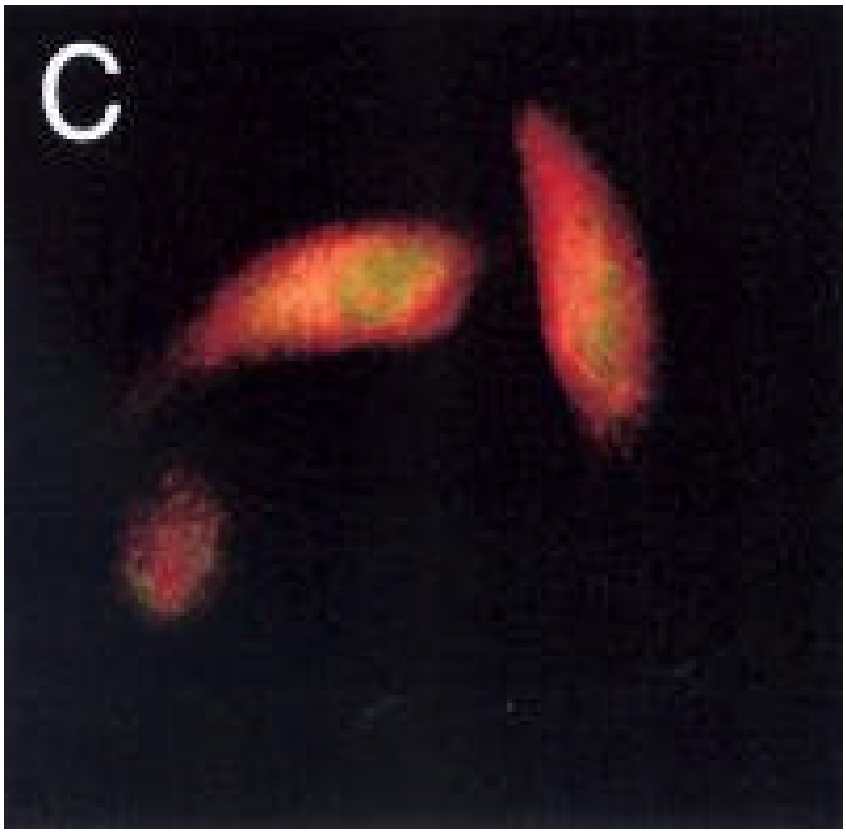
C

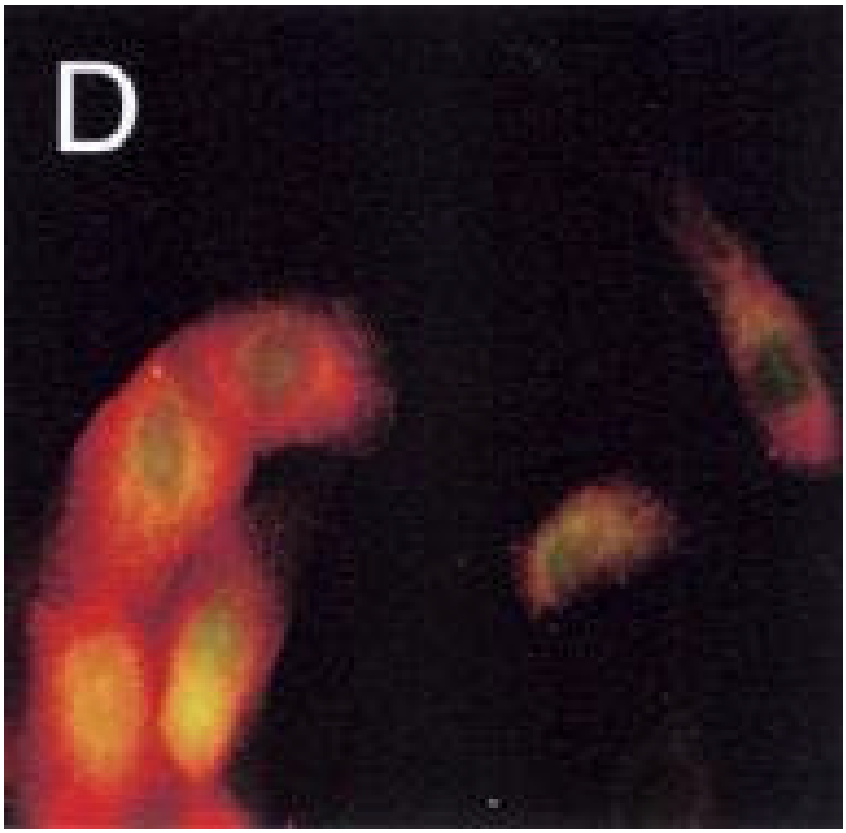
D


E

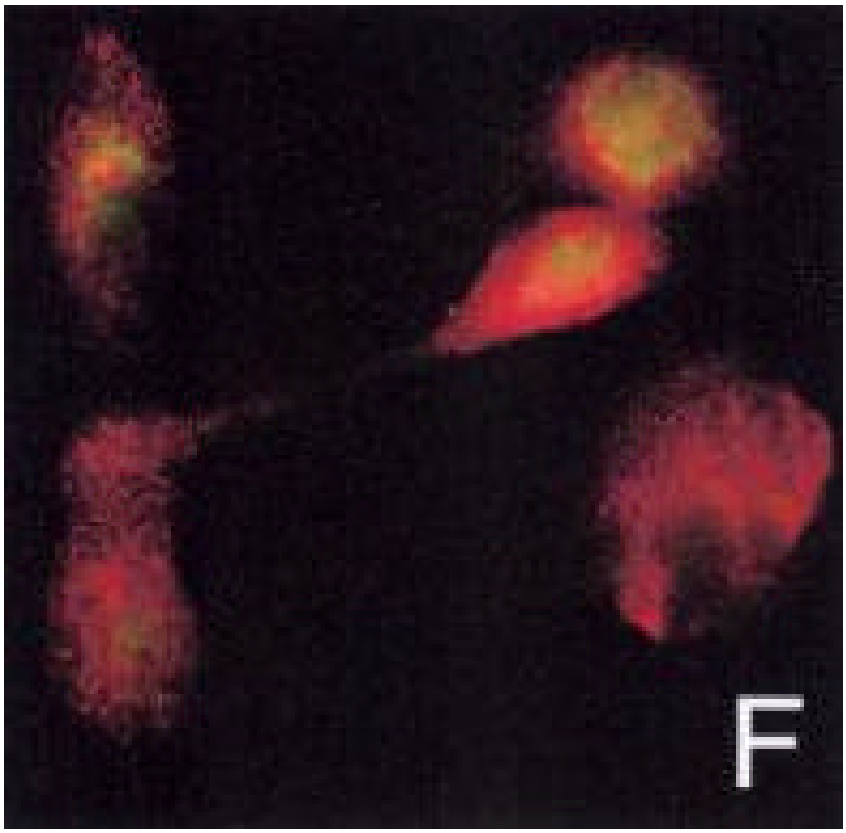
F

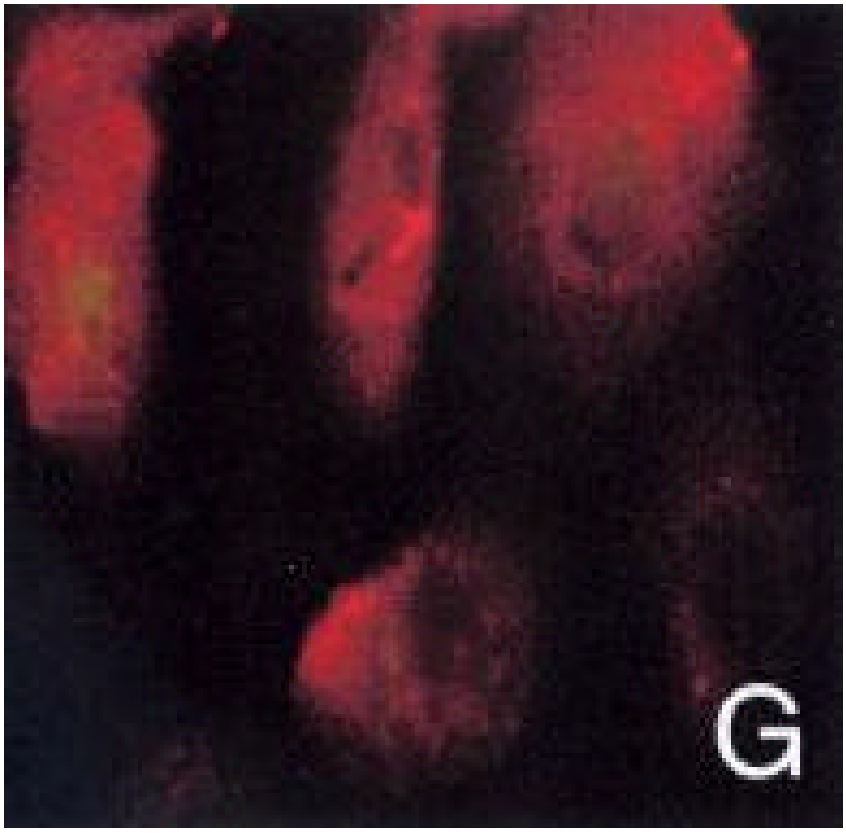

Figure 4-2. Time-dependent translocation of ovine IFNτ in respect to LAMP-1, a lysosomal protein, following ovine IFNτ treatment as shown by indirect immunofluorescence. MDBK cells were grown overnight in chambered glass slides (Lab-Tek). Cells were stimulated with 5000 U/mL of ovine IFNτ and incubated at 4°C for 2 hours; the units per milliliter were standardized by the antiviral activity of the FDA approved human IFNα, Roferon. Cells were then transferred to a 37°C incubator for the indicated time intervals. After fixation with 2% paraformaldehyde, cells were treated with antibodies against ovine IFNτ and LAMP-1 in 0.1% saponin to permeabilize the cells. After three vigorous washings with the saponin:BSA:PBS solution, cells were treated with highly cross-absorbed polyclonal goat anti-mouse secondary antibody coupled to Alexa Green (Molecular Probes) and highly cross-absorbed polyclonal goat anti-rabbit secondary antibody coupled to Texas Red (Molecular Probes) to label ovine IFNτ and LAMP1, respectively. These secondary antibodies were added in the presence of saponin as the permeabilization is temporary. Cells were viewed using a Zeiss fluorescent microscope at a 63X magnification. (A) Localization of ovine IFNτ at 0 minutes. (B) Localization of ovine IFNτ at 4 minutes. (C) Localization of ovine IFNτ at 8 minutes. (D) Localization of ovine IFNτ at 16 minutes. (E) Localization of ovine IFNτ at 32 minutes. (F) Localization of ovine IFNτ at 60 minutes. (G) Localization of ovine IFNτ at 120 minutes.

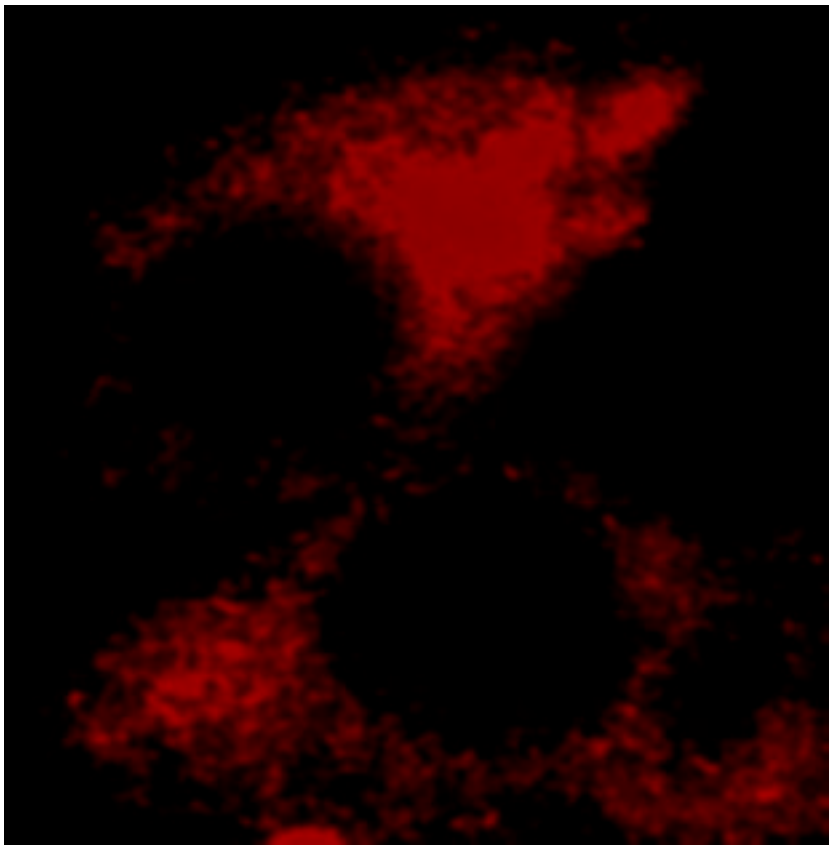

Figure 4-3. The indirect immunofluorescence of LAMP-1. MDBK cells were grown overnight in chambered glass slides (Lab-Tek). Cells were incubated at 4°C for 2 hours. After fixation with 2% paraformaldehyde, cells were treated with antibodies against LAMP-1 in 0.1% saponin to permeabilize the cells. After three vigorous washings with the saponin:BSA:PBS solution, cells were treated with highly cross-absorbed polyclonal goat anti-rabbit secondary antibody coupled to Texas Red (Molecular Probes) to fluorescently label LAMP-1. The secondary antibody was added in the presence of saponin, as the permeabilization is temporary. Cells were viewed using a Zeiss fluorescent microscope at a 63X magnification.

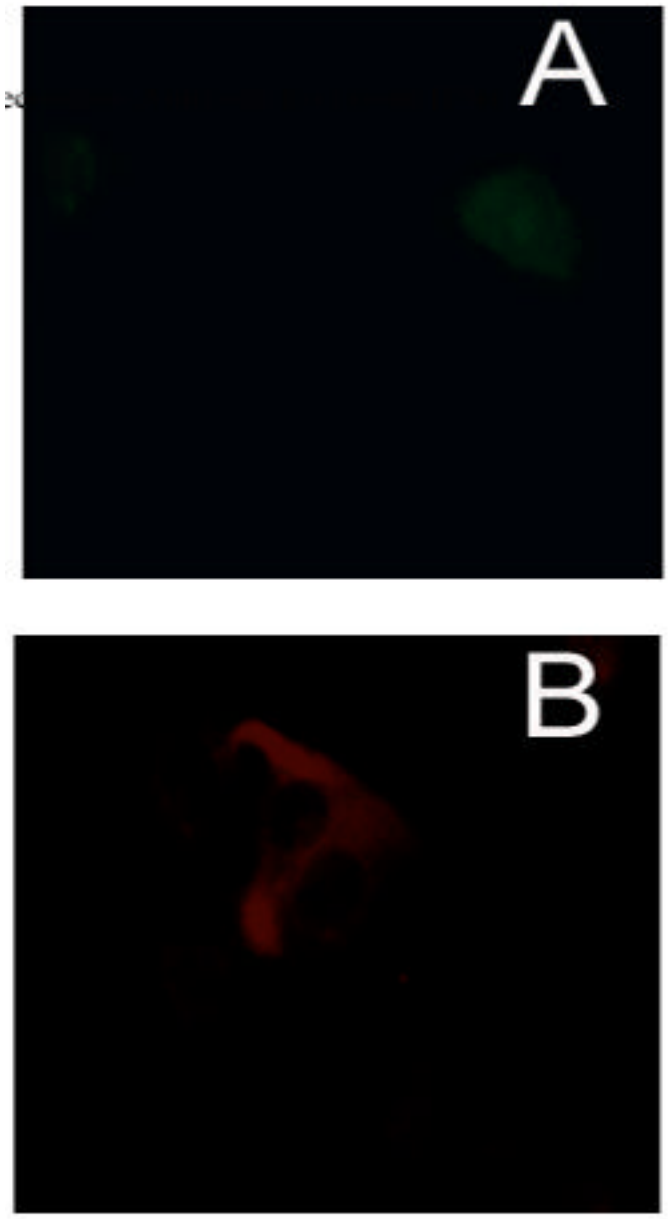

Figure 4-4. MDBK cells treated only with secondary antibodies against primary antibodies specific for (A) ovine IFNτ and (B) LAMP-1. MDBK cells were grown overnight in chambered glass slides (Lab-Tek). Cells were incubated at 4°C for 2 hours. Cells were fixed with 2% paraformaldehyde. Cells were treated with highly cross-absorbed polyclonal goat anti-mouse secondary antibody coupled to Alexa Green (Molecular Probes) specific for ovine IFNτ and highly cross-absorbed polyclonal goat anti-rabbit secondary antibody coupled to Texas Red (Molecular Probes) specific for LAMP-1, in the presence of saponin as the permeabilization is temporary. Cells were viewed using a Zeiss fluorescent microscope at a 63X magnification.

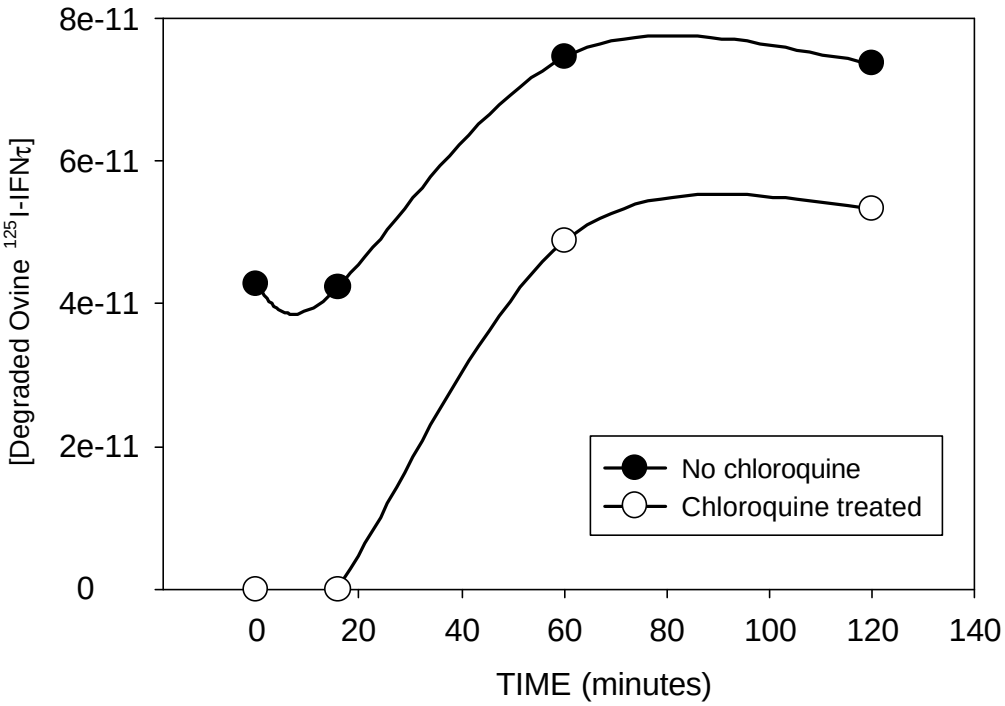

Figure 4-5. Concentration of degraded ovine ^{125}I-IFNτ from 100 μM final concentration of chloroquine-treated MDBK cells. MDBK cells grown to near confluency in 150 cm^2 flasks were treated with a final concentration of 100μM chloroquine in 10 mLs of 10% FBS MEM or 10 mLs of 10% FBS MEM with no chloroquine. The cells were then incubated for 4 hours at 37°C, scraped from the flasks and resuspended in 35 mLs of MEM. The cells were then treated with a final concentration of 0.5 nM of ovine ^{125}I-IFNτ. Cells were incubated on a rocker for 7 hours at 4°C to allow ovine ^{125}I-IFNτ to bind. Cells were aliquoted at a quantity of 2.7 x 10^6 cells/mL to represent the time intervals of 37°C incubation. The specific time intervals were 0, 15, 60, and 120 minutes. The sets of cells were then placed into a 37°C water bath for the specified times. Cells were then removed from the bath at appropriate times and were pelleted using centrifugation. Following centrifugation, each of the 1 mL supernatant fluids was aspirated and treated with 200 μg of BSA followed by a 10% final volume of TCA to precipitate intact ligand, leaving degraded ligand in solution. The TCA treated supernatants were incubated overnight at 4°C to ensure proper separation of degraded and intact ligand.

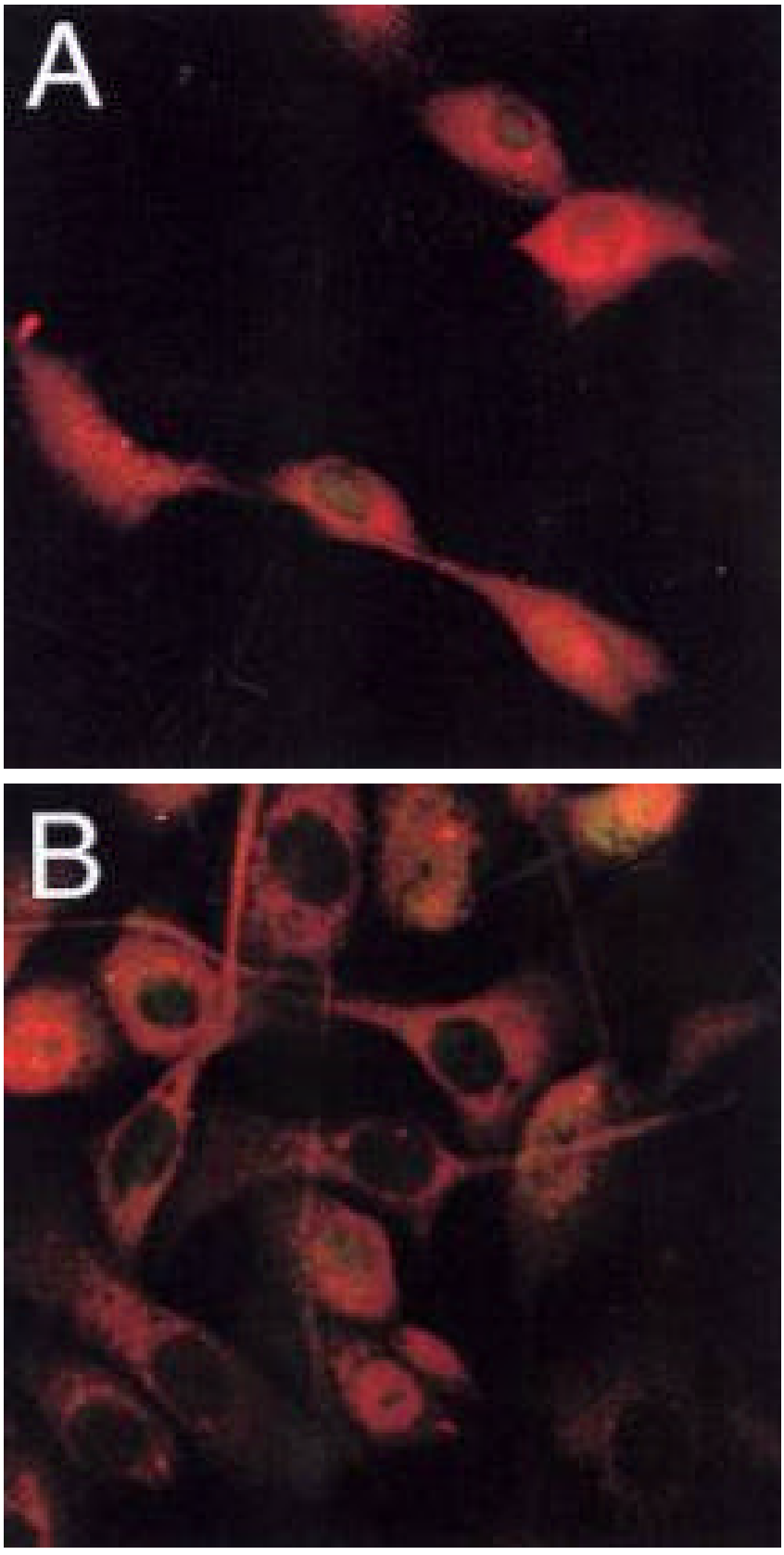
A
B

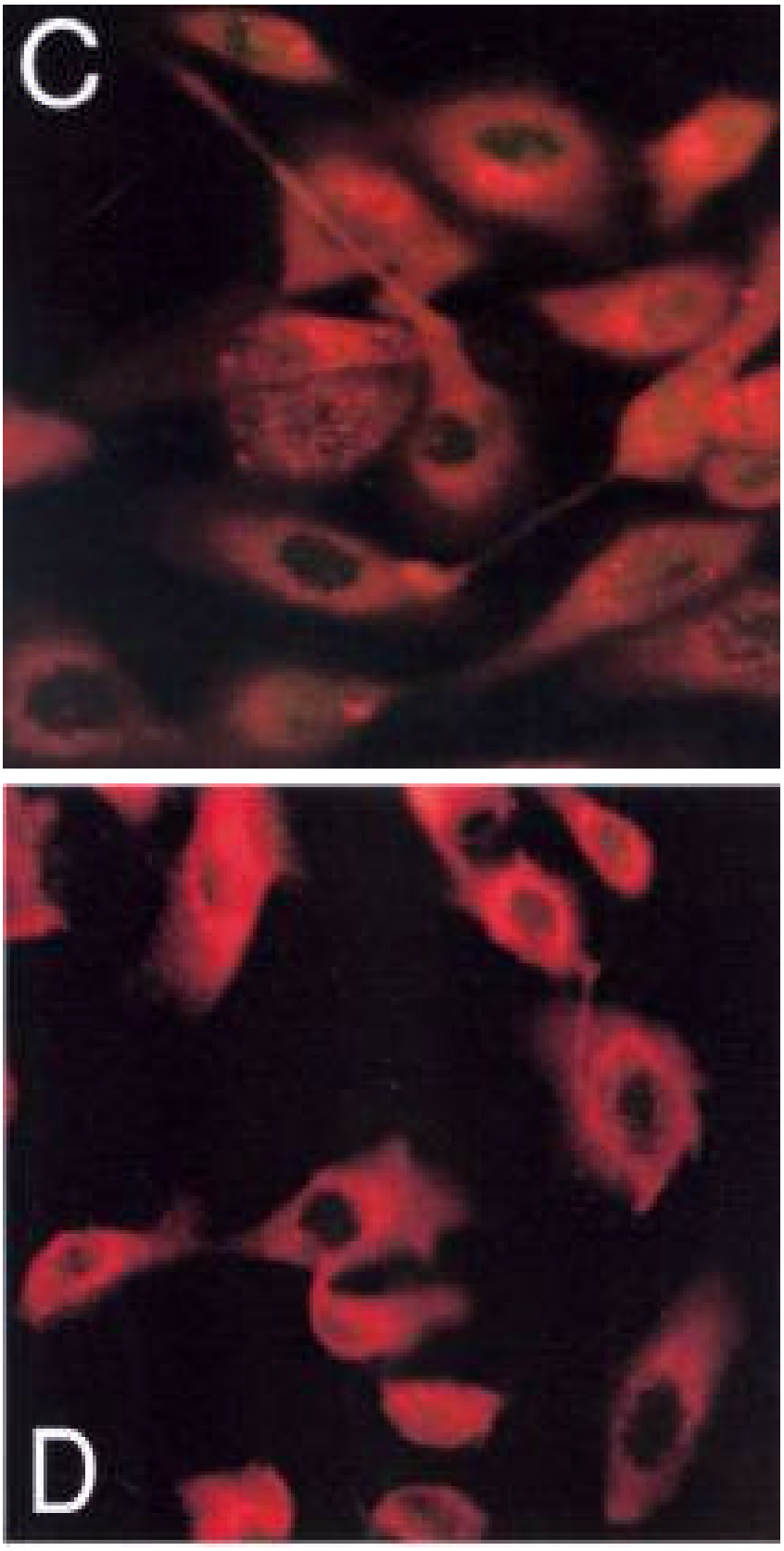
C
D

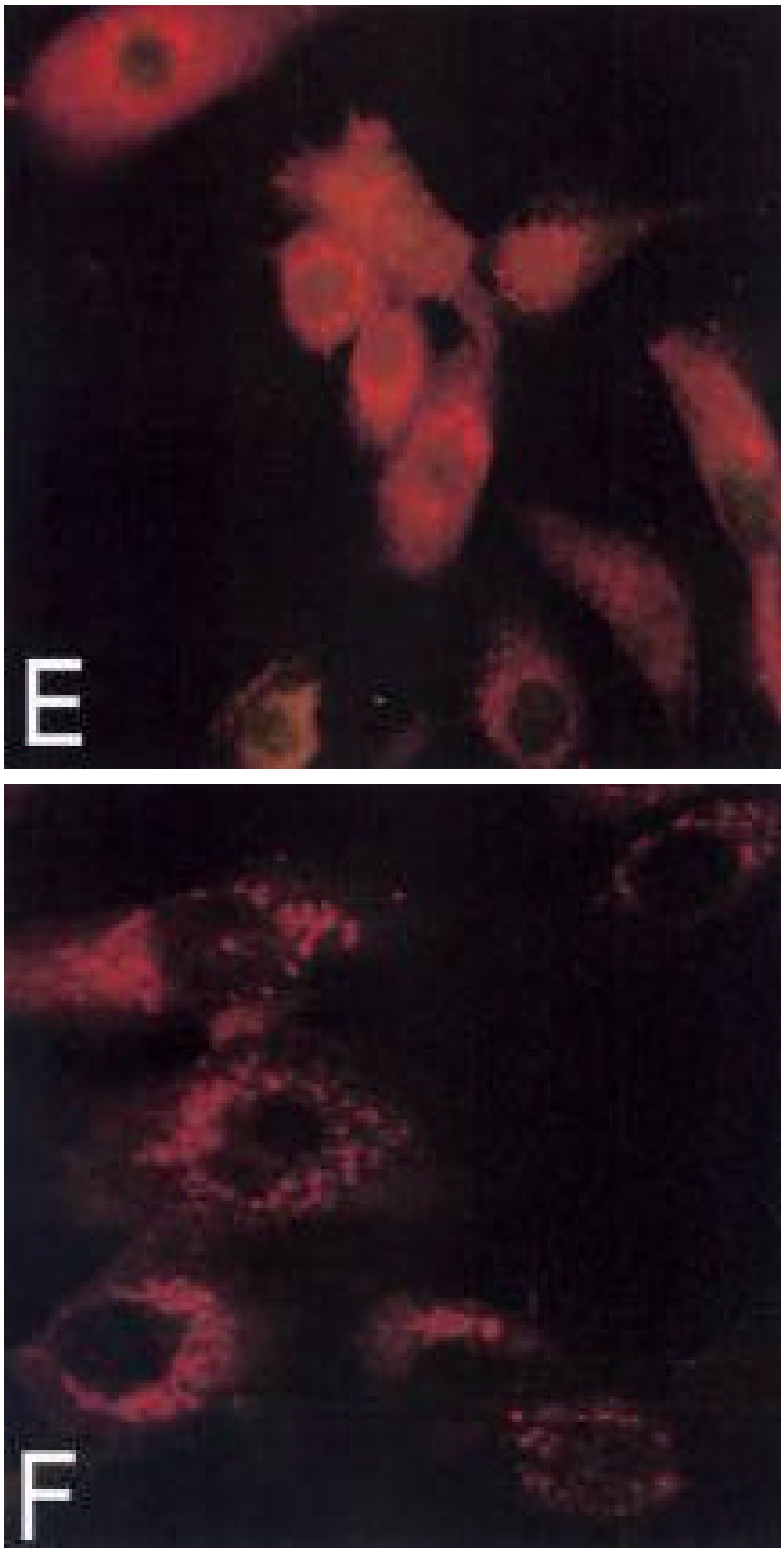
E
F

Figure 4-6. Time-dependent translocation of IFNAR2 following ovine IFNτ treatment as shown by indirect immunofluorescence. MDBK cells were grown overnight in chambered glass slides (Lab-Tek). Cells were stimulated with 5000 U/mL of ovine IFNτ and incubated at 4°C for 2 hours; the units per milliliter were standardized by the antiviral activity of the FDA approved human IFNα, Roferon. Cells were then transferred to a 37°C incubator for the indicated time intervals. After fixation with 2% paraformaldehyde, cells were treated with rabbit anti-IFNAR2 in the presence of 0.1% saponin to permeabilize the cells. After three vigorous washings with the saponin:BSA:PBS solution, cells were treated with goat anti-rabbit secondary antibodies conjugated to Texas Red in 0.1% saponin, as the permeabilization is temporary. Cells were viewed using a Zeiss fluorescent microscope at a 40X magnification. (A) Localization of IFNAR2 at 0 minutes. (B) Localization of IFNAR2 at 8 minutes. (C) Localization of IFNAR2 at 16 minutes. (D) Localization of IFNAR2 at 32 minutes. (E) Localization of IFNAR2 at 60 minutes. (F) Localization of IFNAR2 at 120 minutes.

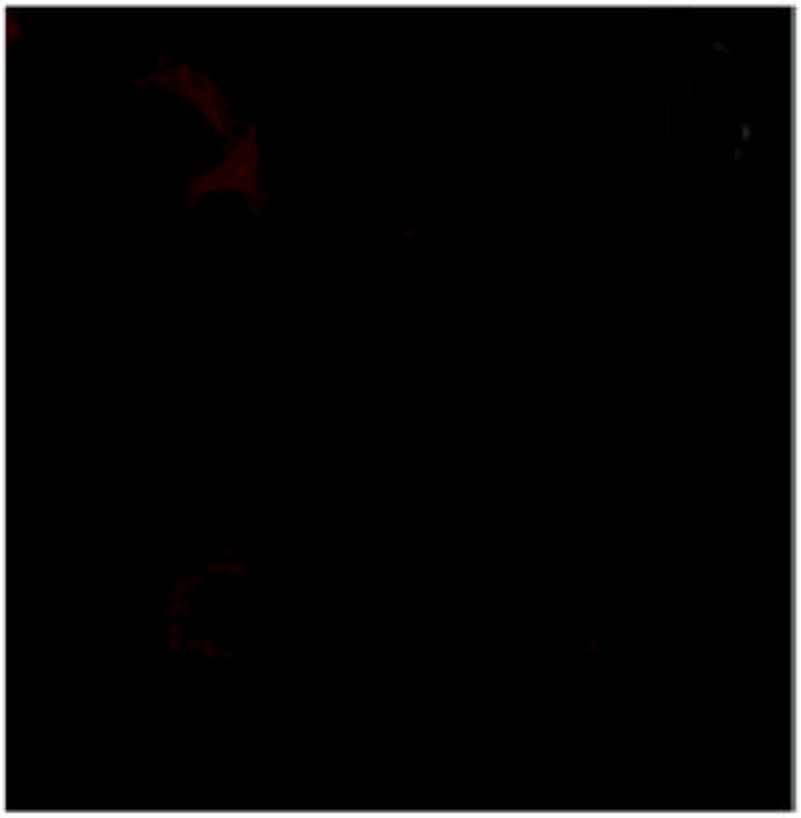

Figure 4-7. MDBK cells treated only with secondary antibodies that were against primary antibodies specific for IFNAR2. MDBK cells were grown overnight in chambered glass slides (Lab-Tek). Cells were incubated at 4°C for 2 hours. Cells were fixed with 2% paraformaldehyde. Cells were treated with goat anti-rabbit secondary antibodies conjugated to Texas Red in 0.1% saponin:BSA:PBS solution. Cells were viewed using a Zeiss fluorescent microscope at a 40X magnification.

within 8 minutes, as seen by the yellow coloration in figures 4-2B and 4-2C. Ovine IFNτ continued to colocalize with LAMP-1 at 16 and 32 minutes, suggesting that ovine IFNτ was trafficking to the lysosomes (Figures 4-2D and 4-2E). After 1 hour very little ovine IFNτ appeared to be associated with the lysosomes and at two hours little ovine IFNτ was detectable, suggesting that ovine IFNτ was degraded (Figure 4-2F and 4-2G).

Ovine IFNτ Appears to be Degraded in the Lysosomes

Previous studies showed that human IFNαA degradation could be blocked by the addition of chloroquine, a lysomotropic agent. This suggests that human IFNαA is internalized and degraded by lysosomes within the cells [76]. Ovine IFNτ degradation was also inhibited by the treatment of MDBK cells with chloroquine (Figure 4-5). The p-value derived from a Student paired t-test was 0.01, suggesting that the inhibition of degradation of ovine IFNτ in MDBK cells by chloroquine treatment is significant [136]. These results, in combination with the results from the indirect fluorescent studies, suggest that ovine IFNτ, like human IFNαA, is degraded in the lysosomes.

IFNAR2 is Internalized in MDBK Cells Following Ovine IFNτ Stimulation

In ovine IFNτ treated cells, fluorescent microscopy showed that the major binding subunit of the type I IFN receptor, IFNAR2 was

internalized following ligand occupancy. By 16 minutes, internalization was apparent (Figure 4-4A, 4-4B, 4-4C) and within 32 minutes IFNAR2 localized to a perinuclear region (Figure 4-4D). However, it appeared that some IFNAR2 remained or was recycled back to the surface prior to one hour of incubation as shown by the diffuse coloration covering the cells [139]. Within one hour, IFNAR2 further accumulated in the perinuclear region and the pattern had a tubular appearance (Figure 4-4E). IFNAR2 appeared to be in microtubules, possibly microtubular extensions of the endosomes or of the trans-Golgi network (TGN). It appears that in some cells, IFNAR2 moved to a more vesicular compartment within one hour, as evident by the punctuate appearance of the red emissions. Within two hours, IFNAR2 appears to traffic to the lysosomes (Figure 4-4F). The fluorescently-labeled IFNAR2 molecules form a pattern typical of homogenously labeled lysosomes [139]. This suggests that IFNAR2 enters the lysosomes of MDBK cells to be degraded.

Discussion

Previous studies have shown that human IFNαA binding to the type I IFN receptor on Daudi cells following stimulation with human IFNαA and IFNβ was reduced by approximately 85% [74]. In addition, biochemical studies showed that occupancy of the type I interferon receptor by IFNα and IFNβ gradually began to decrease after thirty

minutes of interferon treatment. This decrease was attributed to the down regulation of the type I IFN receptor, which is the removal of ligand bound receptors from the cell membrane by internalization without immediate replenishment of the receptor population. In alternative studies receptor binding was significantly inhibited by the addition of low doses of unlabeled human IFNαA on the order of 0.5 U/mL [75]. This suggested that fractional occupancy of the receptors by human IFNαA appeared to either desensitize or down-regulate the type I IFN receptors considerably. Reinsertion of surface-bound type I IFN receptors was significantly prevented by the addition of cycloheximide. Protein synthesis appears to be necessary to replenish the receptor population internalized via receptor-mediated endocytosis.

Once internalized, ligand and receptor may be processed independently by the cells. Several receptors have been shown to transfer to the perinuclear trans-Golgi network (TGN) from endosomal or lysosomal compartments [87-89]. Like the early endosomes, the TGN is connected to the secretory/recycling pathway as well as the degradative pathway [90].

Human ^{125}I-IFNαA was internalized and degraded by Daudi cells [74]. In separate experiments, the cells were treated with chloroquine or methylamine, both lysomotropic agents. Both agents inhibited the

degradation of human IFNαA, suggesting that this ligand is degraded in the lysosomes. Biochemical studies that determined the rates of endocytosis and hydrolysis separately suggested that human IFNαA is degraded in several cell lines, such as A375, A549, Daudi and MDBK. In addition, an accelerated internalization rate of the ligand-occupied receptors also appeared to cause receptor down-regulation [75, 76]. The present study suggests that like human IFNαA, ovine IFNτ is internalized by MDBK cells and traffics to the lysosome, where it is ultimately degraded. Elucidating the processing of ovine IFNτ and the type I IFN receptor may provide important insight into the ligand and receptor dynamics required for a cellular response to the type I IFNs.

CHAPTER 5
BINDING, INTERNALIZATION, AND PROCESSING OF OVINE IFNτ, HUMAN IFNαA, AND THE TYPE I IFN RECEPTOR BY MDBK CELLS: A COMPARATIVE BIOCHEMICAL ANALYSIS

Equilibrium Binding of Ovine IFNτ and Human IFNαA to the Type I IFN Receptor on MDBK Cells

To gain insight into the interactions between human IFNαA and ovine IFNτ at the surface of MDBK cells, equilibrium binding assays were performed. As discussed in the materials and methods, cell suspensions were treated with either radiolabeled human IFNαA or ovine IFNτ in increasing concentrations and then allowed to incubate at 4^{o}C to reach equilibrium. Free ligand was separated from the bound ligand by centrifugation. Radioligand concentrations were determined via measurements on a gamma counter. Unlabeled human IFNαA and ovine IFNτ in excess competed with specific binding of their radiolabeled counterparts to reveal the nonspecific binding. The nonspecific binding was subtracted from the total binding to determine values of specific binding. Scatchard analysis revealed the equilibrium association constant (K_a), the equilibrium dissociation constant (K_d), and the maximum concentration of surface-bound receptors (B_{max}), which allowed the comparison of the aspects of cell surface binding of

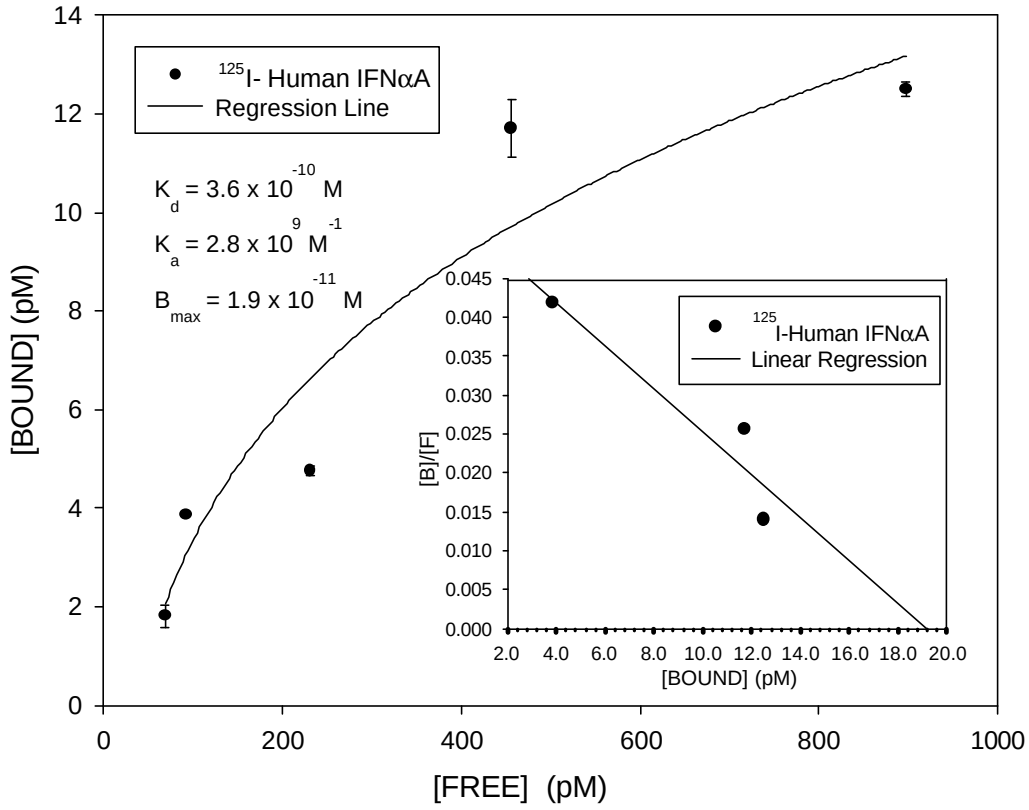

Figure 5-1. The equilibrium surface binding of human IFNαA to MDBK cells as determined by (A) Scatchard analysis and (B) nonlinear regression analysis. Cultures of 2.5 x 10^6 MDBK cells/mL were incubated at 4°C for 9 hours with increasing concentrations of ^{125}I-human IFNαA. Surface bound ligand was separated from free ligand by centrifugation for 10 seconds. The supernatant was removed to determine $[L]_f$. Surface-bound ligand remained on the cell pellets. Non-specific binding was subtracted from total binding to reveal specific binding.

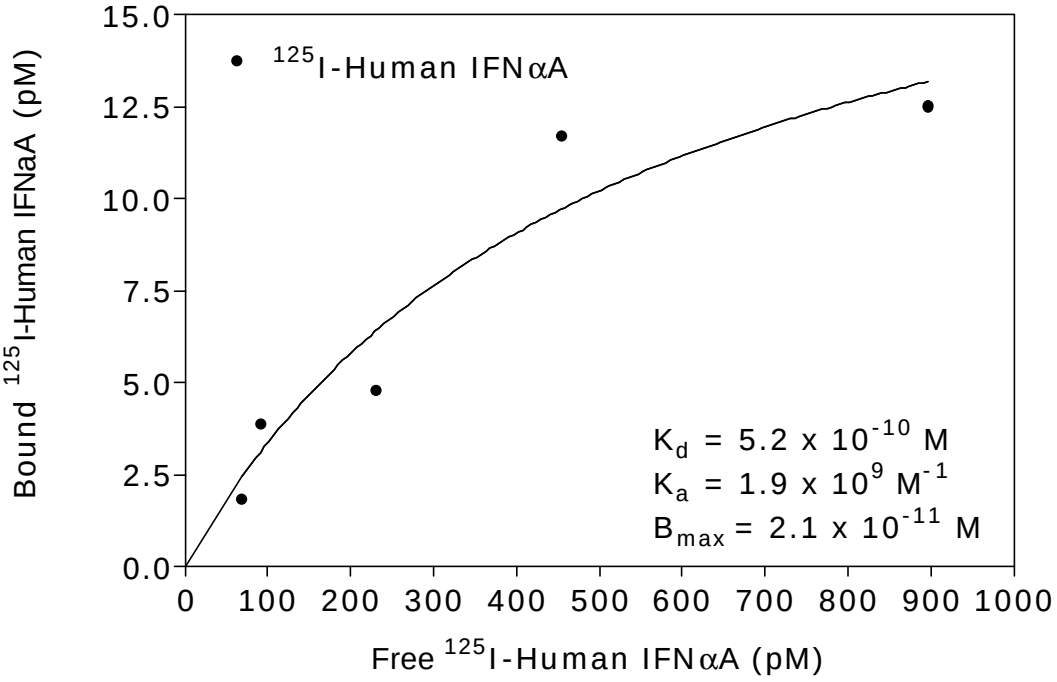
15.0
12.5
10.0
7.5
5.0
2.5
0.0
Bound 125I-Human IFNaA (pM)
125I-Human IFNαA
Kd = 5.2 x 10-10 M
Ka = 1.9 x 109 M-1
Bmax = 2.1 x 10-11 M
0 100 200 300 400 500 600 700 800 900 1000
Free 125I-Human IFNαA (pM)

Figure 5-1B.

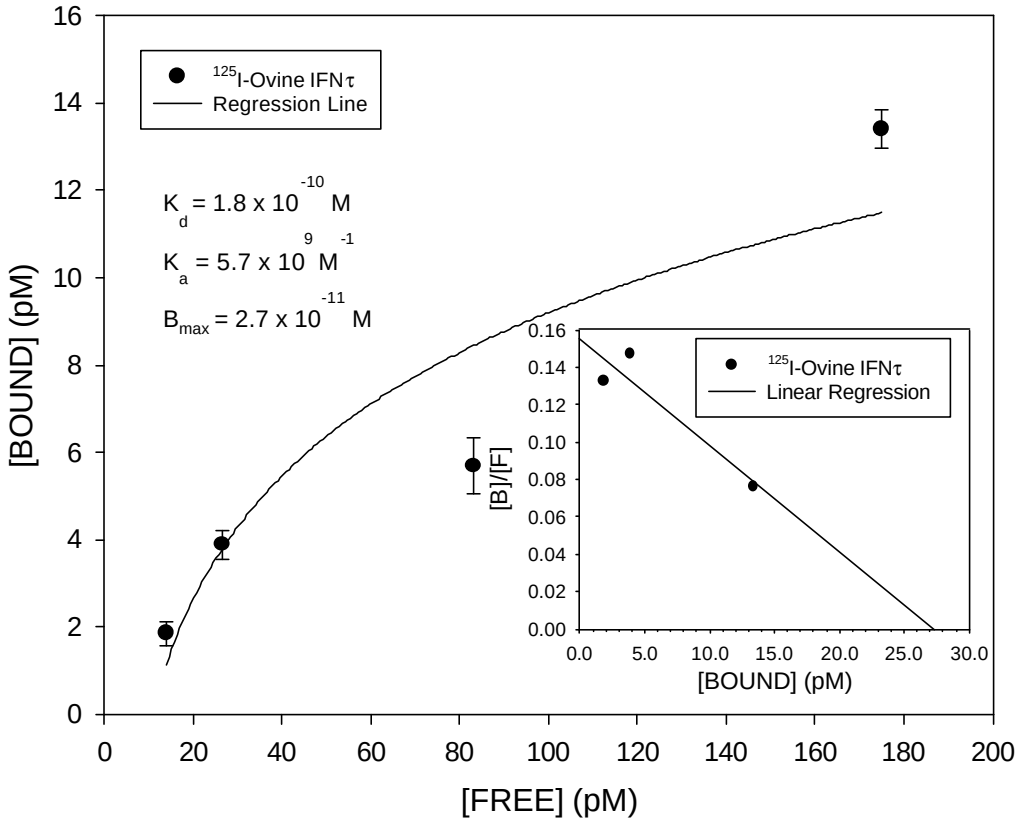

Figure 5-2. The equilibrium surface binding of ovine IFNτ to MDBK cells as determined by (A) Scatchard analysis and (B) nonlinear regression analysis. Cultures of 2.5 x 10^6 MDBK cells/mL were incubated at 4°C for 9 hours with increasing concentrations of ^{125}I-ovine IFNτ. Surface bound ligand was separated from free ligand by centrifugation for 10 seconds. The supernatant was removed to determine $[L]_f$. Surface-bound ligand remained on the cell pellets. Non-specific binding was subtracted from total binding to reveal specific binding.

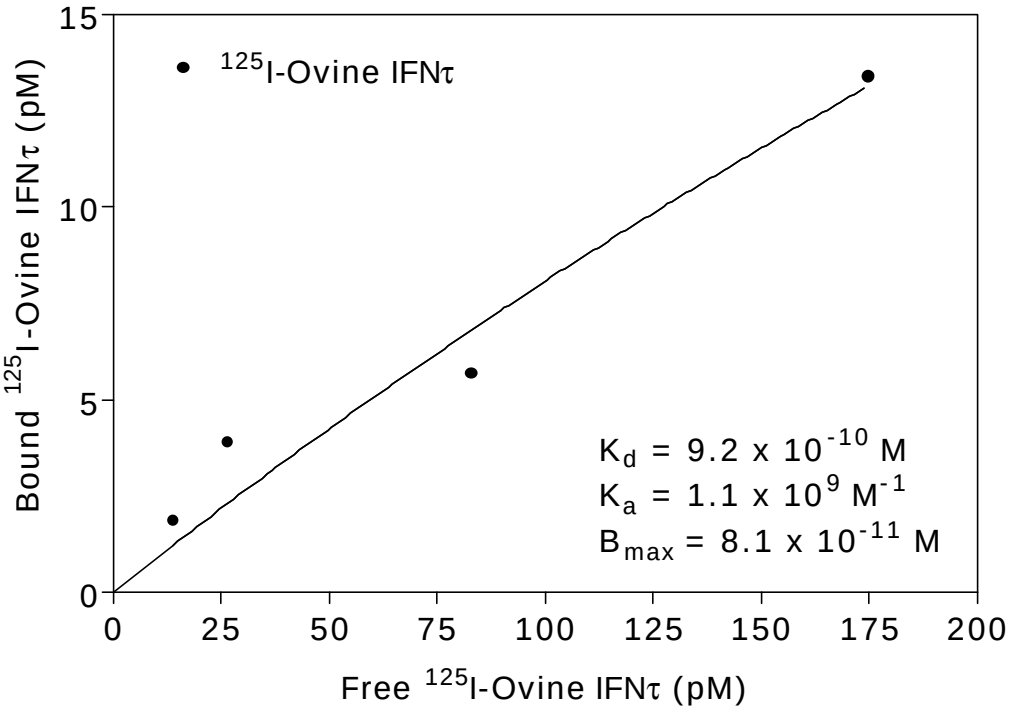
15
10
5
0
0
25
50
75
100
125
150
175
200
^{125}I-Ovine IFNτ
Bound ^{125}I-Ovine IFNτ (pM)
Free ^{125}I-Ovine IFNτ (pM)
K_d = 9.2 x 10^{-10} M
K_a = 1.1 x 10^{9} M^{-1}
B_{max} = 8.1 x 10^{-11} M

Figure 5-2B.

human IFNαA and ovine IFNτ to the type I IFN receptor. For human IFNαA, the K_a, K_d and B_{max} were 2.8 x 10^{9} M^{-1}, 3.6 x 10^{-10} M, and 1.9 x 10^{-11} M, respectively (Figure 5-1A). For ovine IFNτ, the K_a equaled 5.7 x 10^{9} M^{-1}, the K_d was 1.8 x 10^{-10} M, and the B_{max} was 2.7 x 10^{-11} M (Figure 5-2A). The residuals squared (r^2) of the linear regressions of the Scatchard plots were 0.88 and 0.87. Residuals are the difference between the observed points and the predicted linear regression. The r^2 value indicates the goodness of the fit. As r^2 approaches one, the predicted regression line approaches the observed data [136]. The B_{max} values of human IFNαA and ovine IFNτ were comparable which gives evidence that these ligands bind to the same receptor complex. The binding affinity of ovine IFNτ for the type I IFN receptor on MDBK cells appears to be slightly greater than that of human IFNαA according to the K_a and K_d values. However, homogeneity of regression analysis indicated that the slopes of the Scatchard plots were not independent from one another [136]. This suggests that the equilibrium binding constants, which are derived from the slope of the Scatchard plots, are not significantly different. Therefore, the binding affinities of human IFNαA and ovine IFNτ for the type I IFN receptor on MDBK cells appear to be similar.

Although Scatchard analysis is commonly employed to acquire binding constants, the linear transformation of nonlinear data has

disadvantages that may affect the accuracy of the values. For example, the data points are not evenly weighted in their effect on the linear regression of the transformed data. Saturation binding data points transformed from the lowest concentrations and concentrations approaching saturation of free ligand have a greater effect on the slope of the Scatchard graph than points transformed from the curvilinear area of the saturation-binding curve. Another drawback of the Scatchard plot is that it requires the use of its x-axis values, the concentrations of bound radioligand, to calculate the y-axis values, the concentrations of bound radioligand divided by free radioligand [77]. Therefore, to minimize these concerns, the equilibrium binding results were determined using nonlinear regression analysis of the saturation binding curves [77, 101]. The K_d and K_a of human IFNαA were 5.2×10^{-10} M and 1.9×10^{9} M^{-1}, respectively (Figure 5-1B). The K_d and K_a of ovine IFNτ were 9.2×10^{-10} M and 1.1×10^{9} M^{-1}, respectively (Figure 5-2B). The values produced by the nonlinear regression of the saturation-binding curve were of the same order of magnitude as those of the Scatchard analysis. In contrast to the equilibrium constants derived using a linear regression, the values obtained using the nonlinear regression model suggests that human IFNαA may interact with the type I IFN receptor with a slightly higher affinity than ovine IFNτ. However, homogeneity regression analysis showed that

the regression lines of the nonlinear model, like the linear model, were best represented by a single line. Therefore, these data suggest that the binding constants and affinities of human IFNαA and ovine IFNτ for the type I IFN receptor are not different.

The Dissociation Rate Constant (k_d) of Ovine IFNτ and Human IFNαA from the Type I IFN Receptor on MDBK Cells

The physiologically relevant ligand and receptor dynamics for ovine IFNτ and the type I IFN receptor in MDBK cells were compared to those of human IFNαA. To determine the rates of dissociation of ovine IFNτ and human IFNαA, the cells were treated with constant concentrations of the radiolabeled ligands and incubated at 37^{o}C for specified time intervals. After completion of each timed incubation, the cell suspensions were centrifuged at 4^{o}C, separating the free IFNs from receptor-bound IFNs. The surface-bound ligand was then segregated from the internalized ligand by the addition of an acidic buffer to the cell pellets. The k_d values were determined as the slope of the natural log of the concentration of surface-bound ligand at each specific time interval divided by the concentration of surface-bound ligand at time zero. The k_d of human IFNαA and membrane-bound type I IFN receptor on MDBK cells was 1.0×10^{-2} min^{-1} +/- 1.4×10^{-3} min^{-1} (Figure 5-3). The residual squared (r^2) of the line was equal to 0.97. The k_d of ovine IFNτ and the type I IFN receptor appeared to be

equivalent to the rate of dissociation of human IFNαA from the type I IFN receptor. Ovine IFNτ dissociated from the receptor at a rate of 1.2×10^{-2} min^{-1} +/- 4.5×10^{-3} min^{-1} (Figure 5-4). The plot used to determine the k_d of ovine IFNτ and the type I IFN receptor had a r^2 of 0.78.

The p-values of the linear plots used to obtain the dissociation rate constants of human IFNαA and ovine IFNτ from MDBK cells were 0.0001 and 0.0019, respectively; therefore, both plots were best described as linear equations. The linearity of the plots suggests that human IFNαA and ovine IFNτ bind only to one population of receptor. This is consistent with previous studies that indicate that human IFNαA and ovine IFNτ only specifically interact with the type I IFN receptor [42, 43, 47]. The linear plots also suggest that no changes in binding affinity for either human IFNαA or ovine IFNτ to the type I IFN receptor occurred as the incubation time progressed.

Association Rate Constants (k_a) of Ovine IFNτ and Human IFNαA from the Type I IFN Receptor on MDBK Cells

The human IFNαA and ovine IFNτ association rate constants (k_a) were then calculated by dividing the respective k_d values by the equilibrium dissociation constants (K_d). Equilibrium dissociation constants were derived using nonlinear regression analysis of a

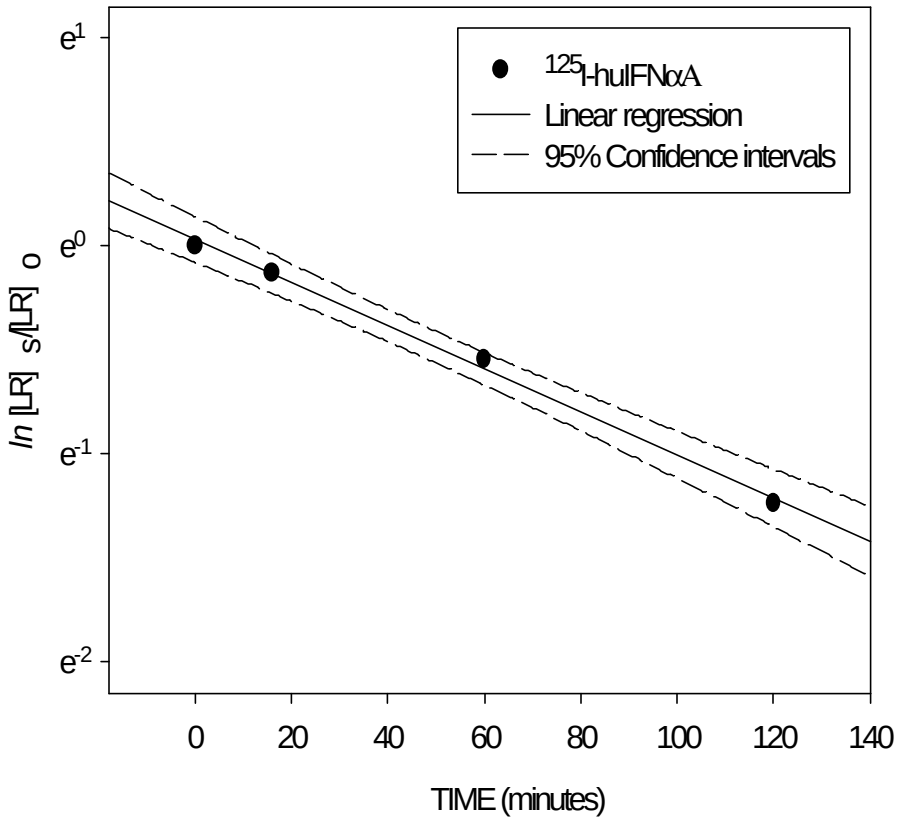

Figure 5-3. The k_d of human IFNαA and the type I IFN receptor on MDBK cells. Cultures of 2.7 x 10^6 MDBK cells/mL were incubated at 4°C for 7 hours with ^{125}I-human IFNαA at a final concentration of 0.5 nM. Cells were then placed at 37°C for the specified time intervals. Surface-bound ligand was removed with a pH 4.0, glycine buffer. Nonspecific binding was determined in a parallel set of cells with the addition of a 200-fold excess of unlabeled human IFNαA. The k_d of ovine IFNτ and the type I IFN receptor on MDBK cells was determined to be 1.0 x 10^{-2} min^{-1} +/- 1.4 x 10^{-3} min^{-1}. The r^2 of the plotted line was 0.97.

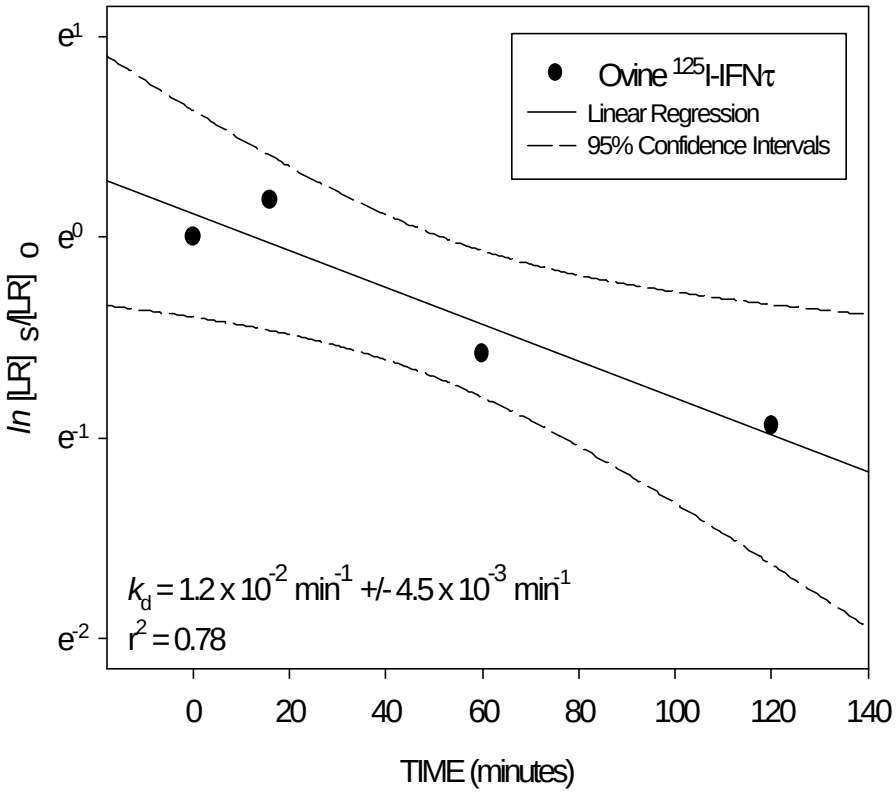

Figure 5-4. The k_d of ovine IFNτ and the type I IFN receptor on MDBK cells. Cultures of 2.7 x 10^6 MDBK cells/mL were incubated at 4°C for 7 hours with ^{125}I-ovine IFNτ at a final concentration of 0.5 nM. Cells were then placed at 37°C for the specified time intervals. Surface-bound ligand was removed with a pH 4.0, glycine buffer. Nonspecific binding was determined in a parallel set of cells with the addition of a 200-fold excess of unlabeled human IFNτ. The k_d of ovine IFNτ and the type I IFN receptor on MDBK cells was determined to be 1.2 x 10^{-2} min^{-1} +/- 4.5 x 10^{-3} min^{-1}. The r^2 of the plotted line was 0.78.

saturation-binding curve to avoid the inaccuracies caused by the linear transformation of nonlinear data. The k_a values of human IFNαA and ovine IFNτ to type I IFN receptors on MDBK cells were 1.9×10^7 min^{-1} M^{-1} and 1.3×10^7 min^{-1} M^{-1}, respectively, suggesting that the rates of association of human IFNαA and ovine IFNτ, like the rates of dissociation, are comparable.

The Endocytotic Rate Constant (k_e) of Human IFNαA is Significantly Faster than that of Ovine IFNτ into MDBK Cells

The rate constants of endocytosis (k_e) of human IFNαA and ovine IFNτ into MDBK cells were measured to determine whether these type I IFNs are differentially internalized. After the cell pellets were treated with an acidic buffer, removing the surface-bound radioligand, radioligand that remained in the cells was removed by solubilization. According to Wiley and Cunningham, if ligand is actively hydrolyzed in cells, the concentration of internalized ligand is not solely based on the surface-bound ligand [108]. Therefore, trichloroacetic acid (TCA) treatment was used to determine the amount of radiolabel associated with intact or degraded ligand. Degraded ligand remained soluble in TCA and intact ligand precipitated in the presence of TCA. The slope of the concentration of internalized ligand at each specific time interval divided by the concentration of surface-bound ligand over time was equivalent to the k_e values of human IFNαA and ovine IFNτ

into MDBK cells. The k_e of human IFNαA into MDBK cells was 3.2 x 10^{-2} min^{-1} +/- 3.9 x 10^{-3} min^{-1} with r^2 equal to 0.97 (Figure 5-5). The k_e of ovine IFNτ into MDBK cells was 8.6 x 10^{-3} min^{-1} +/- 3.2 x 10^{-4} min^{-1} and the r^2 of the plot was 0.99 (Figure 5-6). The p-value of the linear plots created from the data sets to determine the k_e values of human IFNαA and ovine IFNτ were 0.0002 and 0.0044, respectively. Therefore, the p-values suggest that the best fit of the regression lines of the plots were to a linear equation. The linearity of the plots also indicated that degradation did not occur and that the cells had reached a steady state subsequent to ovine IFNτ or human IFNαA treatment [108]. These results suggest that the internalization of ovine IFNτ into viable MDBK cells is 75% slower than that of human IFNαA. The Student paired t-test of the k_e values of ovine IFNτ and human IFNαA revealed a p-value, 0.07, which indicated that the internalization rates of ovine IFNτ and human IFNαA into MDBK cells are significantly different.

Surface Binding and Internalization Patterns of Human IFNαA and Ovine IFNτ in MDBK Cells

The patterns of cell surface binding and internalization of human IFNαA differed from that of ovine IFNτ. The concentration of internal radioligand increased to a maximum within 32 minutes. Internalization remained steady for one hour and then reduced slowly until two hours.

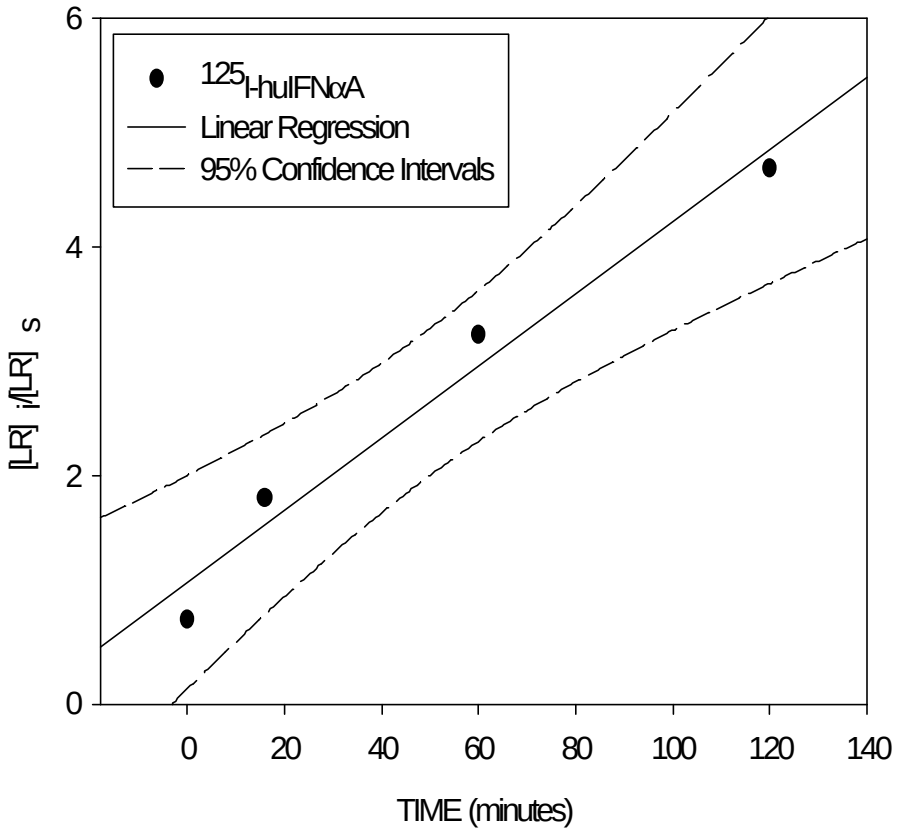

Figure 5-5. The k_e and k_h of human IFNαA and the type I IFN receptor on MDBK cells. Cultures of 2.7 x 10^6 MDBK cells/mL were incubated at 4°C for 7 hours with ^{125}I-ovine IFNτ at a final concentration of 0.5 nM. Cells were then placed at 37°C for the specified time intervals. Surface-bound ligand was removed with a pH 4.0, glycine buffer. Internalized ligand remained in the cells following the glycine buffer treatment. Nonspecific binding was determined in a parallel set of cells with the addition of a 200-fold excess of unlabeled human IFNαA. The k_e of human IFNαA and the type I IFN receptor on MDBK cells was determined to be 3.2 x 10^{-2} min^{-1} +/- 3.9 X 10^{-3} min^{-1}. The k_h was 8.1 x 10^{-3} min^{-1}. The r^2 of the plotted line was 0.97.

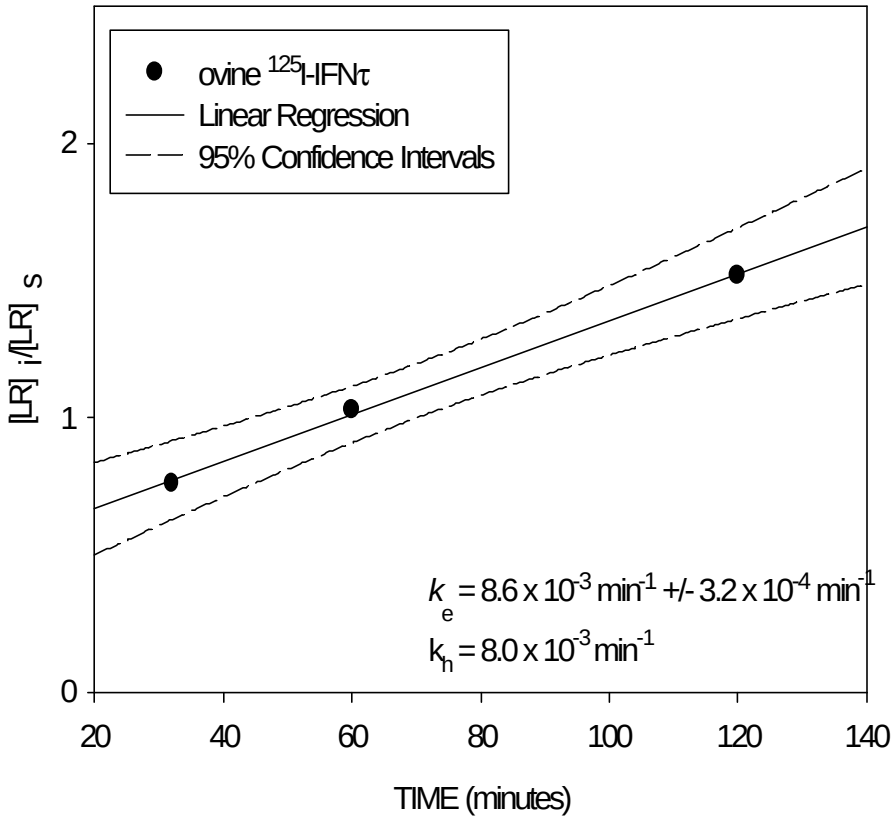

Figure 5-6. The k_e and k_h of ovine IFNτ and the type I IFN receptor on MDBK cells. Cultures of 2.7 x 10^6 MDBK cells/mL were incubated at 4°C for 7 hours with ^{125}I-ovine IFNτ at a final concentration of 0.5 nM. Cells were then placed at 37°C for the specified time intervals. Surface-bound ligand was removed with a pH 4.0, glycine buffer. Internalized ligand remained in the cells following the glycine buffer treatment. Nonspecific binding was determined in a parallel set of cells with the addition of a 200-fold excess of unlabeled ovine IFNτ. The k_e of ovine IFNτ and the type I IFN receptor on MDBK cells was determined to be 8.6 x 10^{-3} min^{-1} +/- 3.2 X 10^{-4} min^{-1}. The k_h was 8.0 x 10^{-3} min^{-1}. The r^2 of the plotted line was 0.99.

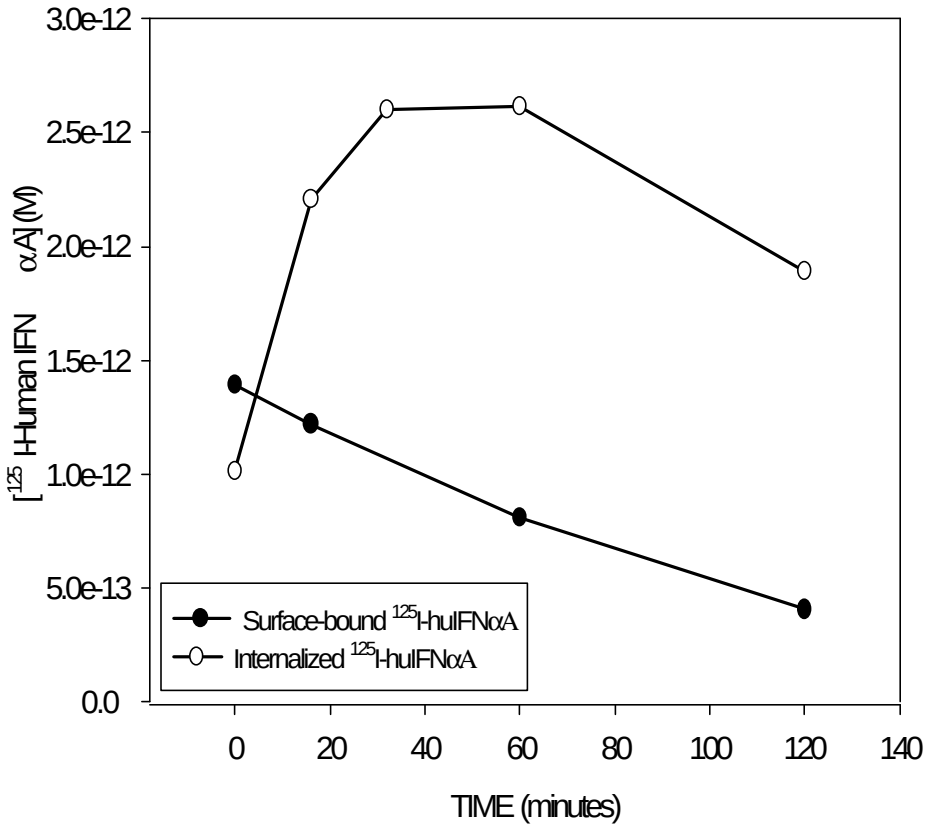

Figure 5-7. The surface binding and internalization pattern of human IFNαA and the type I IFN receptor in relation to MDBK cells. Cultures of 2.7 x 10^6 MDBK cells/mL were incubated at 4°C for 7 hours with ^{125}I-human IFNαA at a final concentration of 0.5 nM. Cells were then placed at 37°C for the specified time intervals. Surface-bound ligand was removed with a pH 4.0, glycine buffer. Internalized ligand remained in the cells following the glycine buffer treatment.

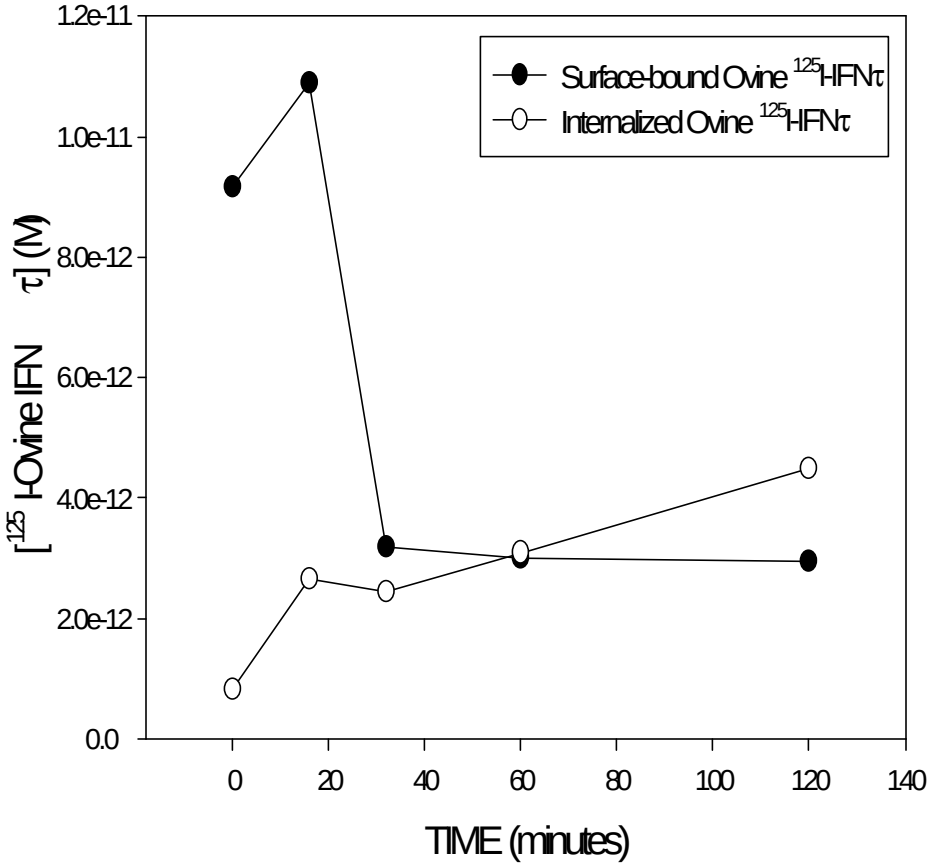

Figure 5-8. The surface binding and internalization pattern of ovine IFNτ and the type I IFN receptor in relation to MDBK cells. Cultures of 2.7 x 10^6 MDBK cells/mL were incubated at 4°C for 7 hours with ^{125}I-ovine IFNτ at a final concentration of 0.5 nM. Cells were then placed at 37°C for the specified time intervals. Surface-bound ligand was removed with a pH 4.0,glycine buffer. Internalized ligand remained in the cells following the glycine buffer treatment.

The surface binding of human IFNαA declined steadily and did not change in respect to the concentration of internalized ^{125}I-human IFNαA beginning at approximately 1 hour (Figure 5-7).

Ovine IFNτ surface binding reached a maximum within 16 minutes followed by a sharp decline. For two hours, the concentration of surface-bound ovine IFNτ remained steady (Figure 5-8). Unlike human IFNαA, the internalization of ovine IFNτ increased steadily for the two-hour period.

The Rate Constants of Hydrolysis (k_h) of Ovine IFNτ and Human IFNαA in MDBK Cells

The rate of hydrolysis (k_h) for human IFNαA and ovine IFNτ was determined at the time steady state was reached. The k_h values for human IFNαA and ovine IFNτ were 8.1 x 10^{-3} min^{-1} and 8.0 x 10^{-3} min^{-1}, respectively. The rates of hydrolysis of human IFNαA and ovine IFNτ appear to be equivalent. In contrast, the ratios of k_e/k_h, for human IFNαA and ovine IFNτ were significantly different. This ratio shows the quantity of ligand internalized in comparison to the quantity that is hydrolyzed. The ratio for human IFNαA was 3.9 and for ovine IFNτ was 1.1. Therefore, for approximately every four human IFNαA molecules endocytosed, only one is hydrolyzed, whereas for every one ovine IFNτ molecule internalized, one is hydrolyzed. The cells appear to accumulate a higher concentration of human IFNαA

because human IFNαA is endocytosed at a faster rate than it is degraded. The differential ratios of k_e/k_h suggest that ovine IFNτ does not accumulate in the cells after it is endocytosed because the rate of hydrolysis is similar. Based on the k_e/k_h ratios, ovine IFNτ is more efficiently removed from MDBK cells than human IFNαA.

Steady State Binding Constants (K_{ss}) of Ovine IFNτ and Human IFNαA for the Type I IFN Receptor

Steady state binding assays were performed at 37°C for human IFNαA and ovine IFNτ treated MDBK cells. The procedure is similar to that of the equilibrium-binding assay, only the temperature is adjusted from 4°C to 37°C to simulate physiological conditions. Unlike the K_a and K_d values which are dependent only on the rate constants k_d and k_a, the steady state constant (K_{ss}) is contingent on additional variables, specifically, the internalization of ligand occupied and unoccupied receptors. Therefore, the steady state constant reflects several aspects of receptor dynamics including surface association and dissociation with ligand, and the internalization of receptor complexes. The results were plotted with Scatchard analysis to reveal a K_{ss} of $3.1 \times 10^9\ M^{-1}$ for human IFNαA and $3.3 \times 10^9\ M^{-1}$ for ovine IFNτ (Figure 5-9A and 5-10A). The r^2 values for the linear regressions of the Scatchard plots that described steady state binding were 0.86 and 0.99 for human IFNαA and ovine IFNτ, respectively. As indicated by

the nonlinear regression of the saturation binding curve, the K_{ss} values of human IFNαA was 4.7 x 10^9 M^{-1} and 5.4 x 10^9 M^{-1} for ovine IFNτ and the type I IFN receptor (Figures 5-9B and 5-10B). Under steady state conditions, the mathematical equivalence of these values was similar; however, the endocytotic rates and the rates of turnover of unoccupied receptor of human IFNαA and ovine IFNτ were different indicating differences between how human IFNαA and ovine IFNτ interact with the type I IFN receptor dynamically. The x-intercept values of the modified Scatchard graphs were 6.4 x 10^{-12} M and 7.5 x 10^{-12} M for human IFNαA and ovine IFNτ, respectively (Figures 5-9A and 5-10A). The concentrations of the receptor population determined using nonlinear regression analysis were 5.0 x 10^{-12} M for human IFNαA and 6.3 x 10^{-12} M for ovine IFNτ (Figures 5-9B and 5-10B). The similar values for the concentrations of receptors further establishes that human IFNαA and ovine IFNτ bind to the same receptor population and suggest that no other specific receptors exist for either one of these type I IFNs on MDBK cells.

Reinsertion of Type I IFN Receptors into the Plasma Membrane Occurs at a Faster Rate in MDBK Cells Stimulated with Human IFNαA than Ovine IFNτ

Using the values determined in the steady state binding experiments, receptor population turnover was analyzed.

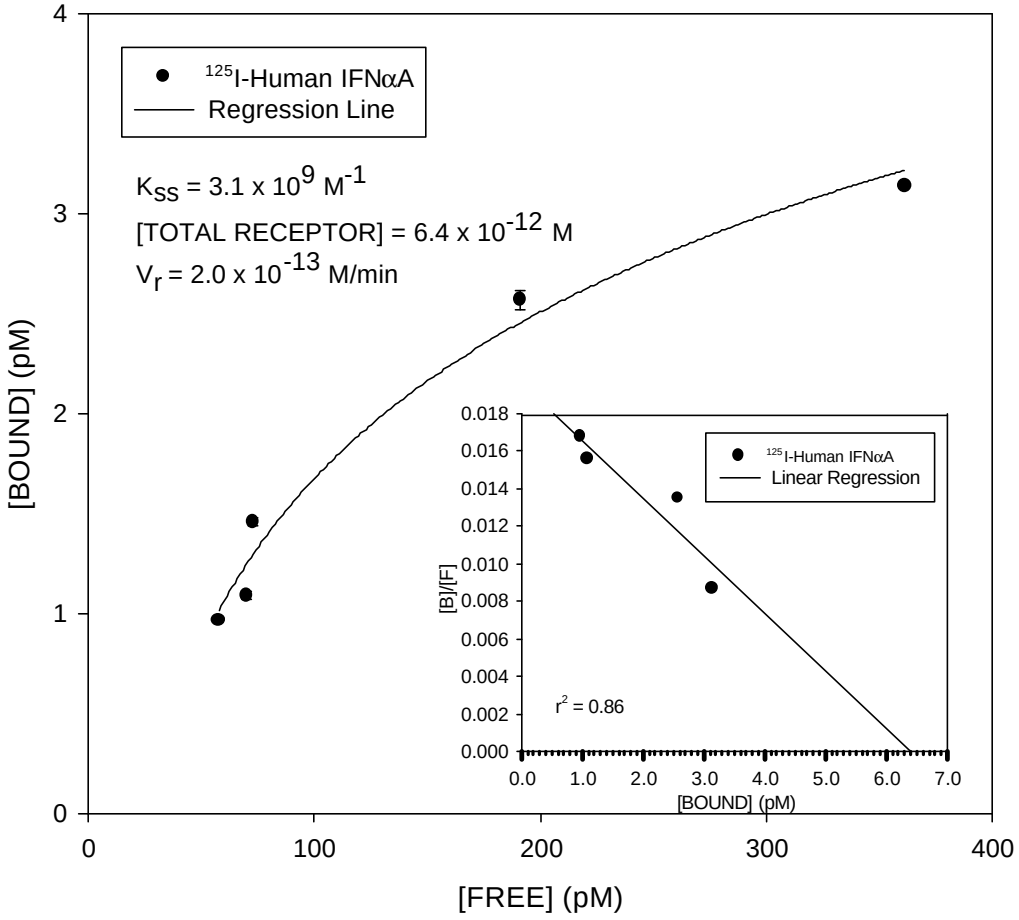

Figure 5-9. The steady state binding of human IFNαA to MDBK cells and the rate of insertion of type I IFN receptors into MDBK cell membranes following human IFNαA stimulation as determined by (A) Scatchard analysis and (B) nonlinear regression analysis. Cultures of 2.5×10^6 MDBK cells/mL were incubated at 37°C for 9 hours with increasing concentrations of ^{125}I-human IFNαA. Surface bound ligand was separated from free ligand by centrifugation for 10 seconds. The supernatant was removed to determine $[L]_f$. Surface-bound ligand remained on the cells. Non-specific binding was subtracted from total binding to reveal specific binding.

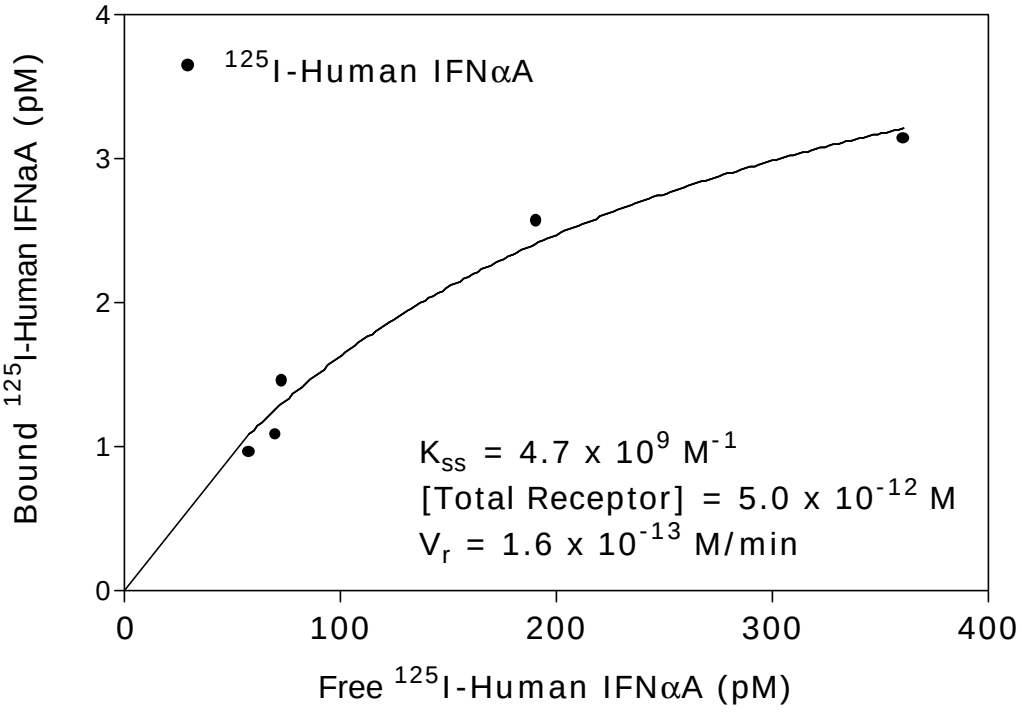
125I-Human IFNαA
Bound 125I-Human IFNaA (pM)
Free 125I-Human IFNαA (pM)
Kss = 4.7 x 10^9 M^-1
[Total Receptor] = 5.0 x 10^-12 M
Vr = 1.6 x 10^-13 M/min
0
1
2
3
4
0
100
200
300
400

Figure 5-9B.

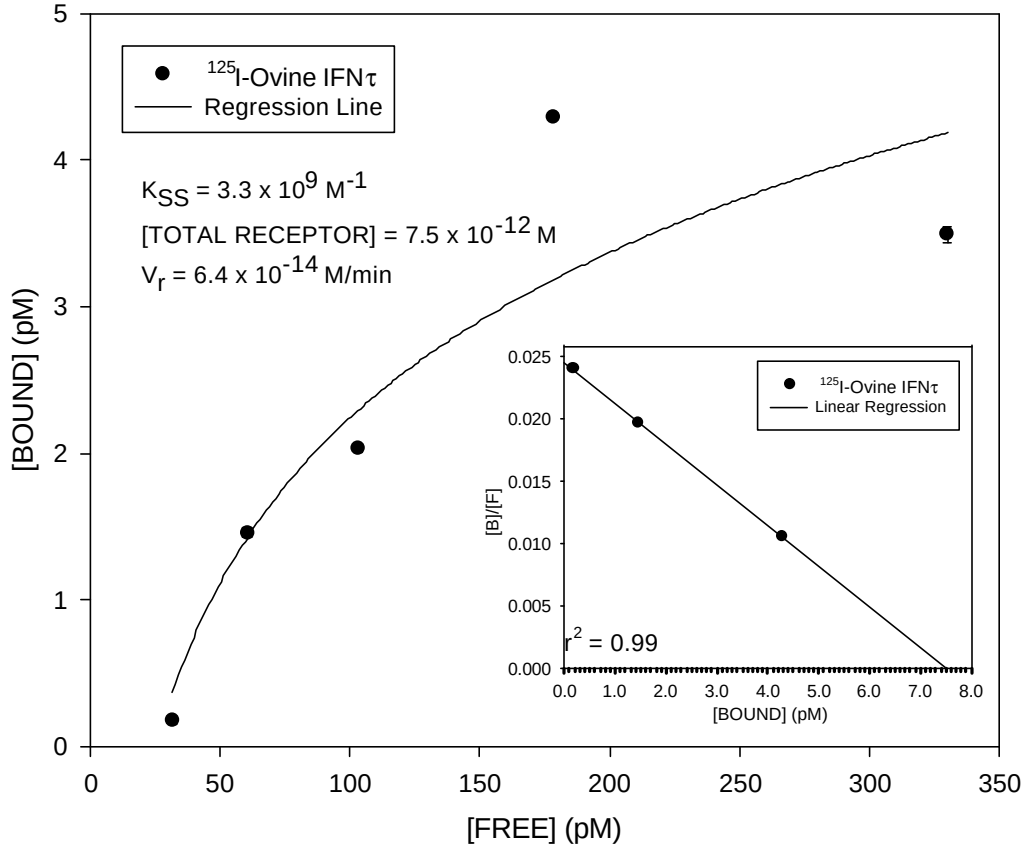

Figure 5-10. The steady state binding of ^{125}I-ovine IFNτ and the rate of insertion of type I IFN receptors into MDBK cell membranes following ovine IFNτ stimulation as determined by (A) Scatchard analysis and (B) nonlinear regression analysis. Madin-Darby bovine kidney cells were incubated at 37°C for 9 hours with increasing concentrations of ^{125}I-ovine IFNτ. Surface bound ligand was separated from free ligand by centrifugation for 10 seconds. The supernatant was removed to determine $[L]_f$. Surface-bound ligand remained on the cell pellets. Nonspecific binding was subtracted from total binding to reveal specific binding.

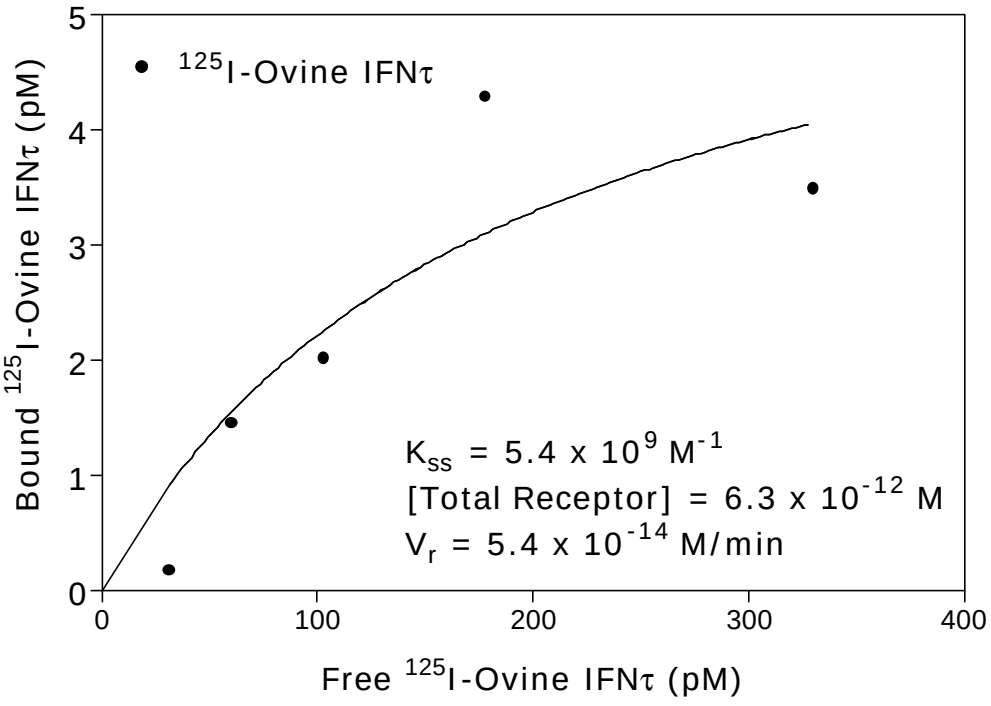
Bound ^{125}I-Ovine IFNτ (pM)
Free ^{125}I-Ovine IFNτ (pM)
^{125}I-Ovine IFNτ
K_{ss} = 5.4 x 10^{9} M^{-1}
[Total Receptor] = 6.3 x 10^{-12} M
V_r = 5.4 x 10^{-14} M/min
0
1
2
3
4
5
0
100
200
300
400

Figure 5-10B.

The x-intercept of the Scatchard plot of a steady state assay multiplied by the k_e yields the value for insertion of receptors into the plasma membrane (V_r). The V_r for human IFNαA was 0.20 pM/min using linear regression and 0.16 pM/min using a nonlinear regression (Figures 5-9A and 5-9B). For ovine IFNτ, receptors were inserted into the cell membrane at a rate of 0.06 pM/min and 0.05 pM/min for the linear and nonlinear regression models, respectively (Figures 5-10A and 5-10B). The differential rates of internalization generated the divergent V_r values because the receptor concentrations for human IFNαA and ovine IFNτ were equivalent. Despite human IFNαA and ovine IFNτ binding to the same receptors with similar affinities, it appears that the cell replenishes the plasma membrane of MDBK cells with type I IFN receptor 70% faster in response to human IFNαA stimulation than ovine IFNτ.

Human IFNαA and Ovine IFNτ Accelerate the Internalization of Ligand-Occupied Type I IFN Receptors into MDBK Cells

`The rate of turnover of unoccupied receptors in response to ligand stimulation is most useful when utilized to demonstrate whether internalization is changed upon ligand occupancy, as internalization of ligand bound receptors has been shown to be a common means of down-regulation [77]. Down-regulation refers to the removal of receptors from the cell membrane by internalization in response to

stimulation by a ligand without immediate replenishment of the receptor population. To determine the rate of turnover of unoccupied receptors (k_t), the suspended cells were allowed to reach steady state in the presence of a constant, subsaturating concentration of either ^{125}I-human IFNαA (22 pM) or ^{125}I-ovine IFNτ (56 pM); this concentration is referred to as $[L]_x$. The bound and free ligand quantities were measured following the incubation. Similar subsets of cells were treated with 22 pM of human IFNαA and 56 pM of ovine IFNτ and placed at 4°C. The receptor population, which was readjusted by the addition of subsaturating amounts of ligand, was therefore prevented from changing any further by reducing the temperature. An equilibrium binding assay was subsequently performed to quantify the new concentration of total cell-surface receptors, which is equal to $[LR]_x + [R]_x$. The cell receptor concentrations, as determined by linear regression, were 2.4×10^{-11} M following cellular stimulation by human IFNαA and ovine IFNτ (Figure 5-11A and 5-12A). The regressions of the linearly transformed data both had a r^2 value of 0.99. Nonlinear regressions revealed type I IFN receptor concentrations of 2.4×10^{-11} M and 4.1×10^{-11} M subsequent to the respective treatments of cells with human IFNαA or ovine IFNτ

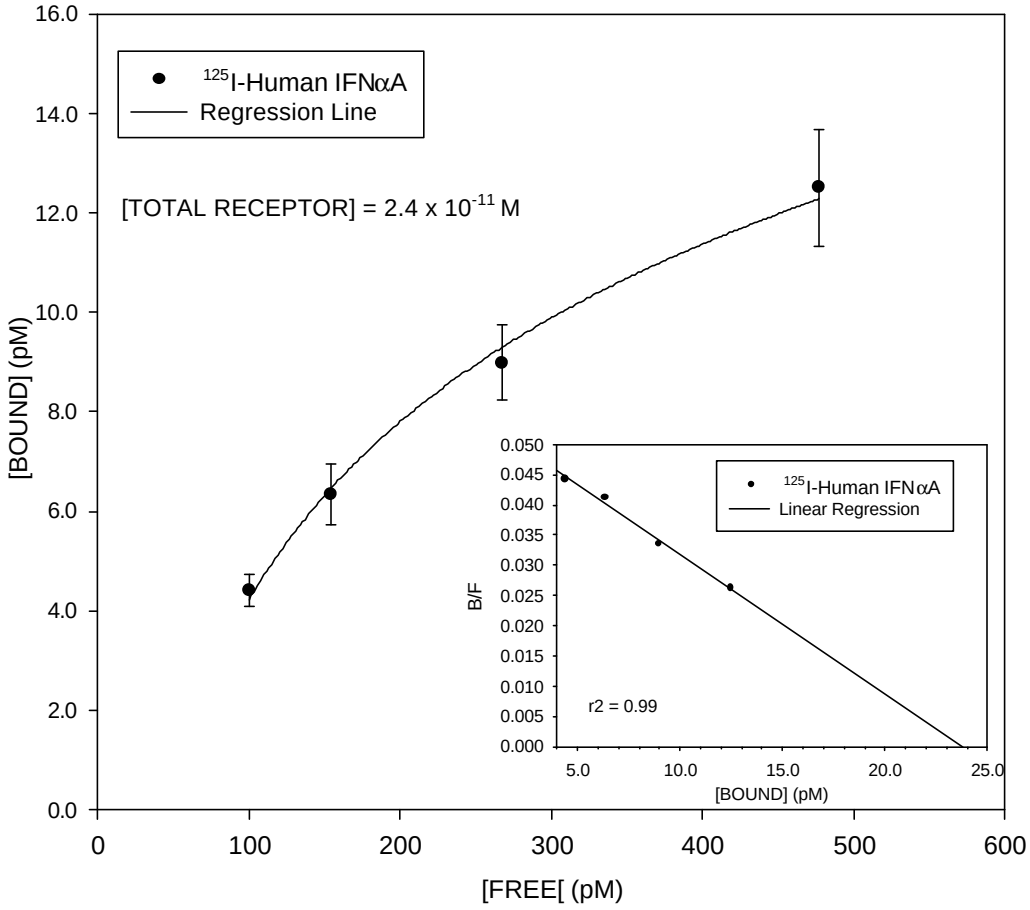

Figure 5-11. Total receptor concentration following human IFNαA stimulation at a final concentration of 22 pM as determined by (A) Scatchard analysis and (B) nonlinear regression analysis. Following the incubation of MDBK cells with the subsaturating concentration of human IFNαA, cells were incubated at 4°C for 9 hours with increasing concentrations of ^{125}I-human IFNαA. Surface bound ligand was separated from free ligand by centrifugation for 10 seconds. Surface-bound ligand remained on the cell pellets. Nonspecific binding was subtracted from total binding to reveal specific binding. The equation to solve for k_t is as follows: k_t, (min^{-1}) = V_r - $k_e([LR]_x)$ / $[R]_x$. The concentration of ligand complexed with receptor ($[LR]_x$) was equal to 1.8 x 10^{-12} M and unoccupied receptor ($[R]_x$) equaled 2.2 x 10^{-11} M.

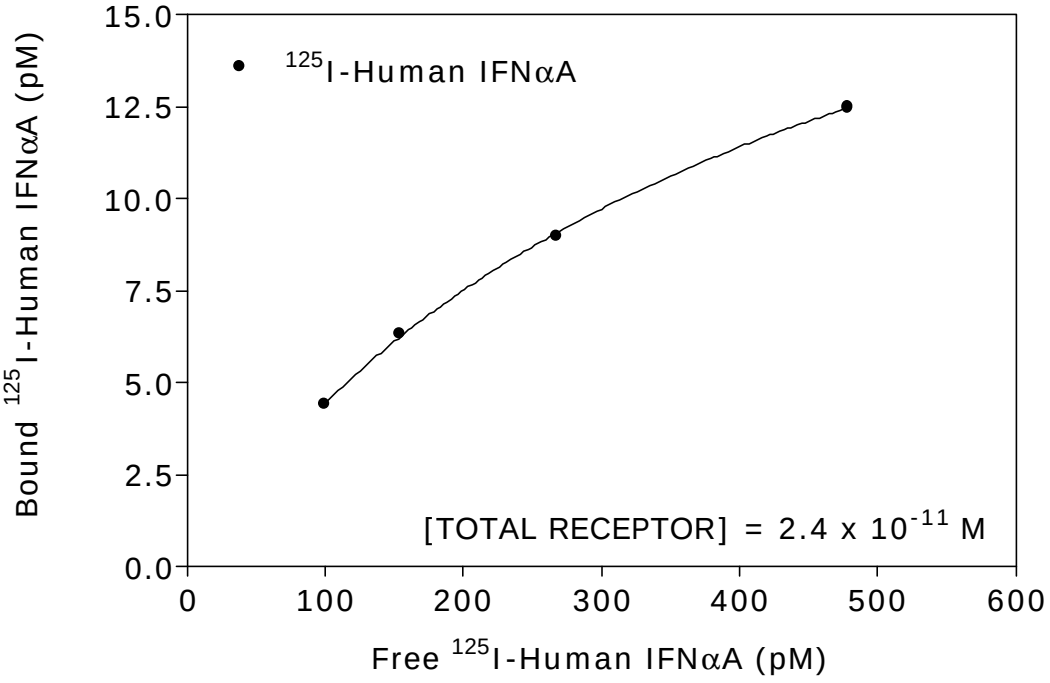
15.0
12.5
10.0
7.5
5.0
2.5
0.0
0
100
200
300
400
500
600
^{125}I-Human IFNαA
[TOTAL RECEPTOR] = 2.4 x 10^{-11} M
Bound ^{125}I-Human IFNαA (pM)
Free ^{125}I-Human IFNαA (pM)

Figure 5-11B.

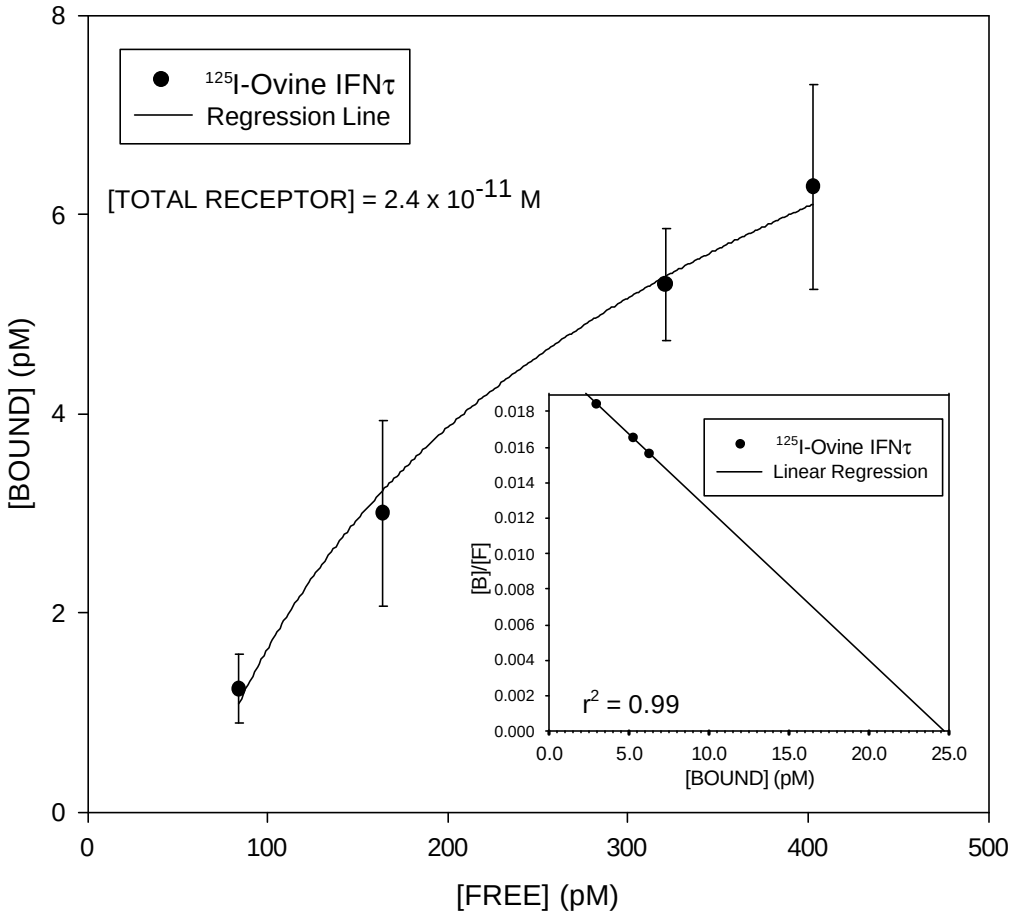

Figure 5-12. Total receptor concentration following ovine IFNτ stimulation at a final concentration of 56 pM as determined by (A) Scatchard analysis and (B) nonlinear regression analysis. Following the incubation of MDBK cells with the subsaturating concentration of ovine IFNτ, cells were incubated at 4°C for 9 hours with increasing concentrations of ^{125}I-ovine IFNτ. Surface bound ligand was separated from free ligand by centrifugation for 10 seconds. Surface-bound ligand remained on the cell pellets. Nonspecific binding was subtracted from total binding to reveal specific binding. The equation to solve for k_t is as follows: k_t, (min^{-1}) = V_r - $k_e([LR]_x)$ / $[R]_x$. The concentration of ligand complexed with receptor ($[LR]_x$) was equal to 2.4 x 10^{-12} M and unoccupied receptor ($[R]_x$) equaled 2.2 x 10^{-11} M.

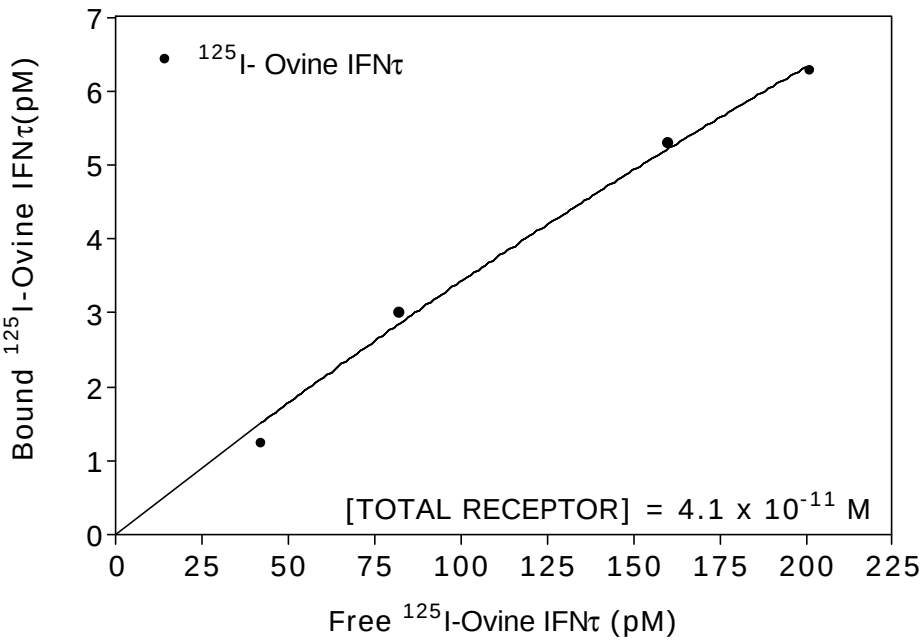
125I- Ovine IFNτ
[TOTAL RECEPTOR] = 4.1 x 10-11 M
Bound 125I-Ovine IFNτ(pM)
Free 125I-Ovine IFNτ (pM)
0
1
2
3
4
5
6
7
0
25
50
75
100
125
150
175
200
225

Figure 5-12B.

(Figure 5-11B and 5-12B). The human IFNαA concentration that bound receptor upon the addition 22 pM of free ligand was 1.8 x 10^{-12} M. The 56 pM pretreatment of ovine IFNτ allowed 2.4 x 10^{-12} M of ovine IFNτ to bind to the type I IFN receptor. The rate constant of the turnover of unoccupied receptor was then determined by the following equation:

$$k_t = (V_r - k_e[LR]_x)/[R]_x$$

Therefore, k_t values of human IFNαA and ovine IFNτ, derived using receptor population concentrations determined using linearly transformed data, were 6.5 x 10^{-3} min^{-1} and 1.8 x 10^{-3} min^{-1}, respectively. These rates were similar to those obtained using the nonlinear regression derived values, which were 6.5 x 10^{-3} min^{-1} for human IFNαA and 1.0 x 10^{-3} min^{-1} for ovine IFNτ. The modes of analysis consistently suggest that receptors unoccupied by ligand are internalized more slowly when MDBK cells are treated with ovine IFNτ instead of human IFNαA. The ratios of k_e/k_t for human IFNαA treated MDBK cells, which revealed the ratio of internalization of ligand occupied type I IFN receptors to unoccupied type I IFN receptors was 4.9 using values acquired from both the linear regression and nonlinear regression models. The ratios of k_e/k_t for ovine IFNτ treated MDBK cells as determined by linear and nonlinear analysis respectively, were 4.8 and 8.6. These data imply that in MDBK cells

human IFNαA and ovine IFNτ occupied type I IFN receptors are internalized approximately 5-9 times faster than unoccupied type I IFN receptors. Therefore, both ovine IFNτ and human IFNαA accelerate the internalization of ligand occupied receptors significantly more than unoccupied receptors.

Discussion

In human lung adenocarcinoma A549, human melanoma A375 cells, and human lymphoblastoid Daudi cells incubated at 37°C with ^{125}I-human IFNαA, internalization of the interferon reached a maximum at 30 minutes and then declined gradually for the remainder of the incubation [74, 76]. These results are similar to the pattern evident in the present study and a previous study in which human IFNαA internalized into MDBK cells after a 30-minute incubation at 37°C [75]. In contrast, ovine IFNτ internalization increased as the incubation progressed. The dynamics of human IFNαA and ovine IFNτ association with surface receptor were significantly different. Ovine IFNτ binding reached a maximum at 16 minutes and then decreased sharply. Binding remained steady for the remainder of the incubation. Surface binding of human IFNαA into MDBK cells diminished linearly. These divergent binding and internalization patterns reflect the differential interactions of human IFNαA and ovine IFNτ with the type I IFN receptor on MDBK cells. Given that the same receptor is

recognized by the type I IFNs, structural variations of the type I IFNs appear to be responsible for disparate surface receptor binding and possibly, the distinct internalization kinetics and localization of individual type I IFNs.

The k_d values of human IFNαA and MDBK cells, 1.0 x 10^{-2} min^{-1}, were of the same magnitude of those found for human IFNαA and A549 cells, which was 5.2 x 10^{-2} min^{-1} [74]. Ovine IFNτ dissociation from receptors on the MDBK cell surface was equivalent to the rate of human IFNαA; the k_d of ovine IFNτ was 1.2 x 10^{-2} min^{-1}.

Although not equivalent, the equilibrium dissociation constant (K_d) values of human IFNαA and ovine IFNτ were comparable to one another from the MDBK cell line. Human IFNαA had a K_d of 5.4 x 10^{-10} M and ovine IFNτ had a K_d of 2.6 x 10^{-10} M when binding reached equilibrium on MDBK cells. Human IFNαA was determined to have a K_d of 2.9 x 10^{-10} M in previous equilibrium binding assays on MDBK cells and ovine IFNτ had a K_d of 3.9 x 10^{-10} M [53, 75]. Equilibrium dissociation constants for human IFNαA binding to the type I IFN receptor on cell lines A549 and A375 were 2.6 x 10^{-10} M and 9.0 x 10^{-10} M, respectively [74, 76]. The K_d values of human IFNαA and these lung and skin tumor cells appear to be similar to those determined on the MDBK cells for human IFNαA and ovine IFNτ. To put these results in perspective, epidermal growth factor (EGF) binds its membrane-

bound receptor on human foreskin (HF) cells substantially differently from those of the type I IFNs to its receptor on various cell lines [74]. The K_d for EGF and the EGF receptor on HF cells is 1.1 x 10^{-8} M versus the K_d for ovine IFNτ and the type I IFN receptor on MDBK cells of 2.6 x 10^{-10} M. Therefore, the binding affinity of the type I IFNs for receptor is greater than that of EGF for its receptor. Because K_a is the inverse of K_d, K_a determinations for human IFNαA and ovine IFNτ were also comparable at 3.8 x 10^9 M^{-1} and 1.8 x 10^9 M^{-1}, respectively. The kinetic k_d values combined with K_d yielded k_a values 1.9 x 10^7 M min^{-1} for human IFNαA and 1.3 x 10^7 M min^{-1} for ovine IFNτ. Similar to the k_a of human IFNαA in MDBK cells determined, the rate constant of human IFNαA association with A375 cells was 5.8 x 10^7 M min^{-1} [76]. The B_{max} values of human IFNαA and ovine IFNτ were 1.9 x 10^{-11} M and 2.7 x 10^{-11}M, respectively. The equivalence of the maximum number of receptors on the cell surface indicates that human IFNαA and ovine IFNτ interact with the same receptor population, the type I IFN receptors, and that no other receptors are specific for either of these ligands on MDBK cells.

The k_e of human IFNαA into MDBK cells was 3.2 x 10^{-2} min^{-1}. The previously determined k_e for human IFNαA on MDBK cells was 3.1 x 10^{-2} min^{-1}. On A549 cells, the k_e, 4.7 x 10^{-2} min^{-1}, was not different from that of human IFNαA in MDBK cells [74]. However, the

k_e of ovine IFNτ in MDBK cells, 8.6 x 10^{-3} min^{-1}, differed considerably from values determined for human IFNαA, as indicated by the p-value of the paired Student's t-test, which was 0.07. In the present study, the k_e of ovine IFNτ into viable MDBK cells was 75% slower than that of human IFNαA. The faster rate of internalization of human IFNαA into MDBK cells when compared to that of ovine IFNτ provide an explanation for the increased toxicity of the IFNαs. Equivalent k_h values of human IFNαA and ovine IFNτ suggest that the cells degrade human IFNαA and ovine IFNτ similarly. However, the ratios of k_e:k_h for human IFNαA and ovine IFNτ, 3.9 and 1.1, respectively, indicate that human IFNαA accumulates in the cells while ovine IFNτ is turned over efficiently. It is a possibility that the increased concentrations of human IFNαA in cells may have toxic effects over time.

The steady state constant (K_{ss}) of 3.2 x 10^9 M^{-1} for human IFNαA and 4.1 x 10^9 M^{-1} for ovine IFNτ, were of the same order of magnitude, which suggest that under steady state conditions there are similarities between human IFNαA and ovine IFNτ interactions with receptor and cellular processing in MDBK cells. Because the K_{ss} value is dependent on k_e, k_a, k_t, and k_d, unlike K_a which depends solely on k_a and k_d, it is not an accurate measurement of affinity of ligand for receptor, but it does reflect the dynamics of the ligand on and in the whole cells. However, the divergence of the V_r values of human IFNαA and ovine

IFNτ, which were 2.4 x 10^{-13} M/min and 6.0 x 10^{-14} M/min, respectively, suggests that type I IFN receptors reinsertion into the cell membrane is faster in response to human IFNαA. The increase in surface receptor availability for human IFNαA may augment the rate of internalization of ligand into cells.

The k_t values of human IFNαA and ovine IFNτ were 6.5 x 10^{-3} min^{-1} and 1.8 x 10^{-3} min^{-1}, respectively. Values in the literature for human IFNαA on A549 and A375 cells were 1.2 x 10^{-3} min^{-1} and 1.5 x 10^{-3} min^{-1}, respectively [74, 76]. Unoccupied receptor turnover reached a rate of 2.3 x 10^{-2} min^{-1} in a previous study using MDBK cells [75]. The previous study coupled with the current study indicates that the k_t of the type I IFN receptor in response to human IFNαA is faster than the rates found in the two tumor cell lines. Possibly, changes in potency or mechanisms of antitumor effects may coincide with the differential rates of internalization of unoccupied receptors by cells in response to type I IFN stimulation. The ratio of k_e:k_t for human IFNαA and ovine IFNτ reflects the acceleration of bound receptor internalization in comparison to unbound receptor. Occupied type I IFN receptors appear to be internalized approximately 5 times faster than unoccupied type I IFN receptors subsequent to human IFNαA treatment. Based on the k_e:k_t ratio, the internalization of ovine IFNτ bound type I IFN receptors is also 5 times faster than unbound

receptors. Accelerated internalization of ligand occupied receptors has been shown to be a means of down-regulation of functional surface receptors in response to various ligands on various cell lines [74-76, 105, 110, 111].

CHAPTER 6
DISCUSSION

The objective of the present study was to provide a comprehensive analysis of the structurally and functionally significant interactions between ovine IFNτ and the type I IFN receptor and the subsequent cellular processing of this ligand and receptor. Because ovine IFNτ has been shown to be less toxic, yet comparable in biological activities than other type I IFNs, including those that have been approved by the FDA for treatment against various cancers, viral diseases, and multiple sclerosis, this research may contribute significantly to the production of hybrid type I IFN therapeutic agents. The differential biochemical aspects of ovine IFNτ, especially the efficient removal of ovine IFNτ from cells when compared to that of human IFNαA and the reduced rate of insertion of receptor into the cell membrane, may be key factors in the reduction of the toxic effects of other type I IFNs. In addition, the display of biochemical characteristics of ovine IFNτ by hybrid type I IFN molecules may be indicative of therapeutic potential.

The present peptide studies show that the C-terminal residues 153-168 of ovine IFNτ are not structurally necessary for ovine IFNτ

interaction with the type I IFN receptor. Previous studies have shown that the last six residues of the C-terminus of ovine IFNτ are not required for antiviral activity in MDBK cells, antiproliferative activity in Daudi cells, as well as antileuteolytic function in ewes. Previous studies have shown that amino acids 154-166 of human IFNα2 are not a required structural element and helix E is not required functionally for IFNβ. The presence of clustered cationic amino acids on the C-terminus of many type I IFNs is interesting because a cluster of cationic residues are also located on the C-terminus of IFNγ. A cluster of cationic amino acids is less apparent on ovine IFNτ. The type II IFN, IFNγ, which is extremely toxic in cell culture and animal models, requires the C-terminus for function. Perhaps, the deletions or substitutions of the cationic amino acids of the C-terminus after residue 153 would reduce the toxicity of the type I IFNs without affecting structural requirements for receptor binding or biological activity.

Although the peptide binding studies provided evidence of a putative intracellular binding site for ovine IFNτ, both equilibrium binding assays and steady state binding assays best fit a one-site binding model. This suggests that ovine IFNτ is binding to only the extracellular region on the type I IFN receptor, without additional binding to an intracellular site. Equilibrium binding assays on viable

cells were expected to fit to a one-site binding based on the peptide binding data, which indicated that ovine IFNτ interacts with the extracellular N-terminal domain of IFNAR2. Equilibrium is reached at a temperature that inhibits internalization, so binding of a ligand is limited to the cell surface. Without the internalization of ovine IFNτ molecules, the interaction of ovine IFNτ with a secondary intracellular region on IFNAR2 would be undetectable. However, steady state binding studies should have theoretically shown if ovine IFNτ was indeed interacting with a second, intracellular region on the type I IFN receptor. Because the attainment of steady state requires that cells are incubated with radioligand at 37^{o}C, internalization of radioligand was expected. If the steady state data would have best fit a two-site binding model, it would have supported the possibility of an intracellular binding site for ovine IFNτ; however, this does not appear to be the case.

A blast search of the extracellular, *N*-terminus of IFNAR2 and the intracellular, N-terminal region of IFNAR2 of the amino acid sequences were performed to determine if these regions were homologous. No sequence similarities were evident. However, extracellular residues 34-67 and intracellular residues 287-315 of IFNAR2 exhibited similar profiles of hydropathy as indicated by comparisons of Kyte and Doolittle hydrophobicity scores of each residue [137]. A strong

correlation has been shown between hydrophobic clusters and protein binding sites [136]. In addition, using hydrophobicity as a guide, sites of protein interaction have been identified [138, 139]. The similar values and patterns of the hydrophobic peaks within residues 34-67 and 287-315, as determined by the Kyte and Doolittle measurments, may be indicative of some similarity in secondary structure. In addition the hydropathy profiles are consistent with IFNAR2(287-315) recognition of ovine IFNτ in a manner that inhibited binding to the extracellular domain of IFNAR2. This suggests that the extracellular and intracellular receptor peptides, although not having amino acid sequence homology, have similar topology of hydrophobic regions, which could account for their interactions with similar sites on ovine IFNτ.

An interesting aspect of the type I IFNs and their relationship with their cell surface receptor is that the ligands must be structurally similar to interact with the same receptor subunit, activate the same signaling pathway and elicit a comparable cell response. However, the type I IFNs must also be inherently different from one another to exert unique and differential biological functions, such as the antileuteolytic activity of ovine IFNτ. The primary sequence of ovine IFNτ is 30% identical to that of IFNβ and 45-55% identical when compared to the amino acid sequences of human, mouse, and pig IFNα subtypes. The

structural similarities and variations of the type I IFNs appear to be responsible for their comparable and distinct surface receptor binding characteristics and internalization kinetics. For example, the ratio of internalization to degradation of human IFNαA and ovine IFNτ in MDBK cells is approximately 4:1 and 1:1, respectively; however, the rates of degradation, 8.0×10^{-3} min^{-1} and 8.1×10^{-3} min^{-1}, of human IFNαA and ovine IFNτ, respectively, are equivalent. Cellular processing of the receptor in response to human IFNαA and ovine IFNτ stimulation has similarities and differences as well. The ligand occupied type I IFN receptors are internalized approximately 5 times faster than unoccupied receptors when cells are stimulated with either human IFNαA or ovine IFNτ. However, the receptors are reinserted into the cell membrane 3 times faster in response to human IFNαA than ovine IFNτ. The internalization of the type I IFN receptor and reinsertion of receptor in response to ovine IFNτ treatment is corroborated by the present fluorescent microscopy studies of IFNAR2. Subsequent to the accumulation of fluorescently-labeled IFNAR2 in intracellular compartments following MDBK cell treatment with ovine IFNτ, some IFNAR2 appears to recycle back to the surface.

LIST OF REFERENCES

1. Jarpe, M.A., Pontzer, C.H., Szente, B.E., Johnson H.M. Structure and Functional Studies of Interferon: A Solid Foundation for Rational Drug Design. In *Structure-Based Drug Design* (Veerapandian P, ed) Marcel Dekker, Inc. 1997.

2. Pestka, S. Interferons. In *Human Cytokines: Handbook for Basic and Clinical Research* (Aggarwal B., Gutterman J., ed) Blackwell Scientific Publications. 1992.

3. Wujcik, D. Update of the Diagnosis of and Therapy for Acute Promyelocytic Leukemia and Chronic Myelogenous Leukemia. Oncol Nurs Forum. 1996. 23(3):478-487.

4. Johnson, H.M., Bazer, F.W., Szente, B.E., Jarpe, M.A. How Interferons Fight Disease. Sci Am. 1994. 270(5):40-47.

5. Pontzer, C.H., Bazer, F.W., Johnson, H.M. Antiproliferative Activity of a Pregnancy Recognition Hormone, Ovine Trophoblast Protein 1. Cancer Res. 1991. 51:5304-5307.

6. Imakawa, K., Anthony R.V., Kazemi, M., Marotti, K.R., Polites H.G., and Roberts R.M. Interferon-like Sequence of Ovine Trophoblast Protein Secreted by an Embryonic Trophectoderm. Nature. 1987. 330:339-379.

7. Stewart, H.J., McCann, S.H.E., Barker, P.J., Lee, K.E., Lamming, G.E., Flint, A.P.F. Interferon Sequence Homology and Receptor Binding Activity of Ovine Trophoblast Antiluteolytic Protein. J Endocrinol. 1987. 115:R13-R15.

8. Ott, T.L. Interferons. In *Human Cytokines: Handbook for Basic and Clinical Research* (Aggarwal B., Gutterman J., ed) Blackwell Scientific Publications. 1992.

9. Radhakrishnan, R., Walter, L.J., Subramaniam, P.S., Johnson, H.M., Walter, M.R. Crystal Structure of Ovine Interferon-tau at 2.1 Angstrom Resolution. J Mol Biol. 1999. 286:151-62.

10. Jarpe, M.A., Johnson, H.M. Bazer, F.W., Ott, T.L., Cutrone, E.C., Krishna, N.R., Pontzer, C.H. Predicted Structural Motif of IFN . Pro Eng. 1994. 7:863-867.

11. Colamonici, O.R., Pfeffer, L.M. Structure of the Human Interferon α Receptor. Pharmac Ther. 1991. 52:227-232.

12. Pestka, S., Langer, J.A., Zoon, K.C., Samuel, C.E. Interferons and Their Actions. Ann Rev Biochem. 1987. 56:727-777.

13. Cutrone, E.C., Langer, J.A. Contributions of Cloned Type I IFN Receptor Subunits to Differential Ligand Binding. FEBS Lett. 1997. 404:197-202.

14. Schindler S., Darnell, J.E. Transcriptional Responses to Polypeptide Hormones: the JAK-STAT pathway. Annu Rev Biochem. 1995. 64:621-51.

15. Roberts, R.M., Cross, J.C., Leaman, D.W. Interferons as Hormones of Pregnancy. Endocrinol Rev. 1992. 13:432-52.

16. Muto, N. F., Martinand-Mari, C., Adelson, M. E., Suhadolnik, R. J. Inhibition of Replication of Reactivated Human Immunodeficiency Virus Type 1 (HIV-1) in Latently Infected U1 Cells Transduced with an HIV-1 Long Terminal Repeat-Driven PKR cDNA Construct. J. Virol. 1999. 73: 9021-9028.

17. Didcock, L., Young, D. F., Goodbourn, S., Randall, R. E. The V Protein of Simian Virus 5 Inhibits Interferon Signalling by Targeting STAT1 for Proteasome-Mediated Degradation. J. Virol. 1999. 73: 9928-9933.

18. Diamond, M. S., Roberts, T. G., Edgil, D., Lu, B., Ernst, J., Harris, E. Modulation of Dengue Virus Infection in Human Cells by Alpha, Beta, and Gamma Interferons. J. Virol. 2000. 74: 4957-4966.

19. Iordanov, M. S., Wong, J., Bell, J. C., Magun, B. E. Activation of NF-{kappa}B by Double-Stranded RNA (dsRNA) in the Absence of Protein Kinase R and RNase L Demonstrates the Existence of Two Separate dsRNA-Triggered Antiviral Programs. Mol Cell Biol. 2001. 21: 61-72.

20. McAveney, K. M., Book, M. L., Ling, P., Chebath, J., Yu-Lee, L.-y. Association of 2',5'-Oligoadenylate Synthetase with the Prolactin (PRL) Receptor: Alteration in PRL-Inducible Stat1 (Signal Transducer and Activator of Transcription 1) Signaling to the IRF-1 (Interferon-Regulatory Factor 1) Promoter. Mol Endocrinol. 2000. 14: 295-306.

21. Price, G. E., Gaszewska-Mastarlarz, A., Moskophidis, D. The Role of Alpha/Beta and Gamma Interferons in Development of Immunity to Influenza A Virus in Mice. J. Virol. 2000. 74: 3996-4003.

22. Silverman, R.H., Cirino N.M. In *mRNA Metabolism and Post-Transcriptional Gene Regulation*. (DR Morris, JB Harford ed.) 1997. 295–309.

23. Lee, S.B., Esteban M. The Interferon-induced Double-stranded RNA-activated Protein Kinase Induces Apoptosis. Virology. 1994. 199(2):491-6.

24. Lee S.B., Rodriguez D., Rodriguez J.R., Esteban M. The Apoptosis Pathway Triggered by the Interferon-induced Protein Kinase PKR Requires the Third Basic Domain, Initiates Upstream of Bcl-2, and Involves ICE-like Proteases. Virology. 1997. 231(1):81-8.

25. Arnheiter H., Frese M., Kambadur R., Meier E., Haller O. Mx Transgenic Mice--Animal Models of Health. Curr Top Microbiol Immunol. 1996. 206:119-47.

26. Dereuddre-Bosquet, N., Clayette, P., Martin, M. Anti-HIV Potential of a New Interferon, Interferon tau (Trophoblastin). J AIDS Human Retroviral. 1996. 11:241-6.

27. Pontzer, C.H., Yamamoto, J.K., Bazer F.B. Potent Anti-feline Immunodeficiency Virus and Anti-human Immunodeficiency Virus Effect of Interferon-tau. J Immunol. 1997. 158:4351-7.

28. Ortaldo, J.R., Mantovani, A., Hobbs, D., Rubenstein, M. Pestka, S., Herberman, R.B. Effects of Several Species of Human Leukocyte Interferon on Cytotoxic Activity of Natural Killer Cells and Monocytes. Int J Cancer. 1983. 31:285-289.

29. Ortaldo, J.R., Mason, A., Rehberg, E., Moschera, J., Kelder, B., Pestka, S., Herberman, R.B. Effects of Recombinant and Hybrid Recombinant Human Leukocyte Interferon on Cytotoxic Activity of Natural Killer Cells. J Biol Chem. 1983. 24:15001-15015.

30. Li, B-L., Zhao, X-Y, Liu, X-Y. Kim, H.S., Raska, K., Ortaldo, J.R., Schwartz, B., Pestka, S. Alpha Interferon Structure and Natural Killer Cell Stimulatory Activity. Cancer Res. 1990. 50: 5328-5332.

31. Fellous, M., Nir, U., Wallach, D., Merlin, G., Rubenstein, M., Revel, M. Interferon-dependent Induction of mRNA for the Major Histocompatability Antigens in Human Fibroblasts and Lymphoblastoid Cells. Proc Natl Acad Sci USA. 1982. 79:3082-3086.

32. Brinkmann, V., Geiger, T., Alkan, S., Heusser, C.H. Interferon Alpha Increases the Frequency of Interferon Gamma-producing Human CD4+ T cells. J Exp Med. 1993. 178(5):1655-63.

33. Evans, S.S., Collea, R.P., Appenheimer, M.M., Gollnick, S.O. Interferon-alpha Induces the Expression of the L-selectin Homing Receptor in Human B Lymphoid Cells. J Cell Biol. 1993. 123(6 Pt 2):1889-98.

34. Tiefenbrun, N., Melamed, D., Levy, N., Resnitzky, D., Hoffman, I., Reed, S.I., Kimchi, A. Alpha Interferon Suppresses the Cyclin D3 and Cdc25A Genes, Leading to a Reversible G0-like Arrest. Mol Cell Biol. 1996. 16(7):3934-44.

35. Zhang K, Kumar R. Interferon-alpha Inhibits Cyclin E- and Cyclin D1-dependent CDK-2 KInase Activity Associated with RB Protein and E2F in Daudi cells. Biochem Biophys Res Commun 1994. 200(1):522-8.

36. Misiani, R., Bellavita, P., Fenili, D., Vicari, O., Marchesi, D., Sironi, P.L., Zilio, P., Vernocchi, A., Massazza, M., Vendramin, G. Interferon alfa-2a therapy in cryoglobulinemia associated with hepatitis C virus. N Engl J Med. 1994. 330(11):751-6.

37. Lifsey, B.J., Baumbach, G.A., Godkin, J.D. Isolation, Characterization and Immunocytochemical Localization of Bovine Trophoblast Protein-1. Biol Reprod. 1989. 40(2):343-52.

38. Martal, J., Lacroix, M.C., Loudes, C., Saunier, M., Wintenberger-Torres, S. Trophoblastin, an Antiluteolytic Protein Present in Early Pregnancy in Sheep. J Reprod Fertil. 1979. 56(1):63-73.

39. Pontzer, C.H., Ott, T.L., Bazer, F.W., Johnson, H.M. Structure/function Studies with Interferon Tau: Evidence for Multiple Active Sites. J Interferon Res 1994. 14(3):133-41.

40. Fish, E.N. Definition of Receptor Binding Domain in Interferon-α. J Interferon Res. 1992. 12:257-266.

41. Piehler, J., Roisman, L.C., Schreiber, G. New Structural and Functional Aspects of the Type I Interferon-receptor Interaction Revealed by Comprehensive Mutational Analysis of the Binding Interface. J Biol Chem. 2000. 275(51):40425-33.

42. Domanski, P., Colamonici O.R. The Type I Interferon Receptor. The long and Short of It. Cytokine and Growth Factor Rev. 1996. 7:143-151.

43. Novick, D. Cohen, B., Rubenstein M. The Human Interferon α Receptor: Characterization and Molecular Cloning. Cell. 1994. 77:391-400.

44. Domanski, P., Witte, M., Kellum, M. Cloning and Expression of a Long Form of the B Subunit of the Interferon α Receptor that is Required for Interferon Signalling. J Biol Chem. 1995. 270:21606-11.

45. Mouchel-Vielh, E., Lutfalla, G., Morgenson, K.E. Specific Antiviral Activities of the Human α-Interferons are Determined at the Level of Receptor (IFNAR) Structure. FEBS Lett. 1992. 313:255-259.

46. Lutfalla, G., Holland, S.J., Cinato, E. Mutant U5A Cells are Complemented by an Interferon αβ Receptor Subunit Generated by Alternative Processing a New Member of a Cytokine Receptor Gene Cluster. EMBO J. 1995. 14:51000-51008.

47. Uze, G., Lutfalla, G., Gresser, I. Genetic Transfer of a Functional Human Interferon Receptor into Mouse Cells: Cloning and Expression of its cDNA. Cell. 1990. 60:225-234.

48. Colamonici, O.R., D'Alessandro, F., M.O. Characterization of Three Monoclonal Antibodies that Recognize the IFNα2 Receptor. Proc Natl Acad Sci USA. 1990. 87:7230-7234.

49. Colamonici, O.R., Domanski, P. Identification of a Novel Subunit of the Type I Interferon Receptor Localized to Human Chromosome 21. J Biol Chem. 1993. 15:10895-9.

50. Colamonici, O.R., Porterfield, B., Domanski, P., Krolewski J.J. Transmembrane Signalling by the α Subunit of the Type I IFN Receptor is Essential for Activation of the Jak Kinases and the Transcription Factor ISGF3. J Biol Chem. 1995. 270:8188-8193.

51. Cohen, B. Novick, D., Barak, S., Rubenstein M. Ligand Induced Association of the Type I IFN Receptor Components. Mol Cell Biol. 1995. 15:4208-4214.

52. Ghislain, J., Sussman, G., Goelz, S., Ling, L.E., Fish, E.N. Configuration of the Interferon-α/β Receptor Complex Determines the Context of the Biological Response. J Biol Chem. 1995. 270:21785-21792.

53. Subramaniam PS, Khan SA, Pontzer CH, Johnson HM. Differential Recognition of the Type I Interferon Receptor by Interferons Tau and Alpha is Responsible for Their Disparate Cytotoxicities. Proc Natl Acad Sci U S A. 1995. 92(26):12270-4.

54. Aguet, M. High Affinity Binding of ^{125}I-labeled Mouse Interferon to a Specific Cell Surface Receptor. 1980. Nature. 284:459-461.

55. Langer, J.A., Pestka, S. Interferon Receptors. Immunol Today. 1988. 9;393-400.

56. Uze, G., Lutfalla, G. Mogenson, K.E. α and β Interferons and Their Receptor and Their Friends and Relatives. J Interferon Cytokine Res. 1995. 15:3-26.

57. Barbieri, G., Velaquez, L., Scrobogna, M. Activation of the Protein Tyrosine Kinase Tyk2 by Interferon α/β. Eur J Biochem. 1994. 223:427-435.

58. Colamonici, O.R., Uyttendale, H., Domanski, P. $p135^{Tyk2}$, an Interferon- α-Activated Tyrosine Kinase, Is Physically Associated with an Interferon-α Receptor. J Biol Chem. 1994. 269:3518-3522.

59. Krishnan, K., Singh, B., Krolewski, J.J. Identification of Amino Acid Residues Critical for the Src-Homology 2 Domain-dependent Docking of Stat2 to the Interferon α Receptor. 1998. J Biol Chem. 273:19495-19501.

60. Colamonici, O.R., Yan, H., Domanski, P. Direct Binding and Tyrosine Phosphorylation of the α–subunit of the Type I IFN Receptor by the $p135^{Tyk2}$ Tyrosine Kinase. Molec Cell Biol. 1994. 14:8133-8142.

61. Pellegrini, S., John, J., Shearer, M., Kerr, I.M., Stark, G.R. Use of a Selectable Marker Regulated by Alpha Interferon to Obtain Mutations in the Signaling Pathway. Mol Cell Biol. 1989. (11):4605-12.

62. Leung, S. Qureshi, S.A., Kerr, I.M., Darnell, J.E.J., Stark, G.R. Role of STAT2 in the Alpha Interferon Signalling Pathway. Molec Cell Biol. 1995. 15:1312-1317.

63. Li XX, Leung S, Kerr IM, Stark GR. Formation of STAT1-STAT2 Heterodimers and Their Role in the Activation of IRF-1 Gene Transcription by Interferon-alpha. Mol Cell Biol. 1997. 17:2048–56.

64. Stancato LF, David M, Carter-Su C, Larner AC, Pratt WB. Preassociation of STAT1 with STAT2 and STAT3 in Separate Signalling Complexes Prior to Cytokine Stimulation. J. Biol. Chem. 1996. 271:4134–37.

65. Ihle, J.N. The Jaks-Stats Pathway. Nature. 1995. 337:591-594.

66. Colamonici, O., Yan, H., Domanski, P., Handa, R., Smalley, D., Mullersman, J., Witte, M., Krishnan, K., Krolewski, J. Direct Binding to and Tyrosine Phosphorylation of the Alpha Subunit of the Type I Interferon Receptor by $p135^{tyk2}$ Tyrosine Kinase. Mol. Cell. Biol. 1994. 14:8133–42.

67. Gauzzi, M.C., Velazquez, L., McKendry, R., Mogensen, K.E., Fellous, M., Pellegrini, S. Interferon-alpha-dependent Activation of Tyk2 Requires Phosphorylation of Positive Regulatory Tyrosines by Another Kinase. J. Biol. Chem. 1996. 271:20494–500.

68. Yan, H., Krishnan, K., Greenlund, A. Phosphorylated Interferon-α Receptor 1 (IFNAR1) Acts as a Docking Site for the Latent Form of the 113 kDa STAT2 Protein. EMBO J. 1996. 15:1064-1074.

69. Stark, G.R., Kerr, I.M., Williams, B.R.G., Silverman, R.H., Schreiber, R.D. How Cells Respond to Interferon. Annu Rev Biochem. 1998. 67:227-264.

70. Williams, B.R.G. Transcriptional Regulation of Interferon Stimulated Genes. Eur J Biochem. 1991. 200:1-11.

71. Renqiu, H., Bekisz, J., Hayes, M., Audet, S., Beeler, J., Petricon, E., Zoon, K.C. Divergence of Binding, Signalling, and Biological Responses to recombinant Human Hybrid IFN. J Immunol. 1999. 163:854-860.

72. Cook, J.R., Cleary, C.M., Mariano, T.M. Differential Responsiveness of a Splice Variant of the Human Interferon Receptor to Interferons. J Biol Chem. 1996. 271:13448-13453.

73. Pfeffer, L.M. Biological Activities of Natural and Synthetic Type I Interferons. Sem Oncol. 1997. 24:Suppl 9 63-69.

74. Myers, A.C., Kovach, J.S., Vuk-Pavlovic, S. Binding, Internalization, and Intracellular Processing of Protein Ligands. J Biol Chem. 1987. 262:6494-6499.

75. Zoon, K.C., Nedden, D.Z., Renqiu, H., Arnheiter, H. Analysis of the Steady State Binding, Internalization, and Degradation of Human Interferon α2. J Biol Chem. 1986. 261:4993-4996.

76. Branca, A.A., Baglioni, C. Down-regulation of the Interferon Receptor. J Biol Chem. 1982. 257:13197-13200.

77. Limbird. L.E. Cell surface receptors: A Short Course on Theory and Methods, Second Edition. Kluwer Academic Publishers, 1996.

78. Heuser, J.E., Anderson, R.G.W. Hypertonic Media Inhibit Receptor-Mediated Endocytosis by Blocking Clathrin Coated Pit Formation. J Cell Biol. 1989. 108:389-400.

79. Doxsey, S.J., Brodsky, F.M., Blank, G.S., Helenius, A. Inhibition of Endocytosis by Anti-clathrin Antibodies. Cell. 1987. 50:453-463.

80. Anderson, R.G.W., Brown, M.S., Goldstein, J.L. Role of the Coated Endocytotic Vesicle in the Uptake of Receptor-bound Low Density Lipoprotein in Human Fibroblasts. Cell. 1977. 10:351-364.

81. Diaz, R. Mayorga, L. Stahl, P.D. *In vitro* Fusion of Endosomes Following Receptor-Mediated Endocytosis. J. Biol. Chem. 1988. 263:6093-7000.

82. Gruenberg, J., Griffith, G., Howell, K.E. Characterization of the Early Endosomes and Putative Endocytotic Carrier Vesicles *in Vivo* and with an Assay of Vesicle Function *in Vitro*. J Cell Biol. 1989. 108:1301-1316.

83. Mellman, I., Fuchs, R., Helenius, A. Acidification of the Endocytotic and Exocytotic Pathways. Annu Rev Biochem. 1986. 55:663-700.

84. Park, R.D., Sullivan, P.C., Storrie, B. Hypertonic Sucrose Inhibition of Endocytotic Transport Suggests Multiple Early Endocytotic Compartments. J Cell Physiol. 1988. 135:443-450.

85. Mellman, I. Endocytosis and Molecular Sorting. Annu Rev Cell Dev Biol. 1996. 12:575-625.

86. Steinman, R.M., Mellman, I.S., Muller, W.A., Cohn, Z.A. Endocytosis and the recycling of the Plasma Membrane. J Cell Biol. 1983. 96:1-27.

87. Schmidt, S.L., Fuchs, R., Male, P., Mellman, I. Two Distinct Subpopulations of Endosomes Involved in Membrane Recycling and Transport to the Lysosome. Cell. 1988. 52:73-83.

88. Silverstein, S.C., Steinman, R.M., Cohn, Z.A. Endocytosis. Annu Rev Biochem. 1977. 46:669-772.

89. Griffiths, G. Simons, K. The *trans*-Golgi Network: Sorting at the Exit Site of the Golgi Complex. Science. 1986. 234:438-443.

90. Yamashiro, D.Y., Tycko, B., Fluss, S.F., Maxfield, F.R. Segregation of Transferrin to a Mildly Acidic (pH 6.5) Para-Golgi Compartment in the Recycling Pathway. Cell. 1984. 37:789.

91. Mori, M., Quintana, A., Yam, J. Studies of the Secretory Process in the Mammalian Exocrine Pancreas. I.: the Condensing Vacuoles. J Cell Biol. 1977. 75(1):148-65.

92. Riezman, H. Endocytosis in Yeast: Several of the Yeast Secretory Mutants are Defective in Endocytosis. Cell. 1985. 40(4):1001-9.

93. Snider, M.D., Rogers, O.C. Intracellular Movement of Cell Surface Receptors after Endocytosis: Resialylation of Asialo-transferrin Receptor in Human Erythroleukemia Cells. 100(3):826-34.

94. Regoeczi, E., Chindemi, P.A., Debanne, M.T., Charlwood, P.A. Partial Resialylation of Human Asialotransferrin Type 3 in the Rat. Proc Natl Acad Sci U S A. 1982. 79(7):2226-30.

95. Anderson, R.G.W., Pathak, R.K. Vesicles and Cisternae in the Trans Golgi Apparatus of Human Fibroblasts are Acidic Compartments. Cell. 1985. 40(3):635-43.

96. Frisch, A., Neufield, E.F. Limited Proteolysis of the Beta-hexosaminidase Precursor in a Cell-free System. J Biol Chem. 1981. 256(15):8242-6.

97. Hedman, K., Goldenthal, K.L., Rutherford, A.V., Pastan, I., Willingham A.C. Comparison of the Intracellular Pathways of Transferrin Recycling and Vesicular Stomatitis Virus Membrane Glycoprotein Exocytosis by Ultrastructural Double-label Cytochemistry. J Histochem Cytochem. 1987. 35(2):233-43.

98. Kornfield, S. The Biogenesis of Lysosomes. Annu Rev Biochem. 1989. 5:483-525.

99. Boeynaems, J.M., Dumont, J.E. Quantitative Analysis of the Binding of Ligands to their Receptors. J Cyclic Nucl Res. 1975. 1:123-142.

100. Wieland, G.A., Molinoff, P.B. Quantitative Analysis of Drug-Receptor Interactions: Determination of Kinetic and Equilibrium Properties. Life Sci. 1981. 29:313-330.

101 Voet, D., Voet, J. Biochemistry. 1995. 1275-1276.

102. Munson, P.J., Rodbard, D. Number of Receptor Sites from Scatchard and Klotz Graph: A Constructive Critique. Science. 1983. 220:979-981.

101. Chang, J-J., Jacobs, S., Cuatrecasas, P. Quantitative Aspects of Hormone-Receptor Interactions of High Affinity. Biochim Biophys Acta. 1975. 406:294-303.

102. Hollenberg, M.D., Cuatrecasas, P. Distinction of Receptor from Non-receptor Interactions in Binding Studies. In *Receptors: A Comprehensive Treatise*. (R.D. O'Brien, ed.). 1979. New York: Plenum Press.

103. Waters, C.M., Kerby, C.O., Carpenter, G., Overhosler, K.A. Rate Constants for Binding, Dissociation, and Internalization of EGF: Effect of Receptor Occupancy and Ligand Concentration. Biochem. 1990. 29:3563-3569.

104. Zoon, K.C., Zur Nedden, D., Arnheiter, H. Procedures for Studying the Binding of Interferon to Human and Bovine Cells in Monolayer Culture. Methods Enzymol. 1986. 119:312-315.

105. Carpenter, G. Binding Assays for Epidermal Growth Factor. Methods Enzymol. 1985. 56:881-894.

106. Wiley, H.S., Cunningham, D.D. The Endocytotic Rate Constant: A Cellular Parameter for Quantitating Receptor-mediated Endocytosis. J Biol Chem. 1982. 257:4222-4229.

107. Wiley, H.S. Receptors: Topology, Dynamics and Regulation. In *Fundamentals of Medical Cell Biology*. JAI Press, Inc. 1992. 5A:113-142.

108. Wiley, H.S., Cunningham, D.D. A Steady State Model for Analyzing the Cellular Binding, Internalization and Degradation of Polypeptide Ligands. Cell. 1981. 25:433-440.

109. Stoscheck, C.M., Gates, R.E., King, L,E. A Search for EGF-elicited Degradation Products of the EGF Receptor. J Cell Biochem. 1988. 38(1):51-63.

110. Heldin CH, Westermark B, Wasteson A. Specific Receptors for Platelet-derived Growth Factor on Cells Derived from Connective Tissue and Glia. Proc Natl Acad Sci USA. 1981. 78(6):3664-8.

111. Motulsky, H.J., Mahan, L.C. The Kinetics of Competitive Radioligand Predicted by the Law of Mass Action. Mol Pharmacol. 1984. 25:1-9.

112. Knauer D.J., Wiley, H.S., Cunningham, D.D. Relationship between Epidermal Growth Factor Receptor Occupancy and Mitogenic Response. Quantitative Analysis using a Steady State Model System. J Biol Chem. 1984. 259:5623-5631.

113. Aggarwal, B.B., Eeasalu, T.E., and Hass, P.E. Characterization of receptors for human tumour necrosis factor and their regulation by gamma-interferon. 1985. Nature. 318:665-667.

114. Klotz, I.M., Hunston, D.L. Properties of Graphical Representation of Multiple Classes of Sites. Biochem. 1971. 10:3065-3069.

115. DeLean, A., Rodbard, D. Kinetics of Cooperative Binding. In *Receptors: A Comprehensive Treatise.* (R.D. O'Brien, ed.). 1979. 1443- 1490. New York: Plenum Press.

116. Demeyts, P., Bianco, A., Roth, J. Site-site Interactions among Insulin Receptors. Characterization of the Negative Cooperativity. J Biol Chem. 1976. 251:187-1888.

117. Krupp, M.N., Connolly, D.T., Lane, M.D. Synthesis, Turnover, and Down-regulation of Epidermal Growth Factor Receptors in Human A431 Epidermoid Carcinoma Cells and Skin Fibroblasts. J Biol Chem. 1982. 257(19):11489-96.

118. Schwartz, A.L., Fridovich, S.E., Lodish, H.F. Kinetics of Internalization and Recycling of the Asialoglycoprotein Receptor in a Hepatoma Cell Line. J Biol Chem. 1982. 257(8):4230-7.

119. Knutson, V.P., Ronnett, G.V., Lane, M.D. The Effects of Cycloheximide and Chloroquine on Insulin Receptor Metabolism. Differential Effects on Receptor Recycling and Inactivation and Insulin Degradation. J Biol Chem. 1985. 260(26):14180-8.

120. Chuntharapai, A., Gibbs, V., Lu, J., Ow, A., Marsters, S., Ashkenazi, A., De Vos, A., Jin Kim, K. J. Determination of Residues Involved in Ligand Binding and Signal Transmission in the Human IFN-alpha Receptor 2. J Immunol. 1999. 163(2):766-73.

121. Chang, C.D., Meienhofer, J. Solid-phase Peptide Synthesis Using Mild Base Cleavage of N Alpha-fluorenylmethyloxycarbonylamino Acids, Exemplified by a Synthesis of Dihydrosomatostatin. J Pept Protein Res. 1978. 11(3):246-9.

122. Hnatowich, D.J., Virzi, F., Rusckowski, M. Investigations of Avidin and Biotin for Imaging Applications. J Nucl Med. 1987. 28(8):1294-302.

123. Smith, P.K., Krohn, R.I., Hermanson, G.T., Mallia, A.K., Gartner, F.H., Provenzano, M.D., Fujimoto, E.K., Goeke, N.M., Olson, B.J., Klenk, D.C. Measurement of Protein Using Bicinchoninic Acid. Anal Biochem. 1985. 150(1):76-85.

124. Bolton, A.E., Hunter, W.M. The Labelling of Proteins to High Specific Radioactivities by Conjugation to a ^{125}I-containing Acylating Agent. Biochem J. 1973. 133: 529-539.

125. Szente, B.S., Weiner, I.J., Jablonsky, M.J.., Krishna, N.R., Torres, B.A., Johnson, H.M. Structural Requirements for Agonist Activity of a Murine Interferon-γ Peptide. J Interferon Cytokine Res. 1996. 16: 813-817.

126. Szente, B.S, Johnson, H.M. Binding of IFNγ and the C-terminal Peptide to a Cytoplasmic Domain that is Essential for Function. Biochem Biophys Res Comm. 1994. 201: 215-221.

127. Salacinski, P.R., McLean, C., Sykes, J.E., Clement-Jones, V.V., Lowry, P.J. Iodination of Proteins, Glycoproteins, and Peptides Using a Solid-phase Oxidizing Agent, 1,3,4,6-tetrachloro-3 alpha,6 alpha-diphenyl glycoluril (Iodogen). Anal Biochem. 1981. 117(1):136-46.

128. Knight, L.C., Budzynski, A.Z., Olexa, S.A. Radiolabeling of Fibrinogen Using the Iodogen Technique. Thromb Haemost. 1981. 46(3):593-6.

129. Chou, P.Y., Fasman, G.D. Prediction of Protein Conformation. Biochem. 1974. 13(2): 222-245.

130. Garnier, J., Osguthorpe, D., Robson, B. Analysis of the Accuracy and Implications of Simple Methods for Predicting the Structure of Globular Proteins . J Mol Biol. 1978 120:97-120.

131. Prevelige, P., Fasman, G.D. Chou-Fasman Prediction of Secondary Structure: in Prediction of Protein Structure and the Principles of Protein Conformation, ed. G.B. Fasman. Plenum, New York. 1989. 1-91.

132. Blank, V.C., Sterin-Prync, A., Retegui, L., Alejandro, V., Criscuolo M., Roguin, L.P. Identification of a Linear Epitope of Interferon-α_{2b} Recognized by Neutralizing Monoclonal Antibodies. Eur J of Biochem. 1999. 265:11-19.

133. Piehler, J. Roisman, L.C., Schreiber, G. New Structural and Functional Aspects of the Type I IFN Receptor Interaction Revealed by Comprehensive Mutational Analysis of the Binding Interface. J Biol Chem. 2000. 275(51):40425-33.

134. Korn, A.P., Rose, D.R., Fish, E.N. Three-dimensional Model of a Human Interferon-alpha Consensus Sequence. J Interferon Res. 1994. 14:1-9.

135. Mujtaba, M.G., Villarete L., Johnson, H.M., IFN-tau Inhibits IgE Production in a Murine Model of Allergy and in an IgE-producing Human Myeloma Cell Line. J Allergy Clin Immunol. 1999. 104(5):1037-44.

136. Agresti, A., Finlay, B. Statistical Methods for the Social Sciences, ed. Heath A. Prentice Hall, Inc. Upper Saddle River, New Jersey. 1997.

137. Chen, J.W., Murphy, T.L., Willingham, M.C., Pastan, I., August, J.T. Identification of Two Lysosomal Membrane Glycoproteins. J Cell Biol. 1985. 101(1):85-95.

138. Kyte J., Doolittle, R.F. A Simple Method for Displaying the Hydropathic Character of a Protein. J Mol Biol. 1982. 157:105-132.

139. Dill, K.A., Bromberg, S., Yue, K., Fiebig, K.M., Yee, D.P., Thomas, P.D., Chan, H.S. Principles of Protein Folding--A Perspective from Simple Exact Models. Pro Sci. 1995. 4:561-602.

140. Young, L., Jernigan, R.L., Covell, D.G. A role for surface hydrophobicity in protein-protein recognitionPro Sci. 1994. 28:717-729.

BIOGRAPHICAL SKETCH

Kendra enjoyed her high school experience at Choctawhatchee senior high school in Fort Walton Beach, Florida. During that time, she was an active member of extracurricular activities such as Wheelettes, a philanthropy group sponsored by the Rotary Club; Latin Honor Society; Thespians drama club; Fellowship of Christian Athletes (FCA), and Harumbee, an organization of minority students that embraced diversity and encouraged the unity of all individuals. She enjoyed competing in debate tournaments throughout Florida. She exercised her leadership abilities by serving as Vice President of Student Council for two years. Although she loved it, she left the varsity tennis team, to strengthen the girl's golf team; the golf team competed in their first state championship that year. The Florida sand and heat was replaced with snow and freezing weather, when she moved to Montana for her first year of college at Montana State University (MSU). Snowboarding and fly-fishing were substituted for tennis and golf. At MSU, she was accepted as an active member of Pi Beta Phi, a sorority that consisted of a group of multi-talented, goal-oriented, young ladies. She completed her undergraduate education with a Bachelor of Science degree in Microbiology at the University of Florida and remained at the

University of Florida for her graduate education. She is a member of the Gamma Sigma Delta Honor Society. When not studying or working, she finds pleasure in playing golf with many outstanding individuals from all walks of life, has philosophical discussions in coffee shops with intriguing people who have much to say, and exercises regularly for her happiness and health.